To the Graduate Council:

I am submitting herewith a dissertation written by Jiahong Zhu entitled "Metallurgical Factors Controlling the Phase Stability and Mechanical Behavior of Transition-Metal Laves Alloy Systems". I have examined the final copy of this dissertation for form and content and recommend that it be accepted in partial fulfillment of the requirements for the degree of Doctor of Philosophy, with a major in Metallurgical Engineering.

Peter K. Liaw, Major Professor

We have read this dissertation
and recommend its acceptance:

Charlie R. Brooks

David C Joy

R. A. Buchanan

Accepted for the Council:

Associate Vice Chancellor and
Dean of The Graduate School

METALLURGICAL FACTORS CONTROLLING THE PHASE STABILITY AND MECHANICAL BEHAVIOR OF TRANSITION-METAL LAVES ALLOY SYSTEMS

A Dissertation

Presented for the

Doctor of Philosophy

Degree

The University of Tennessee, Knoxville

Jiahong Zhu

August 1998

DEDICATION

This dissertation is affectionately dedicated to my wife

Ying Zhang

for

her love, patience, and encouragement.

ACKNOWLEDGMENTS

I am very grateful to Prof. P. K. Liaw for his guidance, support and encouragement during my study at University of Tennessee, Knoxville (UTK). I would like to thank Dr. C. T. Liu, Group Leader of the Alloying Behavior and Design Group at the Oak Ridge National Laboratory (ORNL), for providing me the opportunity to work on Laves phase alloys. His comments and insight are constructive for this research. Thanks are also due to Dr. C. R. Brooks, Dr. R. A. Buchanan, and Dr. D. C. Joy for serving on my dissertation committee and for their helpful comments. I would also thank Dr. J.M. Corum and Dr. J.G.R. Hansen of Engineering Technology Division, ORNL, for their support, instruction, and encouragement during the first year of my study at UTK.

I am very appreciative of Drs. L. M. Pike, J. H. Schneibel and M. P. Brady at ORNL for their friendship and interest in my research. Special thanks go to Dr. L. M. Pike for his kind help and numerous discussions on point defects in intermetallics. Technical assistance by Joe Wright, Elmer Lee and Cecil Carmichael at ORNL is sincerely acknowledged. I owe gratitude to many faculty and staff members in Materials Science and Engineering Department: Dr. Anthony Pedraza for letting me use his equipment; Sandy Maples and Carla Lawrence for providing general service.

This research was sponsored by the DOE Fossil Energy Advanced Research and Technology Development (AR & TD) Materials Program with Dr. R. R. Judkins as the program manager, under subcontract 11X-SP173V to the University of Tennessee with Lockheed Martin Energy Research Corporation. Additional funding was provided by the Southeastern University Research Association (SURA) summer program, with Dr. T. Hutchinson as the contract monitor.

I will always be indebted to my parents, Jianhua Zhu and Jüying Zhu, for their love, understanding and support for so many years. This dissertation is dedicated to my

wife, Ying Zhang, for her love, great patience, constant encouragement, and countless discussions regarding this research.

ABSTRACT

Recent interest in developing ultrahigh temperature intermetallics for structural use has prompted a series of research on Laves-phase based alloys. Alloys based on the $NbCr_2$ Laves phase are shown to be the most promising, since $NbCr_2$ has a high melting point of 1730°C, good creep resistance, high strength, and excellent oxidation resistance. However, the room-temperature fracture toughness of Laves phases is poor. There is a pressing need to (1) understand the scientific principles controlling the phase stability and deformation behavior of the Laves-phase materials, and (2) investigate the ways to toughen these materials so that their applications can be widened.

In this dissertation, the phase stability in transition-metal $NbCr_2$-based Laves phases was first studied following a phase diagram survey. An electron concentration rule for the phase stability of $NbCr_2$-based Laves phase systems was proposed, and the critical electron concentrations for controlling the C15/C14/C15 phase transitions were identified. Pseudobinary $Nb(Cr,X)_2$ (X = Fe or Co) systems with various X contents were investigated to determine the homogeneity ranges of various Laves phases, which was then correlated with the electron concentration factor, e/a. The experimentally determined critical e/a values corresponding to the C15/C14/C15 phase transitions were close to those from the phase diagram survey: at $e/a < 5.77$, the C15 structure was stabilized; at $5.85 < e/a < 7.5$, the C14 structure was stable; and at $e/a > 7.56$, the C15 structure was stabilized again. No intermediate structure was detected between the C15/C14 structures. As the Fe or Co content increased, the volume of a 24-atom unit cell decreased linearly for both C15 and C14 structures, while the Vickers hardness increased over the whole C15 and C14 ranges. The fracture toughness was low for all the alloys, but the fracture toughness of the C15 structure was greater than that of the C14 structure for the two ternary systems. No

improvement in fracture toughness for alloys near the C15 and C14 phase boundaries and in the C15/C14 two-phase regions was observed.

The stability of the Laves phases was also investigated from the consideration of the bonding characteristics and the enthalpy of formation of the Laves phases. A survey on the enthalpies of formation of Laves phases reveals that there are metallic, covalent and ionic bonds, or a mixed metallic-covalent-ionic bond, in Laves phases. A thermodynamic interpretation is offered for the first time to explain the geometric principle for Laves-phase formation. As the deviation from the ideal size ratio increases, the maximum negative enthalpy of formation decreases linearly, which is assumed to be due to the elastic strain energy expended in compressing the atoms. At the atomic size ratios, R_A/R_B, of 1.03 and 1.65, the enthalpy of formation reaches zero. Further deviation in the R_A/R_B ratio will lead to the enthalpy of formation being positive. Thus, the free energy of formation becomes positive, due to the negligible entropy-of-formation term. Consequently, Laves phases can only be stabilized in certain atomic size ratios.

The constitutional defect mechanisms on both sides of stoichiometry in the binary $NbCr_2$, $NbCo_2$ and $NbFe_2$ Laves-phase systems were found to be the anti-site substitution. For the $NbCr_2$ alloys, thermal vacancies exhibiting a maximum at the stoichiometric composition were observed in samples quenched from 1400°C. These vacancies could be completely eliminated by annealing at 1000°C.

Anti-site hardening was found in the $NbCr_2$, $NbCo_2$ and $NbFe_2$ Laves-phase systems. The presence of thermal vacancies in the $NbCr_2$ alloys, on the other hand, was found to soften the Laves phases. Both the anti-site defects and thermal vacancies do not significantly affect the fracture toughness of the Laves phases.

TABLE OF CONTENTS

PART I: GENERAL INTRODUCTION AND OUTLINE OF THIS RESEARCH 1

1. INTRODUCTION 2

2. BACKGROUND INFORMATION AND CRITICAL ISSUES 3
   - 2.1. Phase Stability and Bonding Characteristics 3
   - 2.2. Defects, Deformation Mechanisms and Alloy Development 5
   - 2.3. Critical Issues on Laves Phases 8
     - 2.3.1. Brittleness at Room Temperature 9
     - 2.3.2. Phase Stability 9
     - 2.3.3. Relationship between Deformation Characteristics and Phase Stability 10

3. OUTLINE OF THIS RESEARCH 10
   - 3.1. Effects of Electron Concentration on the Phase Stability of $NbCr_2$-Based Laves Phases (Part II) 12
   - 3.2. Effects of Ternary Additions on the Phase Stability of $NbCr_2$-Based Laves Phases (Part III) 15
   - 3.3. Enthalpies of Formation of Laves Phases (Part IV) 15
   - 3.4. Point Defects in Binary Laves-Phase Alloys (Part V) 15
   - 3.5. Concluding Summary and Suggested Future Work (Part VI) 16

4. IMPACT OF THIS WORK 17

REFERENCES 18

PART II: EFFECTS OF ELECTRON CONCENTRATION ON THE PHASE STABILITY OF $NbCr_2$-BASED LAVES PHASES .. 23

1. INTRODUCTION 24
   - 1.1. Phenomenological Study of Phase Stability in Laves Phases 24
   - 1.2. Theoretical Prediction of Phase Stability of Laves phases 28
   - 1.3. Motivation of This Study 29

2. LAVES PHASES IN BINARY X-Cr AND Nb-X SYSTEMS 30

3. LAVES PHASES IN TERNARY Nb-Cr-X SYSTEMS 33

4. EFFECT OF e/a ON LAVES-PHASE STABILITY 35

5. CONCLUSIONS 39

REFERENCES 41

PART III: EFFECTS OF TERNARY ADDITIONS ON THE PHASE STABILITY OF $NbCr_2$-BASED LAVES PHASES 45

1. INTRODUCTION 46

2. EXPERIMENTAL PROCEDURES 47

3. RESULTS AND DISCUSSIONS 49

4. CONCLUSIONS 58

REFERENCES 59

PART IV: ENTHALPIES OF FORMATION OF LAVES PHASES..... 62

1. INTRODUCTION..... 63
2. MEASUREMENTS OF ENTHALPIES OF FORMATION 64
3. ENTHALPIES OF FORMATION AND BONDING OF INTERMETALLIC COMPOUNDS..... 66
4. SEMIEMPIRICAL CALCULATION..... 68
5. SOME REGULARITIES IN THE ENTHALPIES OF FORMATION OF LAVES PHASES 70
   - 5.1. Effect of Atomic Size Ratio on Enthalpies of Formation..... 79
   - 5.2. Enthalpies of Formation in Non-Transition Metal Laves Phases..... 84
   - 5.3. Enthalpies of Formation in Transition-Metal Laves Phases..... 86
   - 5.4. Enthalpies of Formation in Laves Phases Involving Rare Earth Elements 87
6. SUMMARY 94

REFERENCES 95

PART V: POINT DEFECTS IN BINARY LAVES-PHASE ALLOYS.. 102

1. INTRODUCTION..... 103
   - 1.1. Point Defects in B2 Compounds..... 103
   - 1.2. Point Defects in Laves Phases and Objective of This Study..... 105
2. EXPERIMENTAL PROCEDURES..... 108
3. RESULTS 112
   - 3.1. Microscopic Observation..... 112
   - 3.2. Lattice Parameter, Density, and Vacancy Concentration 118
     - 3.2.1. Binary $NbCr_2$ Alloys 118
     - 3.2.2. Binary $NbCo_2$ Alloys..... 121
     - 3.2.3. Binary $NbFe_2$ Alloys 122
   - 3.3. Hardness and Fracture Toughness Behaviors..... 126
4. DISCUSSION 131
   - 4.1. Defect Mechanisms in Binary Laves Phases..... 131
   - 4.2. Thermal Vacancy in Binary $NbCr_2$ Laves Phases..... 133
   - 4.3. Solid Solution Hardening in Binary Laves Phases 134
   - 4.4. Fracture Toughness in Binary Laves Phases 135
5. CONCLUSIONS 136

REFERENCES 137

PART VI: CONCLUDING SUMMARY AND SUGGESTED FUTURE WORK..... 140

1. CONCLUDING SUMMARY..... 141
2. SUGGESTED FUTURE WORK 143

REFERENCES 146

VITA 148

LIST OF FIGURES

FIGURE PAGE

PART I: GENERAL INTRODUCTION AND OUTLINE OF THIS RESEARCH

1. Diagram showing the integration strategy and interrelationship amongst various research tasks 12

2. The binary Nb-Cr phase diagram 13

PART II: EFFECTS OF ELECTRON CONCENTRATION ON THE PHASE STABILITY OF $NbCr_2$-BASED LAVES PHASES

1. Effect of valence electron concentration on phase stability for several ternary Mg-based alloys 25

2. Effect of average electron concentration factor (e/a) on ordered structures in pseudo-binary Ni_3V-Co_3V and Co_3V-Fe_3V systems 28

3. Effect of average electron concentration (e/a) on phase stability in binary and ternary $NbCr_2$-based systems 36

PART III: EFFECT OF TERNARY ADDITIONS ON PHASE STABILITY IN NbCr2-BASED LAVES PHASES

1. X-ray diffraction patterns of $Nb(Cr,Fe)_2$ alloys with 2, 7, 9 at.% Fe, which have C15, C14/C15, and C14 structures, respectively 49

2. Effect of average electron concentration (e/a) on phase stability in $NbCr_2$-based systems, with the critical e/a values for phase transitions both from experiments and phase diagram information 51

3. Dependence of the volume of 24-atom cell of $Nb(Cr,X)_2$ Laves phase on the Fe or Co content 52

4. The effect of Fe content on the Vickers hardness of $Nb(Cr,Fe)_2$ alloys 54

5. The effect of Co content on the Vickers hardness of $Nb(Cr,Co)_2$ alloys 54

6. Cracking behaviors in (a) C15 $NbCo_2$ alloy and (b) C14 $NbFe_2$ alloy 56

7. Fracture toughness values of the Laves phases as a function of the Fe content 57

8. Fracture toughness values of the Laves phases as a function of the Co content.....57

PART IV: ENTHALPIES OF FORMATION OF LAVES PHASES

1. Enthalpy of formation versus R_A/R_B for C15 Laves phases 80

2. Enthalpy of formation versus R_A/R_B for C14 Laves phases 80

3. Enthalpy of formation versus R_A/R_B for C36 Laves phases 81

4. Enthalpy of formation versus R_A/R_B for C15, C14 and C36 Laves phases.....81

5. Enthalpy of formation versus the axial ratio c/a for C14 Laves phases 83

6. Enthalpy of formation versus R_A/R_B for non-transition metal Laves phases.....85

7. Enthalpy of formation versus the difference in electronegativity of the two components for non-transition metal Laves phases.....86

8. Enthalpy of formation in transition-metal Laves phases 87

9. Experimental enthalpy of formation for 3d transition metal lanthanide Laves phases as a function of lanthanide atomic number 89

10. Experimental enthalpy of formation for 4d transition metal lanthanide Laves phases as a function of lanthanide atomic number 89

11. Experimental enthalpy of formation for 5d transition metal lanthanide Laves phases as a function of lanthanide atomic number 90

12. Experimental enthalpy of formation for VIII transition metal (Fe, Ru, and Os) lanthanide Laves phases as a function of lanthanide atomic number.....90

13. Experimental enthalpy of formation for VIII transition metal (Co, Rh, and Ir) lanthanide Laves phases as a function of lanthanide atomic number.....91

14. Experimental enthalpy of formation for VIII transition metal (Ni and Pt) lanthanide Laves phases as a function of lanthanide atomic number.....91

15. Predicted enthalpy of formation for 3d transition metal lanthanide Laves phases as a function of lanthanide atomic number by Miedema's method 93

16. Predicted enthalpy of formation for aluminum lanthanide Laves phases as a function of lanthanide atomic number by Miedema's method.....93

PART V: POINT DEFECTS IN BINARY LAVES-PHASE ALLOYS

1. The difference in the shapes of the unit cell volume vs. composition curves between anti-site defect and triple defect B2 compounds.....104

2. Optical microstructure of the stoichiometric $NbCr_2$ alloy after quenching from 1000°C (in etched condition).....113

3. SEM micrograph of the $NbCr_2$ alloy #1 after quenching from 1000°C (in as-polished condition).....113

4. EDS spectra of the matrix and the dark phase indicated in Fig. 3, which were $NbCr_2$ Laves phases and Cr precipitate, respectively.....114

5. Optical microstructure of the stoichiometric $NbCo_2$ alloy 115

6. SEM micrograph of the $NbCo_2$ alloy #6.....115

7. EDS spectra of the matrix and the second phase indicated in Fig. 6, which were $NbCo_2$ Laves phase andβ Nb_6Co_7 phase, respectively.....116

8. Optical microstructure of the stoichiometric $NbFe_2$ alloy.....117

9. SEM micrograph of the $NbFe_2$ alloy #7 117

10. EDS spectra of the matrix and the second phase indicated in Fig. 9, which were $NbFe_2$ Laves phase and μ NbFe phase, respectively 118

11. Lattice parameter as a function of the Nb content for $NbCr_2$ alloys.....119

12. X-ray and bulk densities as a function of the Nb content for $NbCr_2$ alloys after quenching from 1400 and 1000°C.....120

13. Vacancy concentration as a function of the Nb content for $NbCr_2$ alloys after quenching from 1400 and 1000°C.....120

14. Lattice parameter as a function of the Nb content for $NbCo_2$ alloys.....121

15. X-ray and bulk densities as a function of Nb content for $NbCo_2$ alloys.....123

16. Vacancy concentration as a function of Nb content for $NbCo_2$ alloys 123

17. Lattice parameters, a and c, as a function of Nb content for $NbFe_2$ alloys.....124

18. X-ray and bulk densities as a function of Nb content for $NbFe_2$ alloys 125

19. Vacancy concentration as a function of Nb content for $NbFe_2$ alloys.....125

20. Vickers Hardness versus Nb content for $NbCr_2$ alloys after quenching from 1400°C and 1000°C.....126

21. Vickers Hardness versus Nb content for $NbCo_2$ alloys after quenching from 1000°C.....127

22. Vickers Hardness versus Nb content for $NbFe_2$ alloys after quenching from 1000°C.....128

23. Fracture toughness versus Nb content for $NbCr_2$ alloys after quenching from 1400°C.....129

24. Fracture toughness versus Nb content for $NbCr_2$ alloys after quenching from 1000°C.....129

25. Fracture toughness versus Nb content for $NbCo_2$ alloys.....130

26. Fracture toughness versus Nb content for $NbFe_2$ alloys 131

LIST OF TABLES

TABLE PAGE

PART II: EFFECTS OF ELECTRON CONCENTRATION ON THE PHASE STABILITY OF $NbCr_2$-BASED LAVES PHASES

I. Atomic size, electron concentration factor (e/a) of alloying element, and existing binary Laves phase 31

II. Atomic size ratio (R_A/R_B), homogeneity range (%A range), corresponding e/a range and Laves phase structure in binary XCr_2 and NbX_2 alloy systems 33

III. Homogeneity range (%X) and corresponding e/a range of C15/C14 structures in ternary Nb-Cr-X systems.....34

PART IV: ENTHALPIES OF FORMATION OF LAVES PHASES

I. List of R_A/R_B, experimental ΔH and ΔS, the experimental temperature and method, and relevant references for binary C15 Laves phases.....71

II. List of R_A/R_B, c/a, experimental ΔH and ΔS, the experimental temperature and methods, and relevant references for binary C14 Laves phases 76

III. List of R_A/R_B, experimental ΔH and ΔS, the experimental temperature and method, and relevant references for binary C36 Laves phases.....78

PART V: POINT DEFECTS IN BINARY LAVES-PHASE ALLOYS

I. Composition, lattice parameter, X-ray density, bulk density and vacancy concentration (c_v) of the $NbCr_2$ alloys quenched from 1400 and 1000°C 109

II. Composition, lattice parameter, X-ray density, bulk density and vacancy concentration (c_v) of the $NbCo_2$ alloys quenched from 1000°C.....109

III. Composition, lattice parameter, X-ray density, bulk density and vacancy concentration (c_v) of the $NbFe_2$ alloys quenched from 1000°C.....110

PART VI: CONCLUDING SUMMARY AND SUGGESTED FUTURE WORK

I. The enthalpies of formation of several B2 compounds 144

PART I: GENERAL INTRODUCTION AND OUTLINE OF THIS RESEARCH

1. INTRODUCTION

Laves phases with AB_2 compositions are a common type of topologically close-packed (TCP) structures [1-3]. There are over 360 binary Laves phases reported in the literature. Furthermore, Laves phases are capable of dissolving considerable amounts of ternary alloying additions. Totally over 900 combined binary and ternary Laves phases have been documented. Although Laves structures are the most abundant among intermetallic compounds, they are the least investigated. So far, most previous studies have concentrated on compounds with structures that have an ordered form of face-centered cubic (f.c.c.), body-centered cubic (b.c.c.), or hexagonal-close packed (h.c.p.) structure. Thus, there is a great need for the study of Laves phases.

Laves phases are being considered for many practical applications. For example, $(Tb,Dy)Fe_2$ has been used as a magnetoelastic transducer because of its great magnetorestriction [4]. Compounds of $(Hf,Zr)V_2$ have demonstrated superconducting properties with a combination of high critical temperature and current density, and great magnetic strength [5, 6]. Laves phases, such as $Zr(Cr,Fe)_2$, have been considered for hydrogen storage applications due to favorable hydriding-dehydriding kinetics and high hydrogen-absorbing capabilities [7]. The $Mo(Co,Si)_2$ Laves phase contributes to the wear-resistance of "Tribaloy" materials [8]. More recently, $HfCr_2$-, $NbCr_2$- and $TiCr_2$-based two-phase alloys are being developed for high-temperature structural uses, because of their high melting points and good retention of mechanical properties at elevated temperatures [9-22]. Despite their useful properties, their low ductility and brittle fracture characteristics at ambient temperatures are the main limitations for structural applications of this large class of alloys.

All these facts indicate that more research needs to be undertaken on Laves phases to further the understanding on the basic phase stability, defect and deformation

mechanism, and fracture behavior. Moreover, ways need to be found to overcome the brittleness in these phases.

In Section 2, some background information on Laves phases is summarized, especially in areas such as phase stability and bonding features, point defects, deformation characteristics and alloy development. The critical issues regarding the Laves-phase study will also be described. An outline of this research is given in Section 3. Section 4 emphasizes the impact of this work on both the alloy phase theory and mechanical properties of ultrahigh temperature structural intermetallic alloys.

2. BACKGROUND INFORMATION AND CRITICAL ISSUES

2.1 Phase Stability and Bonding Characteristics

There are several different crystalline structures of Laves phases, with the following three structures most frequently observed: a cubic C15 - $MgCu_2$ structure, hexagonal C14 - $MgZn_2$ structure and dihexagonal C36 - $MgNi_2$ structure [3, 23]. The structures of Laves phases are most easily characterized with the stacking sequence of four-layer units, in a close analogy to the familiar description of f.c.c. and h.c.p. structures in terms of the stacking series of single close-packed layers [24]. The cubic C15 structure consists of such layers stacked ABCABC, while the hexagonal C14 structure is composed of such layers stacked ABABABAB. C36 may be regarded as a transitional phase between the C15 and C14 structures with a stacking series of ABACABAC. Laves phases are generally stabilized by the size-factor (geometric) principle, i.e., the atomic size ratio, R_A/R_B, is ideally 1.225, with a range of 1.05-1.68 usually observed. Laves phases can be stabilized only in this range of atomic size ratios; no Laves phases are observed outside this range. However, the stability of each crystalline structure is also greatly influenced by the electron concentration factor (e/a) [3, 25-27]. The classic work by Laves and Witte [25, 26]

showed that for several quasi-binary alloy systems involving $MgCu_2$ and $MgZn_2$, with increasing valence electron concentration, the three Laves polytypes, C15, C36 and C14, exist in that order. For some transition-metal Laves phases, the average electron concentration and the d-band hole number were successfully used to relate to the crystalline structures by Bardos, Gupta and Beck [28], and Watson and Bennett [29-31].

The phase stability is also closely related to the nature of bonding in the compound. The bond characteristics of Laves phases were generally considered to be of metallic nature [32, 33]. The enthalpy of formation is an indication of the bond strength and the stability of the compound [33]. The enthalpies of formation of Laves phases were found to be small for alloys without transition metals, which was used to explain the metallic nature of the bond in these alloys. For Laves phases containing transition metals, the enthalpy of formation is usually higher, due to the possible electron transfer to fill the incomplete d-band of the transition metal [32, 34]. Recent experimental data show that some Laves phases have a very high enthalpy of formation [35], and a mixed metallic-covalent-ionic bond can, thus, possibly exist in Laves phases. So far, no one has offered a quantitative interpretation of the observed size ratio range (1.05-1.66) from the viewpoint of the geometric factor, electronic factor, or thermodynamics (enthalpy of formation).

The importance of the phase stability study lies in the fact that many fundamental properties are affected by the crystalline structure. For example, it was found that the stoichiometric compound, $ZrCr_2$, can be stabilized in either of the C14 and C15 types. The hydrogen storage capability of the $ZrCr_2$-based Laves-phase compound is related to the crystalline structure. At room temperature, it absorbs up to 3.4 H/formula unit (f.u.) for the C14 structure, and 4 H/f.u. for the C15 structure [36, 37]. More recently, it is suggested that the deformability of complex Laves phases can be improved by controlling

their crystalline structures in such a way that the stress-assisted phase transformation and/or mechanical twinning can be triggered during plastic deformation [11, 12, 38-42].

It is very important to study the factors controlling the phase stability of Laves phases so that the phase structure can be eventually controlled by alloying additions. Thus, improved mechanical properties, especially fracture toughness, of Laves phases may be achieved.

2.2 Defects, Deformation Mechanisms and Alloy Development

Recently, the interest in developing Laves-phase intermetallics for high-temperature structural applications has provoked a significant amount of work on defects, dislocation behavior, deformation mechanisms, and alloy developments of Laves-phase based alloys.

About 25% of the known binary Laves phases shows certain solubility ranges [43]. For the nonstoichiometric compositions, constitutional defects are incorporated into the intermetallics. The defect mechanisms in some intermetallics, such as the B2 phase, have been extensively documented [44, 45] and have important impacts on the mechanical behavior of the compound [45-49]. However, for the Laves phases, little is known about the possible defect structures that may be associated with the solubility at off-stoichiometric compositions. Defect mechanisms have only been preliminarily studied in some Laves phases. Most studies suggest that anti-site substitutions are present on both sides of the stoichiometry in Laves phases, i.e., the A and B atoms substitute for each other [50]. For Al_2Y, it has been suggested that the Y-rich side is accommodated by vacancies, while the Al-rich compositions result from anti-site substitution [51]. As in the B2-structure, the types of constitutional defects are important, because they may affect mechanical properties of Laves phases. Vacancies have been proposed to assist the movement of synchro-Shockley dislocations of Laves phases [52]. Off-stoichiometry was also found to affect the

hydride stability of $ZrMn_2$ [53] and the hydrogen storage capability of $TiMn_2$ alloys [54]. Therefore, it is imperative to determine the off-stoichiometric defects in the binary Laves phases and study the effect of such constitutional defects on the deformability of the Laves phases.

The extended defects in Laves phases have been characterized. It has been shown that in C15 $TiCr_2$ Laves phases, {111} stacking faults are bounded by two 1/6<112> synchro-Shockley partial dislocations [55]. In $MgCu_2$, splitting of each individual dislocation into two partial dislocations with a spacing of about 10 nm was found in weak-beam TEM (transmission electron microscopy) images, and much larger separations were also observed in extended nodes in dislocation networks [56]. High-resolution TEM of dislocation splitting on the basal plane of $MgNi_2$ shows a spacing of 34 nm, consistent with the low-stacking fault energy expected for the C36 structure [57].

Deformation mechanisms are considered to be related to the atomic structure of defects in Laves phases. Due to the specific arrangement of atoms, a deformation mechanism termed synchroshear involving cooperative movements between planes of atoms may be required [58]. Ternary additions on A and/or B lattice sites in the AB_2 Laves phase may permit enhanced dislocation mobility [56]. In addition, the presence of vacancy defects may assist the synchroshear processes in Laves phases, potentially providing ductility to the intermetallic phase [41].

Plastic deformation in single-phase Laves compounds has been reported only at temperatures approximately two-thirds of the melting point. Cubic C15 compounds deform on the {111}<110> slip system and by {111}<112> mechanical twinning [38, 56, 59]. Hexagonal C14 compounds deform by $<11\bar{2}0>$ slip on both basal and prismatic planes, and several twinning systems have been identified [60-62]. One study of the high-

temperature compression behavior of dihexagonal C36 compounds indicated that basal slip was the dominant deformation mechanism [38].

Recent work on V-Hf-Nb alloys by Chu and Pope [11] and Livingston and Hall [38] demonstrated that the room-temperature deformation mechanism of the HfV_2-based C15 phase was {111}<112> mechanical twinning. The elastic behavior of HfV_2 is anomalous, in that both Young's and shear moduli decrease with decreasing temperature. This lattice instability is related to a martensitic transformation to an orthorhombic structure below about -153 °C [11, 38, 63]. If the room-temperature mechanical twinning in V-Hf-Nb alloys derives from this lattice instability, this mechanism responsible for low-temperature toughness of Laves phases may be limited to only a few alloy systems. One possible general approach to enhance mechanical twinning is to alloy Laves phases with elements that lower the stacking fault energy (SFE). Alloying C15 $MgCu_2$, for example, with Zn or other elements that eventually lead to transitions to hexagonal Laves phases could presumably lower SFE and may, thus, enhance deformation twinning [3].

Another low-temperature deformation mechanism, recently reported in a Laves phase by Liu, Livingston and Allen [39], is the stress-assisted phase transformation. In a Fe-rich $ZrFe_2$ compound of a two-phase Fe-Zr alloy [39], compression at room temperature resulted in a partial shear transformation of the dihexagonal C36 phase to cubic C15 phase. In Laves-phase compositions near the C15/C14 and other structural transitions, such phase transformation can be introduced during plastic deformation, which may offer a general approach for toughening Laves phases. The small difference in the thermodynamic free energies of the different Laves-phase structures makes the transformation possible under stress.

Both the mechanical twinning and stress-induced phase transformation are possible toughening mechanisms for Laves-phase alloys. Obviously, these kinds of toughening

mechanisms are associated with the relative stability of the Laves polytypes. Thus, it is important to study the factors governing the phase stability in Laves alloys.

Recent alloy development of Laves-phase intermetallics has focused on both the improvement of deformability of monolithic Laves phases and the dual-phase approach in systems forming a eutectic structure of a Laves phase plus a b.c.c. matrix. In particular, the dual-phase alloy has exhibited remarkable improvements in toughness [16]. Niobium and chromium both form eutectic structures with $NbCr_2$, and therefore, this "*in situ* composite" has intrinsic stability. Moreover, the precipitation and coarsening kinetics of the Laves phase in Cr-Nb and Cr-Hf systems have been found to be extremely sluggish, even at 1200°C, thus indicating a slow diffusion process in these dual-phase alloys [13, 64]. Ductility and toughness were found to increase with decreasing Laves-phase content, and low-temperature toughness values up to 20 $MPa\sqrt{m}$ have been achieved in a $NbCr_2$-based alloy with a Nb matrix by Chan and Davidson [16]. It is clear that the presence of a Laves phase is still a limiting factor of the dual-phase fracture toughness. Further improvement in the toughness of these composites would require (1) the ductilization of the b.c.c. matrix, (2) the manipulation of the microstructure to relax high plastic strains by the reduction of the Laves-phase size, (3) the optimized distribution of Laves phases in the b.c.c. matrix, and (4) the control of interfacial properties including the CTE (coefficient of thermal expansion) mismatch, and the degree of coherency between the b.c.c. matrix and the Laves phase. In addition, the modification of the Laves-phase properties through alloying is another possibility, and probably the most important aspect to facilitate Laves-phase alloys for practical applications.

2.3 Critical Issues on Laves Phases

There are many issues that need to be addressed to further the understanding of Laves phases and to build up the scientific and technological knowledge base for

developing Laves-phase alloys for both functional and structural applications. The following three areas are some of the most important for studying Laves-phase based alloys, and are addressed in this dissertation.

2.3.1 Brittleness at Room Temperature

Laves phases, including $NbCr_2$, $HfCr_2$, and $TaCr_2$, exhibit very promising high-temperature (> 1000°C) mechanical properties, such as high strength and appreciable creep resistance, high melting points, and usually excellent oxidation and corrosion resistance. However, the brittle fracture behavior and low fracture toughness of the monolithic Laves phases are the major drawbacks for engineering applications of these materials. The introduction of a ductile b.c.c. phase resulting in a dual-phase structure increased the fracture toughness of the Laves-phase alloy. Nevertheless, the low fracture toughness of the Laves phase still dictates the poor ductility of the two-phase alloys. To overcome this drawback of Laves-phase based alloys, it is very important to improve the deformability of the Laves phase, especially through the mechanisms of mechanical twinning and/or phase-transformation toughening. Vacancies have been suggested to assist sychroshear deformation mechanisms in the Laves phases. Thus, it is also imperative to study the point defect mechanisms in the binary Laves alloys, both thermal and constitutional defects, and their effects on the fracture toughness behavior of the Laves phases.

2.3.2 Phase Stability

There are many polytypes of Laves phases. By changing alloy stoichiometry, temperature, and alloying addition, different Laves-type structures can be stabilized. The rules governing the phase stability are very important, since they can be used to guide alloying additions to control the phase structure and deformation mechanisms, and thus, the

mechanical properties. There is a great need to elucidate the effects of ternary alloying additions on phase stability. Thus, the alloying addition can be controlled to achieve desired Laves-type structures.

The bond characteristics and enthalpies of formation of the Laves phases are closely related to their stability. The thermodynamic data of the Laves phases have not been systematically studied and reviewed. Most of such information is scattered in different journals, proceedings, and books. There is a great need to summarize and analyze these data, with the hope that some general trends can be observed and used to predict the enthalpies of formation for Laves phases where such information is not available.

2.2.3 Relationship between Deformation Characteristics and Phase Stability

The deformation mechanisms of various Laves polytypes should be carefully studied, since work in this area is very limited. So far, all of the studies focus on C14 and C15, with a few on C36. Experimentally, intermediate structures other than C36 should be investigated. Also, alloys of the compositions at the phase boundaries are of metastable nature, which may easily be transformed to other structures, and/or mechanical twinning can be triggered. Thus, as in some partially stabilized zirconia ceramics, the stress-induced phase transformation and/or mechanical twinning may offer a general approach to toughening Laves phases. There has been some research performed in this direction [39, 40]. However, more work is clearly needed to further explore this possibility. The effect of point defects on the deformability of the Laves phases should also be studied to verify if the vacancy-assisted synchroshear deformation can be triggered in Laves phases.

3. OUTLINE OF THIS RESEARCH

In order to enhance the low-temperature mechanical properties of the monolithic Laves phase and develop toughened dual-phase alloys, an in-depth and systematic

investigation of the phase stability in Laves phases is undertaken, which is related to their deformation mechanisms. In this manner, a better understanding of the factors controlling the phase stability of Laves phases is obtained, which may facilitate the alloying element selection. Moreover, the desired phase structures and deformation mechanisms of Laves phases can be controlled, which serves as a base for developing tough dual-phase (Laves phase + b.c.c. matrix) alloys for high-temperature structural applications.

The integration strategy and interrelationship amongst the various research tasks are summarized in Fig. 1. Following a phase diagram survey, the electron concentration and phase stability correlation was studied. Various pseudo-binary systems was investigated to clarify the electron concentration factor/phase stability relationship. The stability of the Laves phases was also considered from the viewpoint of the bonding character and enthalpy of formation of the Laves phases. The point defects in the binary Laves alloys was studied, which accompanied the off-stoichiometry. The deformation mechanism and mechanical properties, including fracture toughness, were determined and related to the phase stability of the alloys. The findings could be used in toughening Laves-phase based dual-phase alloys. The pseudo-binary systems for the phase stability study included $Nb(Cr,Co)_2$ and $Nb(Cr,Fe)_2$ systems. Binary $NbCr_2$, $NbCo_2$, and $NbFe_2$ systems were investigated to clarify the point defect mechanisms in these Laves phases. Information from these studies may guide us in the alloy design of the monolithic Laves phases. The items in the dashed boxes, including the ductilization of the matrix, microstructural manipulation and alloy design of dual-phase alloys, are being addressed by a research program at Oak Ridge National Laboratory, and will not be pursued in this dissertation. However, it is understood that these efforts are also needed for designing toughened dual-phase alloys for their practical structural application.

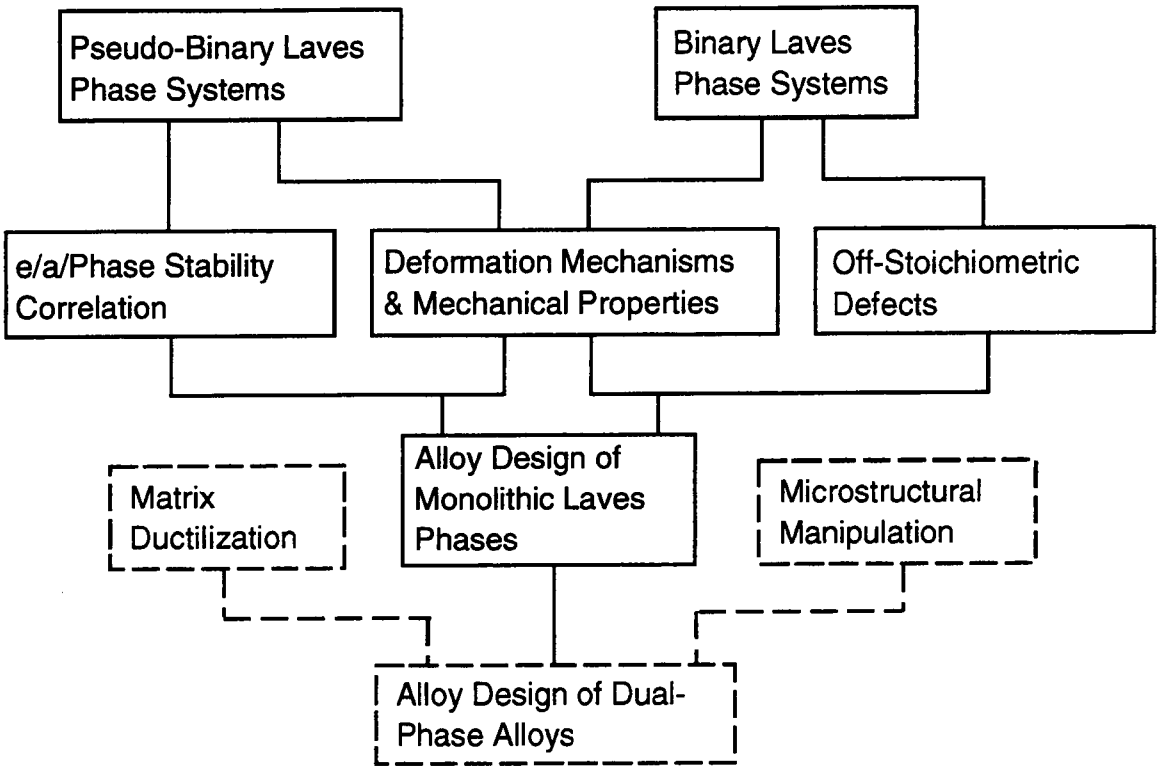


Fig. 1 Diagram showing the integration strategy and interrelationship amongst various research tasks.

Based on the integration strategy in Fig. 1, the following research components were performed in the present dissertation work.

3.1 Effects of Election Concentration on the Phase Stability of $NbCr_2$-Based Laves Phases (Part II)

The Laves phases studied are composed of transition metals. This is because transition-metal Laves phases are most attractive for high-temperature structural applications due to their high melting points and strengths. Furthermore, since the electron concentration factor is important in controlling the phase stability of Laves phases, it is easier to define the e/a values, if we only use transition metals.

$NbCr_2$ is chosen as a model material system, since it is one of the most attractive candidates for mechanical property studies, and however, limited work has been done on

this system. $NbCr_2$ shows the most promise as an ultrahigh temperature (> 1000°C) structural material, since it has a high melting point of 1730°C, appreciable creep resistance, high strength, a density of 7.7 g/cm^3, excellent oxidation resistance, and a relatively large range of binary solubility, see the phase diagram in Fig. 2. The low-temperature phase (T < 1580°C) of $NbCr_2$ has a C15 structure, and the high-temperature phase (T > 1580°C) has a C14 structure. In addition, the congruent intermetallics form a eutectic structure with a chromium or niobium b.c.c. solid solution. The eutectic transformation is an *in situ* processing methodology to obtain the Laves phase/b.c.c. matrix dual-phase alloys, and compression ductility has been demonstrated in the two-phase materials [15].

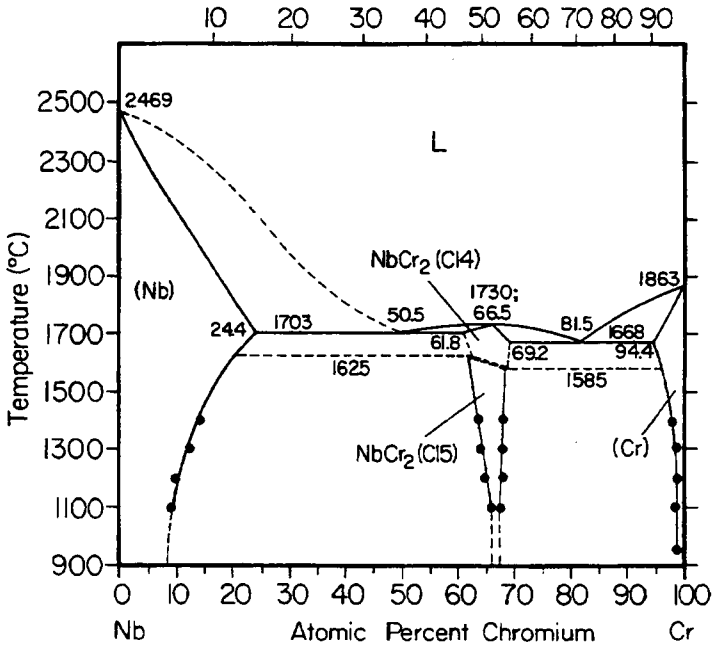


Fig. 2 The binary Nb-Cr phase diagram [14]

Since both geometric and electronic factors contribute to the stabilization of specific Laves-phase structures, it is important to separate these two factors from each other using some specific alloying schemes. The strategy has been to choose alloying elements with an

atomic size identical to either Cr or Nb. In this way, the e/a factor can be easily separated from the atomic size factor in controlling the phase stability.

Using this scheme, the homogeneity ranges reported for binary X-Cr and Nb-X, and ternary Nb-Cr-X phase diagrams are surveyed, and the corresponding average electron concentrations are calculated and correlated to the phase stability in $NbCr_2$-based transition-metal Laves-phase systems. Such information provides guidelines for the experimental study on the phase stability in Part III.

3.2 Effects of Ternary Additions on the Phase Stability of $NbCr_2$-Based Laves Phases (Part III)

In this investigation, the homogeneity ranges of C15 and C14 and critical e/a values for C14/C15 transitions in $NbCr_2$-based transition-metal Laves phases are experimentally determined for several ternary Nb-Cr-X systems (X = Fe or Co). The experimental results are compared with the surveyed data in Part II.

The phase regions between C15 and C14 and between C14 and C15 for the ternary Nb-Cr-X systems (X = Fe and Co) are studied to determine if any intermediate structure is present, by carefully controlling the alloying addition and the electron concentration e/a value.

Furthermore, the lattice parameters and unit cell volumes of the Laves phases as a function of the composition are determined. The hardness and fracture toughness of various Laves phase structures are measured to see if the deformability of the Laves phase can be improved through controlling the phase stability of the alloys, i.e., if stress-assisted phase transformation and/or mechanical twinning can be triggered in some of the alloys with specific phase stability.

3.3 Enthalpies of Formation of Laves Phases (Part IV)

This part first reviews the methods for measuring enthalpies of formation, bonding characteristics in Laves phases, and semiempirical prediction models for calculating the enthalpy of formation. The literature data on the enthalpies of formation of Laves phases are then comprehensively surveyed and listed. Some regularities are then delineated using these surveyed data.

The bond characteristics in Laves phases are inferred from the enthalpy-of-formation data. The bond in Laves phases is generally believed to be metallic in nature. However, considering the recent enthalpy of formation data [35], there may be metallic, covalent and ionic bonds, or a mixed metallic-covalent-ionic bond in Laves phases. A thermodynamic interpretation is also offered to explain the size-ratio limits for the formation of Laves phases. The enthalpies of formation calculated by the semiempirical Miedema model are compared with the available experimental data for transition-metal and Al lanthanide Laves phases.

3.4 Point Defects in Binary Laves-Phase Alloys (Part V)

So far, no systematic study has been undertaken on the point defects of any Laves phase, even though such information is very important in understanding the phase stability and the deformation behavior of the Laves alloys. Two kinds of the defects are possible for accommodating the off-stoichiometry, namely constitutional vacancies and anti-site defects. A series of alloys in binary $NbCr_2$, $NbCo_2$, and $NbFe_2$ Laves phases are prepared, including stoichiometric, Cr, Co, or Fe-rich and Nb-rich alloys, and the vacancy concentrations in these alloys are directly determined by both bulk density and X-ray lattice parameter measurements.

The change of the lattice parameter and vacancy concentration as a function of the composition gives us insight about the point defect mechanisms in the alloys. For example,

as the Nb content increases, the lattice parameter increases correspondingly, due to the fact that the atomic size of Nb is larger than that of Cr. However, the increase of the lattice parameter may slow down or it may even decrease after the alloy becomes Nb-rich, if constitutional vacancies are introduced. Also, if the vacancy concentration is near zero over the whole range of solubility, it is obvious that the anti-site type defects are the main defects.

The hardness of the various binary Laves phases are determined to understand whether solid-solution softening or hardening is operating in the Laves phases. Furthermore, fracture toughness values of these alloys are determined to understand the effect of point defects on the fracture toughness behavior of these alloys.

Some fracture toughness measurements for $NbCr_2$ alloys quenched from different temperatures are also undertaken. Vacancy concentrations after such quenching are different. Whether vacancy-assisted synchroshear mechanisms can be really operative in Laves phases is determined, using alloys of different vacancy concentrations.

The indentation technique is a unique method that can be used to quickly and economically determine the fracture toughness values of brittle materials for comparison purposes [65-67]. This method is used for determining fracture toughness values of all binary and ternary alloys in this study.

3.5 Concluding Summary and Suggested Future Work (Part VI)

A general summary of the findings in this dissertation is provided, and several promising future research areas are suggested and described.

4. IMPACT OF THIS WORK

This research is the first attempt to systematically study the phase stability and point defects in transition-metal Laves phase alloys. Phase stability criteria in transition-metal

$NbCr_2$ based Laves phases are established for the first time, which can be easily extended to other transition-metal Laves-phase systems. Moreover, the deformability of the Laves-type structures are related to their phase stability, which may pave a way to toughen the topologically close-packed Laves phases. The comprehensive survey on the enthalpy of formation of Laves phases has sheded some light on the stability and the size-factor (geometric) principle of Laves phases. The point defect study gives us some insight into the solubility limit in the Laves phases and also the deformation mechanisms of these alloys. Such effort is scientifically important and expands the knowledge base of Laves phases, and therefore, encourages wide applications of Laves-phase alloys.

Based upon the present results, alloying schemes may be developed in order to optimize the low-temperature mechanical properties of the $NbCr_2$-based Laves phases. Through the enhancement of the low-temperature mechanical properties of monolithic Laves phases by proper alloying additions, the $NbCr_2$-based dual-phase alloys with a Cr or Nb matrix can be developed with optimized low-temperature mechanical properties. This research helps to develop the scientific and technological principles for the alloy design of $NbCr_2$-based alloys that are one of the most promising candidates for ultrahigh temperature structural applications.

REFERENCES

1. J.H. Wernick, in *Intermetallic Compounds*, J. H. Westbrook, ed., Wiley, New York, (1967) 197.
2. A.K. Sinha, A. K., Progr. in Mater. Sci. 15 (Part 2) (1972) 79.
3. T.B. Massalski, in *Physical Metallurgy Part 1*, R. W. Cahn and P. Hassen, eds., North-Holland Physics Publishing, NY (1983) 190.
4. M.B. Moffett, A.E. Clark, M. Wun-Fogle, J. Lindberg, J.B. Teter, and E.A. McLaughlin, J. of Acoust. Soc. Amer. 89 (1991) 1448.
5. K. Inoue and K. Tachikawa, IEEE Trans. Magnetics 15 (1979) 635.
6. E. Olzi, F.C. Matacotta, and P. Setina, J. of Less-Common Met 139 (1988) 123.
7. D. Ivey and D. Northwood J. of Less-Common Met. 115 (1986) 23.
8. A. Halstead and R.D. Rawlings, J. Mater. Sci. 20 (1985) 1248 & 1693.
9. D.L. Anton and D.M. Shah, Mater. Res. Soc. Symp. Proc. 194 (1990) 45.
10. J.D. Livingston, Phys. Status Solidi (a) 131 (1992) 415.
11. F. Chu and D.P. Pope, in *High-Temperature Ordered Intermetallic Alloys V*, MRS Symp. Proc. 288 (1993) 561.
12. F. Chu and D.P. Pope, Mater. Sci. and Eng. A170 (1993) 39.
13. K.S. Kumar and D.B. Miracle, Intermetallics 2 (1994) 257.
14. D.J. Thoma and J.H. Perepezko, Mat. Sci. and Eng. A156 (1992) 97.
15. M. Takeyama and C.T. Liu, Mater. Sci. and Eng. A132 (1991) 61.
16. K.S. Chan and D.L. Davidson, JOM 48 (Sept. 1996) 62.
17. J.A. Cook, P.K. Liaw, and C.T. Liu, in *Fatigue and Fracture of Ordered Intermetallics*, W. O. Soboyejo, T. S. Srivatsan and R. O. Ritchie, eds., TMS, Warrendale, PA (1995) 155.
18. J.A. Cook, P.K. Liaw, C.T. Liu, and S.B. Bhaduri, in *Proc. of The Johannes Weertman Symposium*, R. J. Arsenault, D. Cole, T. Gross, G. Kostorz, P. K. Liaw, S. Parameswaran and H. Sizek, eds., TMS, Warrendale, PA (1996) 47.

19. R.L. Fleischer and R.J. Zabala, Metall. Trans. 21A (1990) 2149.

20. K.C. Chen, S.M. Allen, J.D. Livingston, Mater. Res. Soc. Symp. Proc. 288 (1993) 373.

21. K.C. Chen, S.M. Allen, and J.D. Livingston, J. Mater. Res. 12 (1997) 1472.

22. K.C. Chen, *"Compositional Influences on the Microstructures, Phase Stability and Mechanical Properties of $TiCr_2$ Laves Phase Alloys,"* Ph.D. Thesis, Massachusetts Institute of Technology (1996).

23. J.D. Livingston, J. Met. 42(2) (1990) 30.

24. Y. Komura, Acta Cryst. 15 (1962) 770.

25. F. Laves and H. Witte, Metallwirschaft 15 (1936) 840.

26. F. Laves and H. Witte, Metallwirschaft 14 (1935) 645.

27. T.B. Massalski, J.L. Murray, L.H. Bennett, and H. Baker, Binary Alloy Phase Diagram, American Society for Metals, Metals Park, OH (1986).

28. D.I. Bardos, K.P. Gupta, and P.A. Beck, Trans. Met. Soc. AIME 221 (1961) 1087.

29. R.E. Watson and L.H. Bennett, Scripta Metall. 12 (1978) 1165.

30. R.E. Watson and L.H. Bennett, Acta Metall. 32 (1984) 477.

31. R.E. Watson and L.H. Bennett, Acta Metall. 32 (1984) 491.

32. R.C. King and O.J. Kleppa, Acta Metall. 12 (1964) 87.

33. P.M. Robinson and M.B. Bever, in *Intermetallic Compounds*, J. H. Westbrook, ed., John Wiley & Sons, Inc. (1967) 38.

34. J.H. Wernick, S.E. Haszko, and D. Dorsi, J. Phys. Chem. Solids 23 (1962) 567.

35. M. Ellner and B. Predel, in *Intermetallic Compounds: Vol. 1, Principles*, J. H. Westbrook and R. L. Fleischer, eds., John Wiley & Sons Ltd. (1994) 91.

36. A. Pebler and E.A. Gulbransen, Electrochem. Technol. 4 (5-6) (1966) 211.

37. D. Shaltiel, I. Jacob, and D. Davidov, J. of Less-Common Met. 53 (1977) 117.

38. J.D. Livingston and E.L. Hall, J. of Mater. Res. 5 (1990) 5.

39. Y. Liu, J.D. Livingston, and S.M. Allen, Metall. Tran. A23 (1992) 3303.

40. M. Grujicic, S. Tangrila, O.B. Cavin, W.D. Porter, and C.R. Hubbard, Mater. Sci. and Eng. A160 (1993) 37.

41. P.M. Hazzledine, in *Twinning in Advanced Materials*, M. H. Yoo and M. Wuttig, eds., TMS, Warrendale, PA (1994) 403.

42. D.P. Pope and F. Chu, Phil. Mag. A69 (1994) 409.

43. D.J. Thoma and J.H. Perepezko, J. of Alloys and Compounds 224 (1995) 330.

44. Y.A. Chang and J.P. Neumann, (1982), Prog. Solid State Chem. 14 (1982) 221.

45. L.M. Pike, Y.A. Chang, and C.T. Liu, Acta Mater. 45 (1997) 3709.

46. J. Westbrook, J. Electrochem. Soc. 54 (1956) 103.

47. P. Nagpal and I. Baker, Metall. Trans. 21A (1990) 2281.

48. Y.A. Chang, L.M. Pike, C.T. Liu, A.R. Bibrey, and D.S. Stone, Intermetallics 1 (1993) 107.

49. D.B. Miracle, Acta Metall. 41 (1993) 649.

50. G.E.R. Schultze, in *Reinststoffe in Wissenschaft und Technik*, Akademie-Verlag, Berlin (1972) 641.

51. J.C. Foley, D.J. Thoma, and J.H. Perepezko, Metall. Trans. 25A (1994) 230.

52. P.M. Hazzledine and P. Pirouz, Scripta Metall. et Mater. 28 (1993) 1277.

53. D.G. Ivey and D.O. Northwood, Z. Phys. Chem. N. F. 147 (1986) 191.

54. G. Sicking, E. Magomedbekov and R. Hempelmann, Ber. Bunsenges. Phys. Chem. 85 (1981) 686.

55. C.W. Allen, P. Delavignette, and S. Amelincks, Phys. Stat. Sol. (a) 9 (1972) 237.

56. J.D. Livingston, E.L. Hall, and E.F. Koch, MRS Symp. Proc. 133 (1989) 243.

57. Y. Liu, *"Microstructures, Deformation and Phase Transformation of Laves Alloys,"* Ph.D. Thesis, Massachusetts Institute of Technology (1993).

58. J.D. Livingston, MRS Symp. Proc. 322 (1994) 395.

59. J.B. Moran, Trans. Met. Soc. AIME 233 (1965) 1473.

60. H. Kubsch, P. Paufler, and G.E.R. Schulze, Phys. Stat. Sol. (b) 56 (1973) 231.

61. H. Kubsch, P. Paufler, and G. E. R. Schulze, Phys. Stat. Sol. (a) 25 (1974) 269.

62. P. Paufler and G.E.R. Schulze, Naturwissenschaften 54 (1967) 69.

63. H.C. Jain, L. Freise, and M. Forker, J. Phys.: Condens. Matter 1 (1989) 2157.

64. K.S. Kumar and C.T. Liu, Acta Materialia 45 (1997) 3671.

65. A.G. Evans and E.A. Charles, J. of Amer. Ceram. Soc. 59 (7-8) (1976) 371.

66. M. Sakai and R.C. Bradt, Inter. Mat. Rev. 38 (2) (1993) 53.

67. G.R. Anstis, P. Chantikul, B.R. Lawn, and D.B. Marshall, J. of Amer. Ceram. Soc. 64 (9) (1981) 533.

PART II: EFFECTS OF ELECTRON CONCENTRATION ON THE PHASE STABILITY OF $NbCr_2$-BASED LAVES PHASES

1. INTRODUCTION

Laves phases are size compounds, and the abundance of Laves structures among intermetallic compounds has been attributed to geometric principles for the arrangement of atoms on ordered lattice sites [1]. Laves phases are predominantly metallic in the bonding nature and largely governed by geometric space-filling principles. The metallic Goldschmidt radius, R, of the atoms forming the compound was used to evaluate atomic size factors involved in the formation of the Laves phases for a long time [1]. The metallic atomic size for a coordination number (CN) of 12, as reported by Teatum, Gschneidner, and Waber [2], however, is now generally used for geometric analyses of many studies on the phase stability and occurrence of Laves phases. It has been found that Laves phases occur between the metallic radius ratios of 1.05-1.68 [3-5]. The atoms forming the compound need to adjust in size to accommodate the ideal space-filling ratio (R_A/R_B = 1.225, where R is the atomic size in the Laves phase) in the ordered Laves-phase lattice. As a result, the occurrence of the Laves phases is generally related to the ability of the A and B atoms to expand or contract so that the ideal ratio is approached. Thoma and Perepezko [6] have successfully used the geometric arguments to analyze the solubility limits of Laves phases.

Although the geometric consideration provides insight into appropriate alloying additions, the inter-atomic bonding and the polytypic stability are more specifically related to the electronic structures. The stability of each individual Laves-phase polytype is a function of electron concentration.

1.1 Phenomenological Study of Phase Stability in Laves Phases

Laves and Witte [7, 8] studied the phase stability of Mg-based Laves-phase systems. A valence electron concentration rule was found to control the occurrence of

various Laves structures, with C15 stabilized at low e/a values, C14 stabilized at high e/a values, and C36 in between, see Fig. 1 [7-9]. The correlation between the valence electron concentration and phase stability is reasonably good; however, both non-transition and transition metals are involved in forming some Laves phases in their study. This fact makes it difficult to analyze the valence electron concentration factor in the alloys, since for a transition element, the valence electron number is not a constant value, varying in different alloy systems. This may contribute to the scattering in the critical e/a values corresponding to the phase transitions for different ternary systems, as shown in Fig. 1 (i.e., there is overlapping of the C14 and C36 structures for the e/a values between 1.8 and 2.0).

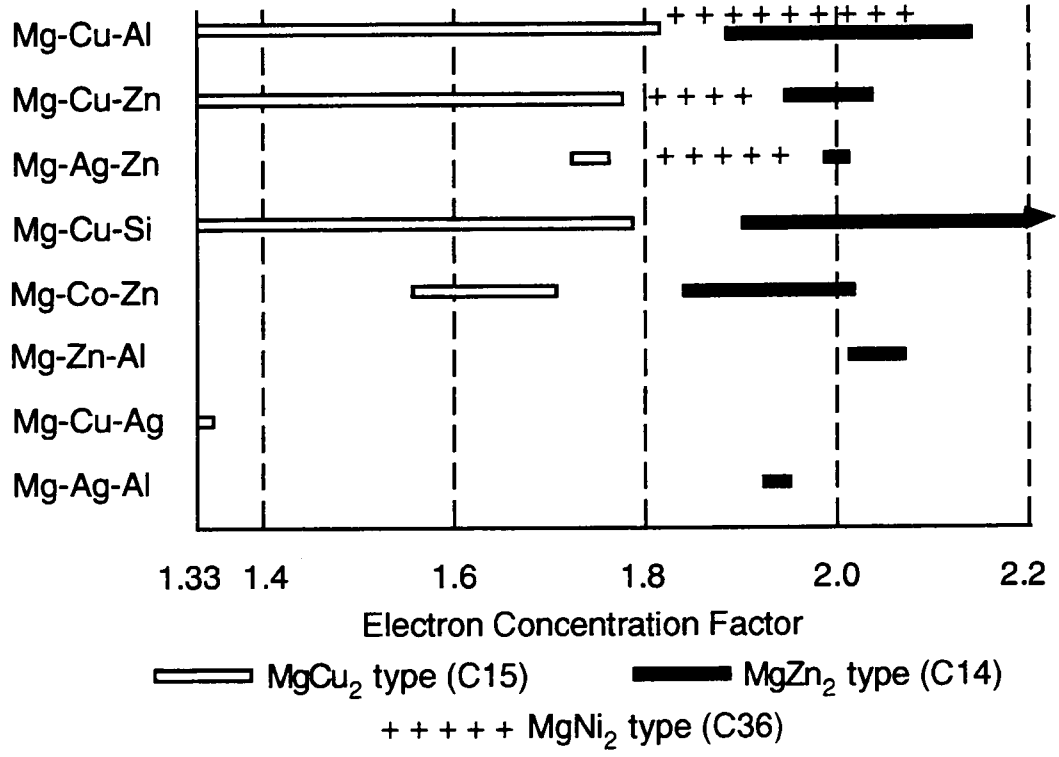


Fig. 1 Effect of valence electron concentration on phase stability for several ternary Mg-based alloys (after Massalski [9])

Komura and his coworkers [10-14] have shown that additional Laves-type structures exist in at least some of these quasi-binary Mg-based systems. The hexagonality of the stacking arrangement decreases, and then, increases with increasing valence electron concentration, i.e., the variation of percent hexagonality followed the sequence of 50 → 33 → 0 → 50 → 57 → 60 → 62 → 66 → 71 → 75 → 100. The intermediate structures corresponding to different percentages of hexagonality were also characterized, which were multi-layer-type superstructures.

Wallace and Craig [15] extended the above treatment of electron concentration to Laves phases formed by transition elements. These variable valency elements cause difficulty in determining electron concentration. However, they applied various criteria and arrived at a valency scheme, which, used in conjunction with low-temperature specific-heat measurements, indicated that the stability limit of each type of Laves phases is related to the fill-up of the respective Brillouin zone. Elliot and Rostoker [16] also successfully used a valency scheme to correlate the phase stability with electron concentration.

Watson and Bennett [17-19] used the d-band hole number, instead of valence electron concentration, as a parameter for characterizing the phase stability in binary Laves phases. A good correlation was found, and a C15 → C14 → C15 transition with increasing the d-band hole number was observed. This method overcomes the variance of valence electron numbers for transition elements. However, this approach was not extended to ternary or quaternary systems.

For a few transition-metal Laves phases, the average electron concentration factor, e/a, which is defined as the average number of electrons per atom outside the closed shells of the component atom, was also successfully used for the correlation purpose by Bardos,

Gupta and Beck [20] and Savin [21]. Such a scheme is the simplest one, and yet, a good correlation was obtained.

The effect of average electron concentration on phase stability has also been examined in some transition-metal A_3B intermetallic compound systems, usually with a very good correlation obtained [22-24]. For example, Liu [23] found that the stacking character of the $(Fe,Co,Ni)_3V$ ordered alloys can be altered systematically by controlling the e/a ratio of the alloys, see Fig. 2. Here, the basic A_3B one-layer structure is the (111) close-packed plane, which is different from the case for Laves phases where a quadruple layer forms a close-packed plane. Different ordered structures can be obtained depending on their stacking sequence. As e/a increases, the stacking character changes from a purely cubic, through a mixture of cubic and hexagonal layers, to purely hexagonal structure. The critical e/a ratio for stabilizing the f.c.c. structure is ≤ 7.89, and for stabilizing the h.c.p. structure ≥ 8.54 in A_3B compounds. Also, similar to the Mg-based Laves-phase alloys, different ordered mixtures of cubic and hexagonal layers were obtained between the cubic and hexagonal structures for the A_3B ordered alloys, i.e., Co_3V, with e/a = 8, exhibits 33.3 percent hexagonality, and $(Co,Ni)_3V$, with e/a = 8.43, shows 66.7 percent hexagonality (Fig. 2).

All these results indicate that the electron concentration factor has a determinate effect on the phase stability of transition-metal intermetallic compounds. The physical origin of such correlation is not clear now. However, the nature of the atomic bonding depends exclusively on the band structure, which provides a clue to understand the underlying reason for the characteristic atomic arrangement of a particular crystalline structure. The phase transition in transition metals is known to be related to the filling of an appropriate Brillouin zone [22, 23], and can be predicted from the ground-state phase stability map [25, 26].

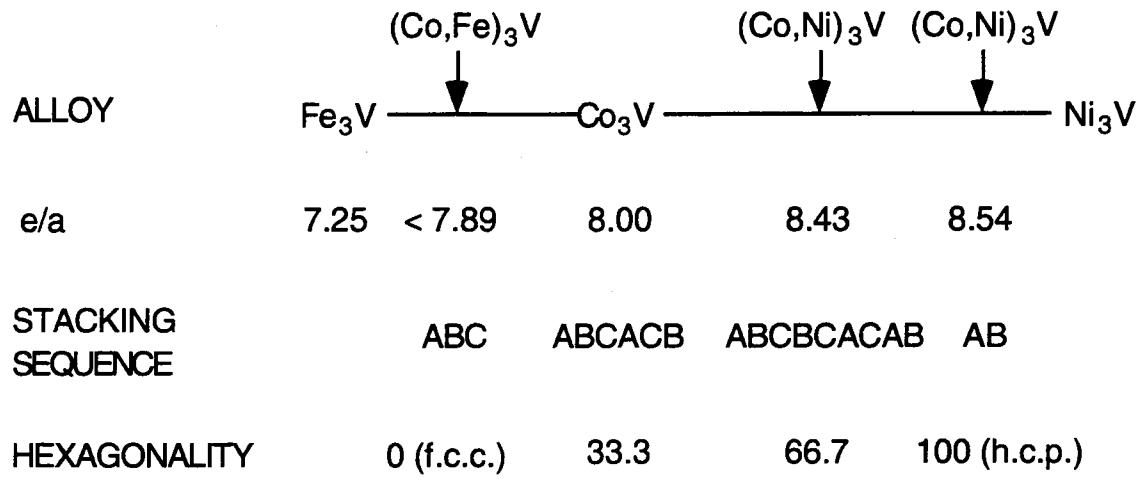


Fig. 2 Effect of average electron concentration factor (e/a) on ordered structures in pseudo-binary Ni_3V-Co_3V and Co_3V-Fe_3V systems (after Liu [23])

1.2 Theoretical Prediction of Phase Stability of Laves Phases

The theoretical development to analyze the ground-state phase stability can be ascribed mainly to two approaches. The first one is to extract common parameters, such as band width, electron concentration, atomic interaction energies, etc., that are inherent to the cohesion of a crystalline lattice and to specify the region where a particular phase appears in the multi-dimensional space spanned by those parameters. The development of various structural maps is a typical example of this approach. The ground-state stacking stability map also falls into this category. The advantage of such an approach is that one may grasp general trends of the phase stability over a wide range of systems. Furthermore, effective parameterization with a small number of variables enables the appearance of a particular phase to be focused on from the viewpoint of the underlying physics. The second approach to ground-state stability is to investigate the detailed band structures of a given phase by performing first-principles electronic structure calculations. Since the cohesive

properties depend exclusively on the electronic structure, this approach provides a more direct clue to the stabilization mechanisms.

To quantify the importance of the electronic structure, Johannes et al. [27] conducted a successful first-principles calculation of the correlation between the crystal structure and the d-electron to atom ratio in the transition-metal Laves alloys. The d-band binding is the main determinant of the structure, and the common-band model is well obeyed. Ohta and Pettifor [28] used a simple bond-order, tight-binding analysis to study the relative phase stability of C15, C14, C36 and C11b structures in some AB_2 compounds. Their research indicates that electron densities and band fitting are also important in determining the relative stability of these compounds. The detailed alloying behavior is not well predicted, but some trends can be captured by the simple methods.

The stability of $NbCr_2$ and HfV_2 has recently been examined using a linear-muffin-tin-orbital method with an atomic sphere approach (LMTO-ASA) [29, 30]. The current equilibrium phase diagrams of these two systems indicate that only the C15 phase is stable at room temperature. However, the calculations indicate that the C14 phase is more stable than C15 at -273 °C for HfV_2, whereas the C15 phase is the stable $NbCr_2$ phase at -273 °C. The effect of alloying additions on the phase stability has not been studied yet.

The approach taken by Pei and Massalski [26] to investigate the phase stability of topologically close-packed structures is quite unique. A simple one-dimensional stacking model involving only a few inter-planar interactions was explored, and the ground-state phase stability maps obtained can be used to explain the seemingly complex stacking sequence changes observed in topologically close-packed phases including A_3B and Laves phases. By considering only up to fourth-adjacent-layer interactions, the ground-state phases were determined using the effective potential method [26].

1.3 Motivation of This Study

Transition-metal Laves phases are currently being considered for many practical applications, e.g., $(Hf,Zr)V_2$ as a superconducting material, $Zr(Cr,Fe)_2$ as a hydrogen storage material, etc. More recently, HfV_2-, $HfCr_2$- and $NbCr_2$-based two-phase alloys [7-13] are being developed for high-temperature structural uses, because of their retention of good mechanical properties at elevated temperatures. However, their low ductility and brittle fracture characteristics at ambient temperatures are the main concerns for structural applications of these materials.

One attractive way to improve the deformability of complex Laves phases is to control their crystalline structure in a way that stress-assisted phase transformation and/or mechanical twinning can be introduced during plastic deformation [14, 15]. It is, thus, important to understand the factors governing the phase stability in transition-metal Laves alloys.

In this investigation, a number of binary and ternary phase diagrams were surveyed, and the phase stability criteria in the $NbCr_2$-based Laves phase systems, binary X-Cr and Nb-X and ternary Nb-Cr-X, were studied. The electron concentration factor (e/a) was identified as the key parameter in controlling the C14/C15 phase stability in $NbCr_2$-based transition-metal Laves alloys.

2. LAVES PHASES IN BINARY X-Cr AND Nb-X SYSTEMS

Since Laves phases are size compounds, we should choose the X elements in the X-Cr systems with an atomic radius close to Nb, and X elements in the Nb-X systems with an atomic radius close to Cr. In this scheme, we can easily separate the e/a factor from the atomic size factor in controlling the phase stability. According to this scheme, the X

elements selected in the X-Cr systems are Ti, Ta, and Nb, and the X selected in the Nb-X systems are Cr, Mn, Fe, Co, Ni, and Cu. The selection of atom size is based on the consideration of the atomic radius with CN 12 [2]. With a minimum disturbance of the atomic size factor, the electron concentration ratio, e/a, should become a dominant factor in controlling the phase stability of the binary Laves phases. The e/a ratio is defined as the average number of electrons per atom outside the closed shells of the component atoms. According to this definition, the e/a ratio of a transition element is the number of electrons (s + d electrons) outside its inert gas shell.

Table I. Atomic Size, Electron Concentration Factor (e/a) of Alloying Element, and Existing Binary Laves Phase

Element	Atomic Radius (Å)	e/a	XCr_2/NbX_2
Nb	1.468	5	$NbCr_2$
Ti	1.462	4	$TiCr_2$
Ta	1.467	5	$TaCr_2$
Cr	1.282	6	$NbCr_2$
Mn	1.304	7	$NbMn_2$
Fe	1.274	8	$NbFe_2$
Co	1.252	9	$NbCo_2$
Ni	1.246	10	None
Cu	1.278	11	None

Table I lists the atomic radii (CN = 12), and the e/a ratios of all the alloy components, together with the existing Laves phases observed in the binary X-Cr and Nb-X systems. It is interesting to note that Ti and Ta have atomic radii close to Nb, and thus, they are postulated to substitute for Nb in the $NbCr_2$ Laves phase. Mn, Fe, Co, Ni and Cu have atom sizes close to Cr and occupy the Cr positions in the $NbCr_2$ Laves phase. From the binary X-Cr and Nb-X phase diagrams [40], we can determine if the XCr_2 or NbX_2

Laves phase exists in the X-Cr and Nb-X systems, as indicated in Table I. Also, the homogeneity ranges of XCr_2 or NbX_2 Laves phases can be determined from the binary phase diagrams. The homogeneity range (or mutual solubility) is defined as the difference between the maximum and minimum atomic percents of A in the AB_2 phase. Corresponding to the homogeneity ranges, we can calculate the e/a ranges for the different binary Laves phases using the e/a ratios for various transition elements listed in Table I according to the following equation:

$$(e/a)_{Laves-phase} = \sum_i [(e/a)_i \times f_i] \qquad (1)$$

where $i = i_{th}$ alloying element, and f_i is the atomic fraction of the corresponding component in the Laves phase.

The binary Laves phase, R_A/R_B ratio, homogeneity range (%A range), e/a range, and corresponding Laves phase structure are listed in Table II. Since temperature is also a factor affecting the phase stability of Laves phases, polytypes may exist at different temperatures in some binary systems. To minimize or eliminate the temperature effect, the Laves structure investigated in the present study is the one stabilized at lower temperatures, if more than one Laves structure exists in the binary system. Also note that no Laves phases were observed in the binary Nb-Ni and Nb-Cu systems, and that the calculation of the e/a ratio was based on the imaginary "$NbNi_2$" and "$NbCu_2$" phases.

In Table II, the R_A/R_B ratios were maintained at approximately the same value for all of the Laves phases. The C15 structure was stabilized at low values of e/a (≤ 5.70) in Table II. A change of the structure from C15 to C14 occurred when e/a ≥ 6.20. Interestingly, C15 was stabilized again, when e/a was equal to or greater than 7.67. As the e/a value further increases (≥ 8.34), no ordered Laves phases exist in the binary system.

Table II. Atomic Size Ratio (R_A/R_B), Homogeneity Range (%A Range), Corresponding e/a Range and Laves Phase Structure in Binary XCr_2 and NbX_2 Alloy Systems

Laves Phase	R_A/R_B	%A Range	e/a Range	Structure
$TiCr_2$	1.140	35-37	5.26-5.30	C15
$TaCr_2$	1.144	33-36	5.64-5.67	C15
$NbCr_2$	1.145	30-39	5.61-5.70	C15
$NbMn_2$	1.161	25.5-40	6.20-6.49	C14
$NbFe_2$	1.152	27-38	6.86-7.19	C14
$NbCo_2$	1.173	27-33.3	7.67-7.92	C15
"$NbNi_2$"	1.178	33.3	8.34	None
"$NbCu_2$"	1.149	33.3	9.00	None

3. LAVES PHASES IN TERNARY Nb-Cr-X SYSTEMS

As postulated in the previous section, Ti and Ta occupy the Nb lattice sites in the $NbCr_2$ Laves phase. From the ternary Nb-Cr-Ta and Nb-Cr-Ti phase diagrams [41], Ti or Ta can substitute for Nb from 0% to 100% without changing the C15 structure of $NbCr_2$. This behavior further confirms our above postulation that Ti and Ta will mainly substitute for Nb in the $NbCr_2$ Laves phase, as the atomic radii of Ta, Ti and Nb are essentially the same. For Mn, Fe, Co, Ni, and Cu, they are postulated to substitute for Cr in the $NbCr_2$ phase. There is no ternary Nb-Cr-Mn phase diagram reported so far, and the ternary Nb-Cr-Cu phase diagrams are incomplete, with the reported data mainly concentrated at the copper-rich corner. On the other hand, the Nb-Cr-Co, Nb-Cr-Fe and Nb-Cr-Ni phase diagrams have been reported in the literature [41, 42]. From these phase diagrams, common trends were observed: Fe, Co and Ni have some solubility in the $NbCr_2$ phase without changing the C15 structure. However, above a certain critical amount of Fe, Co or

Ni added to the stoichiometric $NbCr_2$ to substitute for Cr, a phase modification from C15 to C14 was observed (Table 3). The C14 phase is stable over a wide range of Fe, Co or Ni content. For the Nb-Cr-Co system, a further increase in the Co content results in the reappearance of the C15 structure [42], as shown in Table III.

Table III. Homogeneity Range (%X) and Corresponding e/a Range of C15/C14 Structures in Ternary Nb-Cr-X Systems

	C15		C14		C15	
X	%X	e/a	%X	e/a	%X	e/a
Ti	0-33.3	5.33-5.67	--	--	--	--
Ta	0-33.3	5.67	--	--	--	--
Fe	0-4	5.67-5.75	9-66.7	5.85-6.69	--	--
Co	0-3	5.67-5.76	8-62	5.91-7.53	66-68	7.65-7.72
Ni	0-2.5	5.67-5.77	5-52	5.87-8.05	--	--

The stability ranges of C14 and C15 phases in the ternary Nb-Cr-X systems at around 1000°C are summarized in Table III, together with the corresponding e/a values that were calculated using Equation 1. This temperature range was chosen due to the lack of pertinent ternary phase diagrams at lower temperatures. From Table III, it should be noted that the solubility of Fe, Co, and Ni in $NbCr_2$ with the C15 structure decreases in the order of Fe, Co, and Ni. However, the e/a ratios corresponding to the change of the C15 to C14 structure are almost identical (i.e., 5.75, 5.76, and 5.77) for the different systems of Nb-Cr-Fe, Nb-Cr-Co and Nb-Cr-Ni, respectively. This trend implies that the average electron concentration may play a key role in determining the C15/C14 phase stability. The average maximum e/a for the C15 structure is 5.76, and the average minimum e/a ratio to stabilize the C14 structure is about 5.88. A transition from C14 to C15 was observed in the Nb-Cr-Co system, when $e/a \geq 7.65$. Note that the transition from C14 to C15 was also found in the binary Laves phases, as shown in Table II.

4. EFFECT OF e/a ON LAVES-PHASE STABILITY

Laves phases are compounds of the general formula AB_2, with three crystal types, C15, C36, and C14, typically observed. There is a marked similarity among the three structures. These crystalline structures consist of double layers of hexagonal arrays of A atoms surrounded by tetrahedra of the B elements. One stacking layer consists of 4 sub-layers, and thus, they are called quadruple layers. The cubic C15 structure consists of such layers stacked ABCABC, while the C14 consists of such layers stacked ABABABAB. C36 may be regarded as a transitional phase between the C15 and C14 structures with a stacking of these layers ABACABAC. As noted previously, Laves phases are size compounds, and therefore, the size difference between A and B atoms is predominant in stabilizing the Laves phase. Since we purposely chose some alloying elements with roughly the same atomic sizes with either Cr or Nb (see Tables I and II), the atomic size difference between A and B is similar in the AB_2 Laves phases investigated. This approach simplifies our analysis, since we can separate the other factors from the size factor in stabilizing different Laves phase structures. Also, we only chose transition metals to form Laves phases, which made it ideal to study the e/a effect on the Laves-phase stability. In transition metals, filling the d-band is important for the phase stability.

In Laves and Witte's studies [7, 8], ternary Mg-based systems were selected. The valence electron concentration rule was found to control the occurrence of various Laves structures, with C15 stabilized at low e/a values, C14 stabilized at high e/a values, and C36 in between. The correlation is reasonably good; however, both non-transition and transition metals were involved in forming some Laves phases in their study, thus making it difficult to analyze the valence electron concentrations in the alloys. This difficulty results from the fact that for a transition element, the valence electron number is not a constant

value, but varies in different systems. This behavior may contribute to the scattering in the critical e/a values corresponding to the phase transitions for the different ternary systems.

In the present evaluation, all the elements chosen to form Laves phases were transition metals. Instead of using the valence electron concentration, the average electron concentration was chosen for correlation purposes. This concept of average electron concentration has been successfully used to obtain a correlation between the e/a value and the phase stability in some transition metal alloy systems [18, 20-22, 24, 43]. If the data in Tables II and III for both binary and ternary alloy systems are combined, we can clearly demonstrate the e/a effect on the phase stability (C14/C15) in $NbCr_2$-based Laves alloys (see Fig. 3).

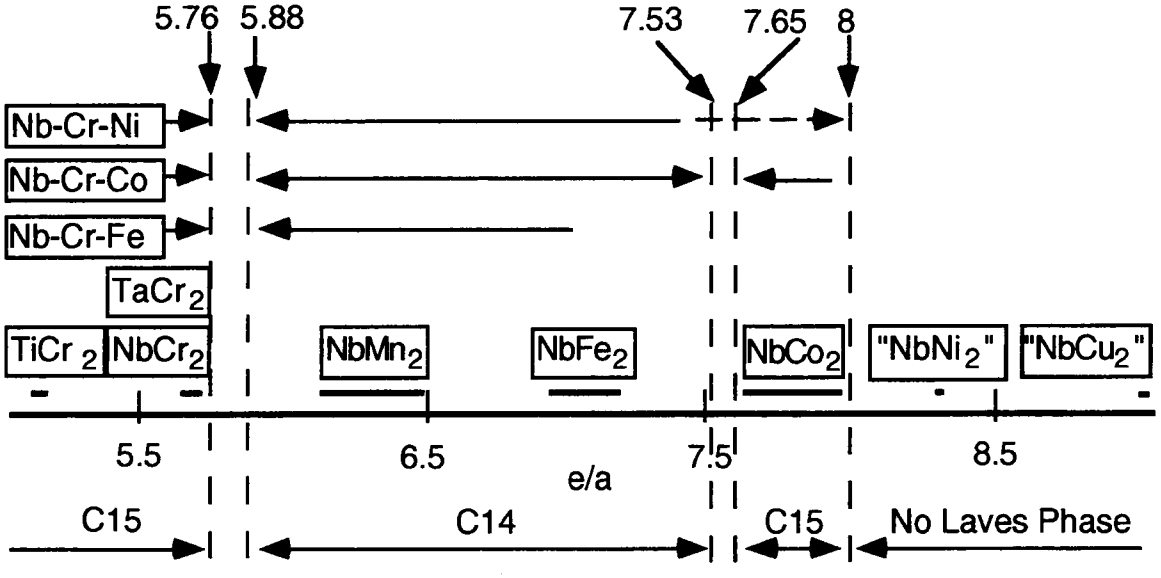


Fig. 3 Effect of average electron concentration (e/a) on phase stability in binary and ternary $NbCr_2$-based systems

At e/a values lower than 5.76, the C15 structure was stabilized for both binary and ternary Laves alloys (Fig. 3). By increasing e/a to 5.88, the C14 structure was stabilized. Over the e/a range of 5.88-7.53, the C14 structure is more stable than the C15 structure.

This trend is similar to that observed in the Mg-based Laves phases [7, 8], where the C15→C36→C14 phase modification was observed with an increasing e/a value.

In ternary $NbCr_2$-based Laves phases, the e/a ratio for the C15/C14 phase boundaries is very precise, with C15 existing at e/a ≤ 5.76, and C14 occurring at e/a ≥ 5.88 (Fig. 3). This may be associated with the fact, as mentioned previously, that all the components of the ternary $NbCr_2$-based Laves phases are transition metals. The region between the two single-phase regions should be a two-phase mixture of C14 and C15 from thermodynamic considerations. However, in reality, it is possible to obtain different intermediate structures, due to the metastable transformation of the one to the other and/or the low chemical free energies of some intermediate structures. For example, the C36 phase exists in some Mg-based Laves alloys. Moreover, Komura and his coworkers have shown that additional Laves-type structures exist in at least some of these quasi-binary Mg-based systems [10-14]. The hexagonality of the stacking arrangement decreases, and then increases with increasing valence electron concentration.

However, no existence of C36 and other intermediate structures was indicated in the reported phase diagrams of binary and ternary $NbCr_2$-based systems between the C14 and C15 phase fields. This is probably due to the fact that no detailed work on crystal structures was undertaken to determine the various intermediate structures in this region. Thus, it is postulated that at least in some of the $NbCr_2$-based Laves-phase systems, C36 and other intermediate structures may exist in the e/a regime of 5.76-5.88, probably around 5.7-5.9 due to the variability in the literature data. In fact, a C36 phase was detected in a recent study of the Nb-Cr-Fe system [39]. Even though it is difficult to calculate the exact e/a value for the C36 Laves phase, since that system is basically a dual-phase alloy with a Nb solid solution and a Laves phase, it does indicate that it is possible to stabilize at least the C36 structure at certain e/a ratios.

Over the e/a range considered, the atomic size difference has no effect on the e/a correlation with the phase stability in both binary and ternary $NbCr_2$-based systems. Actually, the solubility of Fe, Co and Ni in $NbCr_2$ has different values, yet the same critical e/a value is yielded, with respect to the change of the crystal structure from C15 to C14 (Fig. 3). This may result from the fact that the atomic size difference (R_A/R_B) is kept similar in our investigation. Recently, a geometry analysis of solubility ranges in Laves phases was performed by Thoma and Perepezko [6].

The effect of the average electron concentration on phase stability has been shown in some transition-metal A_3B intermetallic compound systems, usually with a very good correlation obtained [22-24]. For example, Liu found that the stacking character of the (Fe, Co, Ni)$_3$V ordered alloys can be altered systematically by controlling the e/a ratio of the alloys [23]. The basic A_3B one-layer structure is the (111) close-packed plane, which is different from the case for Laves phases, where a quadruple layer forms a close packed plane. Different ordered structures can be obtained depending on their stacking sequence. Similar to our observation in Laves phases, as e/a increases, the stacking character changes from a purely cubic structure, through a mixture of cubic and hexagonal structures, to purely hexagonal structure. Also, similar to Mg-based Laves phase alloys, different ordered mixtures of cubic and hexagonal layers were obtained between the cubic and hexagonal structures for the A_3B ordered alloys. All the results indicate that the average electron concentration factor has a determinate effect on the phase stability of transition-metal intermetallic compounds. The reason leading to such a correlation is not clear now; however, the phase transition in transition metals is known to be related to the filling of an appropriate Brillouin zone [22-24] and can be predicted from the ground-state phase stability map [26].

From Fig. 3 and Table III, it can also be seen that for the Nb-Cr-Co system, when

the e/a ratio increases further to 7.65, the C15 structure was stabilized again over the C14 structure. Similarly in the binary systems, there is a C14→C15 transition when e/a > 7.65 (Fig. 3 and Table II). This structure modification from C14 to C15 with a further increase in the e/a ratio has been observed in a number of transition-metal Laves phases [44]. It is a general trend, rather than an exception. In the ternary Nb-Cr-Fe system, such a C14 to C15 transition cannot be observed, since we are unable to obtain an e/a ratio higher than 7.6 in this system (Fig. 3 and Table III). No $NbNi_2$ (with e/a = 8.34) and $NbCu_2$ (with e/a = 9) Laves phases exist in binary Nb-Ni and Nb-Cu systems (Table II), a fact consistent with the observation by Bardos et al. [20] that at e/a > 8, a disordered structure is stabilized over the Laves phase in transition-metal systems. Also in agreement with Bardos et al., the maximum e/a ratio for the Laves phases in the Nb-Cr-Ni system is around 8. However, no C14 → C15 transition in the Nb-Cr-Ni system was reported at e/a ratios > 7.65, possibly due to the fact that many ternary phase diagrams containing Laves phases are inaccurate with regard to the identification of C14/C36/C15 structures. Note that as discussed before, it is postulated that C36 and other intermediate structures may exist between C14 and C15 structures at 7.65 > e/a > 7.53.

5. CONCLUSIONS

Binary X-Cr and Nb-X, and ternary Nb-Cr-X phase diagrams were surveyed, and some interesting phase stability features were identified in these transition-metal systems. The average electron concentration factor (e/a) has been shown to be a dominant factor in controlling the phase stability of $NbCr_2$-based transition-metal Laves alloys. With e/a ≤ 5.76, the C15 structure is stabilized; at an e/a range of 5.88-7.53, the C14 structure is stabilized; with e/a ≥ 7.65, the C15 structure is stabilized again. A further increase in electron concentration (e/a > 8) leads to the disordering of the alloy. It is postulated that at

5.88 > e/a > 5.76 and 7.65 > e/a > 7.53, the C36 and other intermediate structures may be stabilized. Such an e/a correlation is found to be analogous to that in A_3B transition-metal intermetallic compounds and Mg-based Laves phases, and the physical ground leading to such a correlation should be further studied.

REFERENCES

1. F. Laves, in *Theory of Alloy Phases*, American Society for Metals, Metals Park, OH (1956) 124.
2. E. Teatum, K. Gschneidner, and J. Waber, LA-2345, U.S. Department of Commence, Washington, D.C. (1960); also see: W.B. Pearson, *The Crystal Chemistry and Physics of Metals and Alloys*, Wiley, New York, NY (1972) 151.
3. A.E. Dwight, Trans. Amer. Soc. Met. 53 (1961) 479.
4. M.V. Nevitt, in *Electronic Structure and Alloy Chemistry of the Transition Elements*, P.A. Beck, ed., Interscience Publishers, New York (1963) 101.
5. W.B. Pearson, Acta Cryst. B24 (1968) 7.
6. D.J. Thoma and J.H. Perepezko, J. of Alloys and Compounds 224 (1995) 330.
7. F. Laves and H. Witte, Metallwirschaft 14 (1935) 645.
8. F. Laves and H. Witte, Metallwirschaft 15 (1936) 840.
9. T.B. Massalski, in *Physical Metallurgy Part 1*, R. W. Cahn & P. Hassen, eds., North-Holland Physics Publishing, NY (1983) 190.
10. Y. Komura, Acta Cryst. 15 (1962) 770.
11. Y. Komura, E. Kotera, and M. Mitarai, Acta Cryst. A25 (1969) S96.
12. Y. Komura, M. Mitarai, I. Nakatani, H. Iba, and T. Shimizu, Acta Cryst. B26 (1970) 666.
13. Y. Komura, A. Nakaue, and M. Mitarai, Acta Cryst. B28 (1972) 727.
14. Y. Komura and Y. Kitano, Acta Cryst. B33 (1977) 2496.
15. W.E. Wallace and R.S. Craig, in *Phase Stability in Metals and Alloys,* P. S. Rudman, J. Stringer and R. I. Jaffee, eds., McGraw-Hill, Inc. (1967) 225.
16. R.P. Elliott and W. Rostoker, Trans. Am. Soc. Met. 50 (1958) 617.
17. R.E. Watson and L.H. Bennett, Scripta Metall. 12 (1978) 1165.
18. R.E. Watson and L.H. Bennett, Acta Metall. 32 (1984) 477.

19. R.E. Watson and L.H. Bennett, Acta Metall. 32 (1984) 491.

20. D.I. Bardos, K.P. Gupta, and P.A. Beck, Trans. Met. Soc. AIME 221 (1961) 1087.

21. V.V. Savin, Phys. Met. Metall. 68 (1989) 140.

22. A.K. Sinha, (1972), Progr. in Mater. Sci. 15 (Part 2) (1972) 79.

23. C.T. Liu, Inter. Met. Rev. 29 (1984) 168.

24. A.K. Sinha, (1969), Tran. Met. Soc. AIME 245 (1969) 911.

25. S. Pei, *"Stacking Sequence in Topologically Close Packed Structures"*, Ph.D. Thesis, Carnegie Mellon University (1988).

26. S. Pei and T.B. Massalski, Acta Metall. Mater. 43 (1995) 2385.

27. R.L. Johannes, R. Haydock, and V. Heine, Phys. Rev. Letters 36(7) (1976) 372.

28. Y. Ohta and D.G. Pettifor, J. Phys.: Condens. Matter. 2 (1990) 8189.

29. F. Chu, M. Sob, R. Siegl, T.E. Mitchell, D.P. Pope, and S.P. Chen, Phil. Mag. B70 (1994) 881.

30. F. Chu, D.J. Thoma, Y. He, T.E. Mitchell, S.P. Chen, and J.H. Perepezko, Mat. Res. Soc. Symp. Proc. 364 (1995) 1089.

31. F. Chu and D.P. Pope, in *High-Temperature Ordered Intermetallic Alloys V*, MRS. Symp. Proc. 288 (1993) 561.

32. K.S. Kumar and D.B. Miracle, Intermetallics 2 (1994) 257.

33. M. Takeyama and C.T. Liu, Mater. Sci. & Eng. A132 (1991) 61.

34. J.A. Cook, P.K. Liaw, and C.T. Liu, in *Fatigue and Fracture of Ordered Intermetallics*, W. O. Soboyejo, T. S. Srivatsan & R. O. Ritchie, eds., TMS, Warrendale, PA (1995) 155.

35. J.A. Cook, P.K. Liaw, C.T. Liu, and S.B. Bhaduri: in *The Johannes Weertman Symposium*, R. J. Arsenault et al., eds., TMS, Warrendale, PA (1996) 47.

36. K.S. Chan and D.L. Davidson, JOM 48 (Sept. 1996) 62.

37. D.J. Thoma and J.H. Perepezko, Mater. Sci. & Eng. A156 (1992) 97.

38. Y. Liu, J.D. Livingston, and S.M. Allen, Metall. Tran. A23 (1992) 3303.

39. M. Grujicic, S. Tangrila, O.B. Cavin, W.D. Porter, and C.R. Hubbard, Mater. Sci. & Eng. A160 (1993) 37.

40. T.B. Massalski, J.L. Murray, L.H. Bennet, and H. Baker, *Binary Alloy Phase Diagram*, American Society for Metals, Metals Park, OH (1986).

41. P. Villars, A. Prince, and H. Okamoto, *Handbook of Ternary Phase Diagrams*, ASM International (1995).

42. N.I. Kaloev et al., Soviet Non-Ferrous Metals Research 14 (1986) 503.

43. D.I. Bardos, R.K. Malik, F.X. Spiegel and P.A. Beck, Trans. Met. Soc. AIME 236 (1966) 40.

44. K. Kuo, Acta Metall. 1 (1953) 720.

PART III: EFFECTS OF TERNARY ADDITIONS ON THE PHASE STABILITY IN $NbCr_2$-BASED LAVES PHASES

1. INTRODUCTION

Laves phases with an AB_2 composition comprise the single largest class of intermetallics, yet they are the least studied, compared with the conventional intermetallics, such as B2, L12, etc. Transition-metal Laves phases are currently being considered for many practical applications, e.g., $(Hf,Zr)V_2$ as superconducting material, $Zr(Cr,Fe)_2$ as hydrogen storage material, etc. [1, 2]. More recently, HfV_2-, $HfCr_2$- and $NbCr_2$-based two-phase alloys are being developed for high-temperature structural uses [3-9], because of their good retention of mechanical properties at elevated temperatures. However, their low ductility and brittle fracture characteristics at ambient temperatures are the main concerns for structural applications of these materials.

Laves phases generally crystallize into one of the three topologically close-packed structures: a cubic C15 – $MgCu_2$ structure, hexagonal C14 – $MgZn_2$ structure, and dihexagonal C36 – $MgNi_2$ structure [10]. Although Laves phases are generally stabilized by the size-factor principles, the stability of each crystalline structure is also influenced by the electron concentration factor (e/a). The classic work by Laves and Witte [11, 12] showed that for several quasi-binary alloy systems involving $MgCu_2$ and $MgZn_2$, with increasing valence electron concentration, the three Laves types, $MgCu_2$, $MgNi_2$, and $MgZn_2$, exist in that order. One attractive way to improve the deformability of complex Laves phases is to control their crystalline structure in a way that stress-assisted phase transformation and/or mechanical twinning can be triggered during plastic deformation [13, 14]. It is, thus, important to know the factors governing the phase stability in transition-metal Laves alloys.

In our previous investigation [15] (also see Part II), a number of binary and ternary phase diagrams were surveyed, and the phase stability criteria in the $NbCr_2$-based Laves phase systems, binary X-Cr and Nb-X and ternary Nb-Cr-X, were studied. It was shown

that when the atomic size ratios are kept identical, the average electron concentration factor, e/a, is the dominating factor in controlling the phase stability of $NbCr_2$-based transition-metal Laves phases. The e/a ratios for different Laves polytypes were determined as follows: with e/a < 5.76, the C15 structure is stabilized; at an e/a range of 5.88 - 7.53, the C14 structure is stabilized; with e/a > 7.65, the C15 structure is stabilized again. A further increase in the electron concentration factor (e/a > 8) leads to the disordering of the alloy. The results are summarized in Fig. 3 of Part II.

In this investigation, the Laves phase stability in the pseudo-binary $Nb(Cr,X)_2$ (X = Fe or Co) systems was studied experimentally to verify the observed e/a/phase stability correlation. Since Fe and Co have 8 and 9 outshell electrons, respectively, the addition of Fe or Co to substitute for Cr (e/a = 6) in $NbCr_2$ is very effective in increasing the average electron concentration. By a systematic replacement of Cr with Fe, Co, or Cu, it is possible to obtain a whole spectrum (e.g., C15 $\rightarrow$ C14 $\rightarrow$ C15) of changes in the crystal structure of the Laves phase based on $Nb(Cr,X)_2$ alloys. Also, the critical e/a values for phase transition can be determined precisely, which will be compared with the previously surveyed data. Furthermore, the phases between the C15/C14 homogeneity ranges will be carefully studied to examine if any intermediate structures, such as C36, will be stabilized.

The phase structure, unit cell volume, hardness, and fracture toughness of the Laves phases as a function of Fe or Co content in pseudo-binary $Nb(Cr,X)_2$ systems have been determined. The effects of phase stability on the deformability of the $Nb(Cr,X)_2$ Laves phases were also discussed in light of the experimental findings.

2. EXPERIMENTAL PROCEDURES

A series of pseudo-binary $Nb(Cr,X)_2$ alloys with various Fe or Co additions were produced by replacing Cr with either Fe or Co, while keeping the percentage of Nb constant (33.3 at.%). The Fe or Co content of the alloys varied from 0 to 66.7 at. %.

All the alloys of about 50 grams were prepared by arc-melting techniques using high-purity starting materials. An excess amount (typically less than 0.1 gram) of Cr was added to compensate for the evaporation loss of Cr during melting. Arc-melting was carried out in a chamber which was evacuated by a mechanical pump and flushed with ultrahigh purity (UHP) argon gas four or five times, and finally backfilled with UHP argon gas. A Zr sample was melted prior to melting the alloy charge each time in order to getter the oxygen in the chamber. The arc-melting was done using a thoriated tungsten electrode on a water-cooled copper hearth. Each ingot was inverted and remelted at least 7 times to ensure macroscopic compositional homogeneity. The alloys were homogenized in vacuum at 1300°C for 10 hours, then slowly cooled in the furnace. Finally, all the alloys were heat treated at 1000°C for 7 days, then water-quenched to retain the equilibrium condition at 1000°C.

X-ray diffraction measurements were made using a Scintag XD2000 diffractometer with Cu K_α radiation (the wavelengths of Cu $K_{\alpha 1}$ and $K_{\alpha 2}$ are 0.154056 and 0.154439 nm, respectively). Powdered samples were used, and the lattice parameter determination was obtained using 13-15 peaks. The microhardness was measured using a load of 500 g with a holding time of 15 seconds, and crack lengths were measured immediately after the indentation to eliminate the possibility of slow crack propagation following the removal of the indenter. The following equation was used to calculate the fracture toughness of the alloy [16, 17]:

$$K_{IC} = A\left(\frac{E}{H}\right)^n \frac{P}{L^{3/2}} \qquad (1)$$

where K_{IC} = fracture toughness ($MPa\sqrt{m}$), E = Young's modulus (GPa), which is assumed to be 218 GPa for all of the investigated alloys [18], H = Vickers hardness (GPa), P = load (N), and L = average length of the four radial cracks from the center of the indent

to the crack tip. A and n are constants, which are taken as 0.016 and 0.5 respectively, for relatively brittle materials [17].

3. RESULTS AND DISCUSSIONS

For the pseudo-binary $Nb(Cr,Fe)_2$ system, X-ray diffraction results show that the Laves phase after the addition of up to 5 at.% Fe maintains its original C15 structure, while the C14 structure is stabilized for alloys with the Fe content higher than 9 at.%. The corresponding critical e/a values are calculated to be 5.77 and 5.85, using Eq. 1 in Part II. For the alloys with Fe content between 5 and 9 at.%,. a two-phase mixture of C14 and C15 was detected. No intermediate structures, such as C36, were found between the C14 and C15 regions. Figure 1 shows that diffraction patterns for $Nb(Cr,Fe)_2$ alloys with 2 at.% Fe (C15 structure), 7 at.% Fe (C14/C15 structures), and 9 at.% Fe (C14 structure).

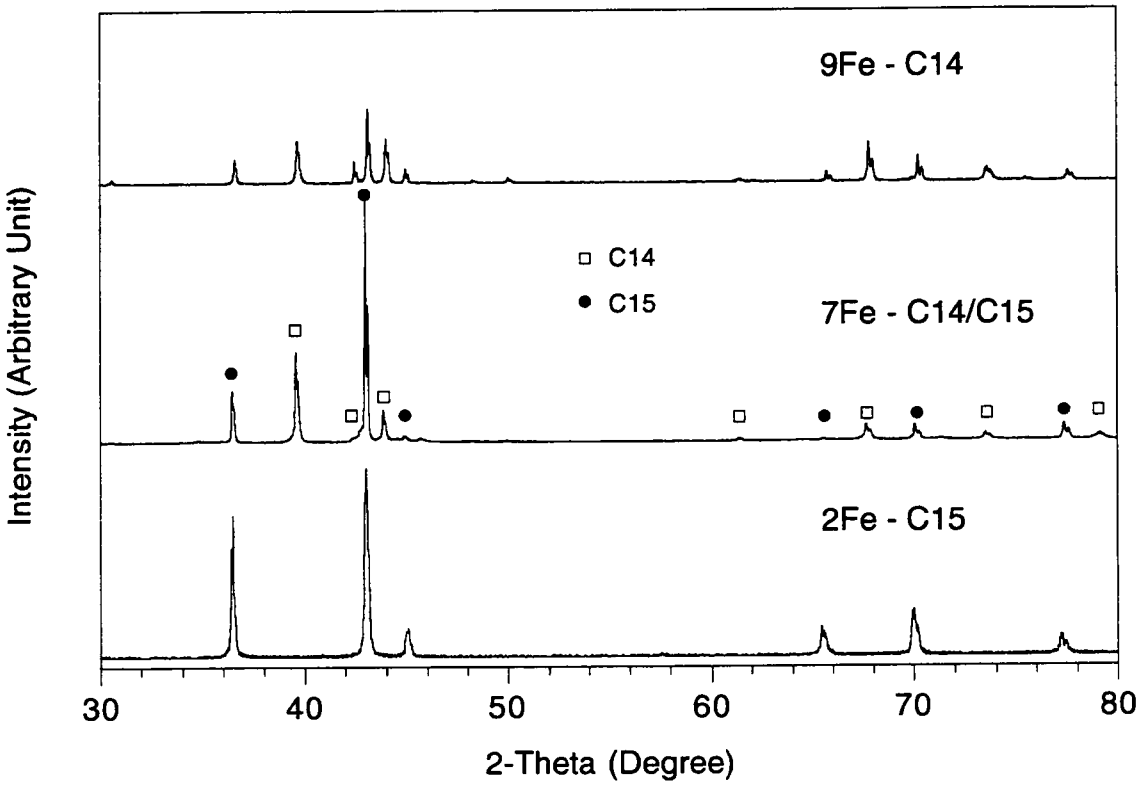


Fig. 1 X-ray diffraction patterns of $Nb(Cr,Fe)_2$ alloys with 2, 7 and 9 at.% Fe, which have C15, C14/C15 and C14 structures, respectively

For the pseudo-binary $Nb(Cr,Co)_2$ system, X-ray diffraction results indicate that the Laves phase after the addition of up to 3.5 at.% Co retains its C15 structure, while the C14 structure is stabilized for alloys with the Co content higher than 6 at.%. The alloys retain the C14 structure, until the Co content is higher than 61.2 at.%. With the Co content higher than 63.2 at.%, the C15 structure is stabilized again. The alloys between C15 and C14 present a mixture of C14 and C15 phases, with no intermediate structures observed. The critical electron concentrations corresponding to the C15/C14/C15 phase transition are calculated to be 5.77 for C15 on the Co-rich side, 5.85 and 7.50 for the C14 structure, and 7.56 for the C15 on the Cr-rich side. It should be noted that the critical e/a values for the C15/C14 transition are exactly same at the low X content side for the two pseudo-binary systems of $Nb(Cr,Fe)_2$ and $Nb(Cr,Co)_2$.

It is clear that the electron concentration rule is obeyed in these two pseudo-binary systems. The phase transition between C14 and C15 is determined by the average electron concentration in these alloys. As has been pointed out in Part II, the difference in atomic size between Cr and X (Fe or Co) is small, which makes the geometric factor similar in all the alloys. Therefore, the electronic factor, i.e., the average electron concentration, e/a, becomes the dominant factor in determining the stability of the different polytypes in these two pseudo-binary systems. Furthermore, the phase boundaries of the C15/C14/C15 transitions are very close to the values predicted using phase diagram information in Part II. The critical e/a values corresponding to the C14/C15 phase transitions shown in Fig. 3 of Part II, however, do need to be modified using the new experimental determined values obtained in the present work. Fig. 3 of Part II is replotted in Fig. 2 in this part by including the new critical e/a values determined experimentally. These data are the first experimental determination of the critical compositions, and therefore, the critical e/a values, for the different phases in the pseudo-binary $Nb(Cr,X)_2$ systems.

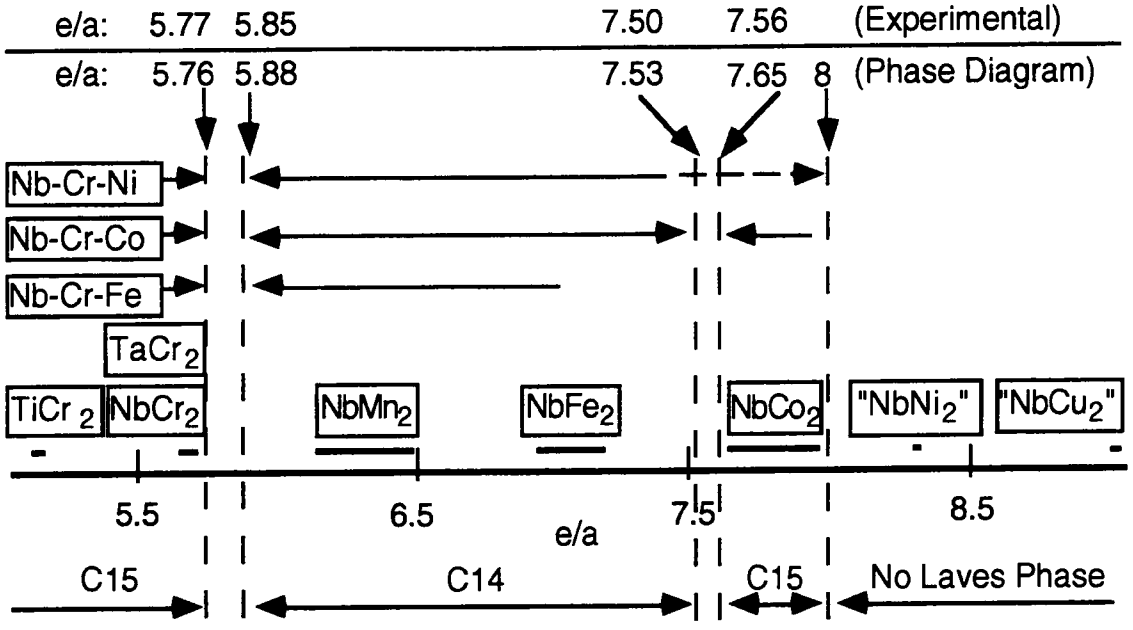


Fig. 2 Effect of average electron concentration (e/a) on phase stability in $NbCr_2$-based systems, with the critical e/a values for phase transitions both from experiments and phase diagram information

No intermediate structures were observed between the C14 and C15 single-phase regions and only a two-phase mixture of C14 and C15 was detected. This observation is in accord with the ternary Nb-Cr-Fe and Nb-Cr-Co phase diagrams [19]. However, this is in contrast to the situation in the pseudo-binary Mg-based system [20-24], where intermediate structures with different percentages of hexagonality, such as C36, were identified. Furthermore, a C36 phase was detected in a recent study of the Nb-Cr-Fe system [25]. The heats of formation of the C14, C36, and C15 polytypes of $NbCr_2$ Laves phase have been studied recently by first-principles calculations [26]. These structures are very close in bonding energy. Thus, the appearance or disappearance of the C36 structure may be affected by small change in temperature or impurity contents in the Laves phases. It will be of interest to see if any intermediate structure may be stabilized after quenching from 1200°C for the pseudo-binary $Nb(Cr,Fe)_2$ Laves phases. This remains an area for future investigation.

The crystal lattice parameters of the C15 and C14 Laves phases were measured for the pseudo-binary $Nb(Cr,X)_2$ alloys with various Fe or Co contents. The volume for the unit cells of C14 and C15 structures can be calculated using the experimentally determined lattice parameters, which are plotted in Fig. 3 as a function of Fe and Co contents. The cubic C15 structure has 24 atoms per unit cell, while the hexagonal C14 structure has 12 atoms per unit cell. Therefore, the volumes of the unit cells of C14 and C15 structures were normalized as the volume of a cell with 24 atoms, for easy comparison between C15 and C14 structures. The normalized unit-cell volume of the C14 structure is twice its original volume, while that of the C15 structure is equal to its original volume. The volumes for C14 and C15 structures presented in Fig. 3 are those after normalization.

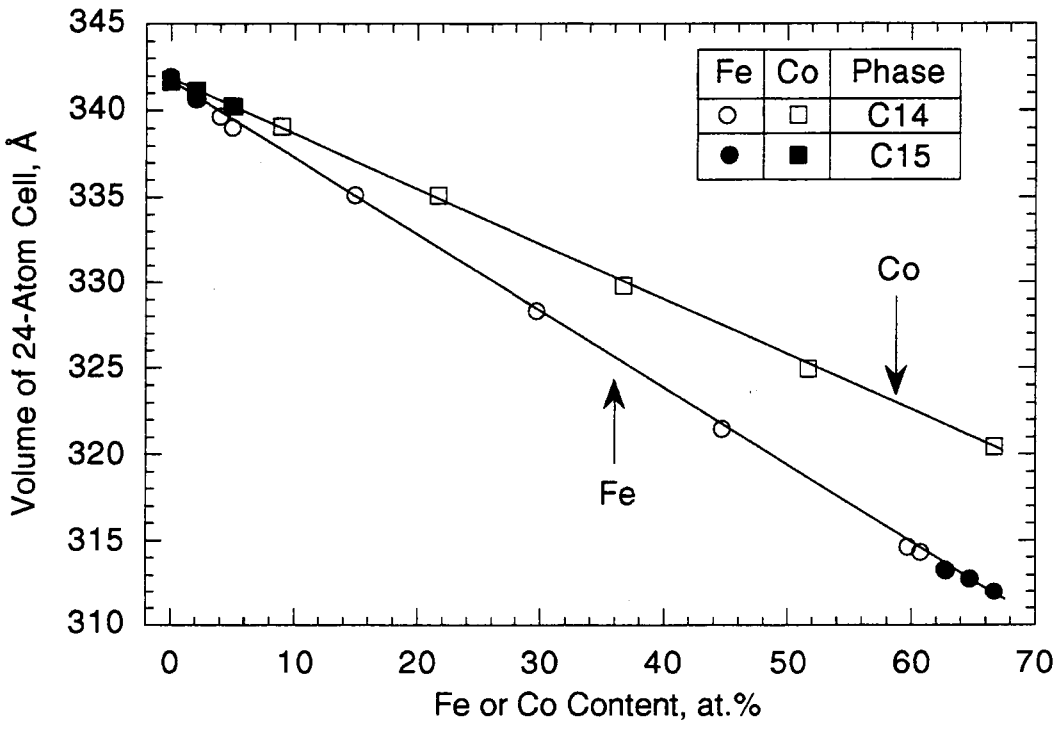


Fig. 3 Dependence of the volume of 24-atom cell of $Nb(Cr,X)_2$ Laves phase on the Fe or Co content

As the Fe or Co content increases, the volume per 24-atom cell decreases linearly. This is not surprising, considering that the atomic sizes of Fe and Co are smaller than that of Cr. Since the atomic size of Fe is larger than that of Co, the Fe addition leads to a slower decrease in the volume of the 24-atom cell than the Co addition at the same doping levels. The slopes of the two lines can be calculated to be -0.323 and -0.448 for $Nb(Cr,Fe)_2$ and $Nb(Cr,Co)_2$ Laves phases, respectively. This linear relation of 24-atom unit cell volume as a function of the ternary X addition indicates that the ternary element, Fe or Co, is exclusively substituting for the Cr atoms in the Laves phase, and Vegard's law is obeyed in these two pseudo-binary systems. The exclusive replacement of Cr by Fe and Co has also been confirmed by our density measurements, which clearly show that no vacancies are created in the pseudo-binary Laves phases, and the measured density is in agreement with the calculated density by assuming that Fe or Co is replacing Cr in $Nb(Cr,X)_2$ Laves phases [27].

It is interesting to note that the change in the crystal structure does not affect the slope of the line, indicating that the substitution of Cr by Fe or Co does not influence the bonding characteristics in the Laves phases. Furthermore, the volume difference between the C14 and C15 structures of the same composition should be small, and there is no disrupt change in volume during the C14/C15 phase transition.

The Vickers hardness of the pseudo-binary $Nb(Cr,X)_2$ alloys with various Fe or Co contents is plotted in Figs. 4 and 5. It is clear from these figures that the addition of Fe or Co to substitute for Cr increases the hardness of the Laves phase linearly. Also, the trend is that the addition of Fe or Co increases the hardness of the C15 and C14 structures in a similar rate. The enthalpies of formation for $NbCo_2$ and $NbFe_2$ are more negative than that of $NbCr_2$ (see Table I and II of Part IV), indicating that the bonding is stronger in $NbCo_2$ and $NbFe_2$ than in $NbCr_2$. This can be used to explain the hardness increase, as the Fe or Co content in the alloy increases in Figs. 4 and 5.

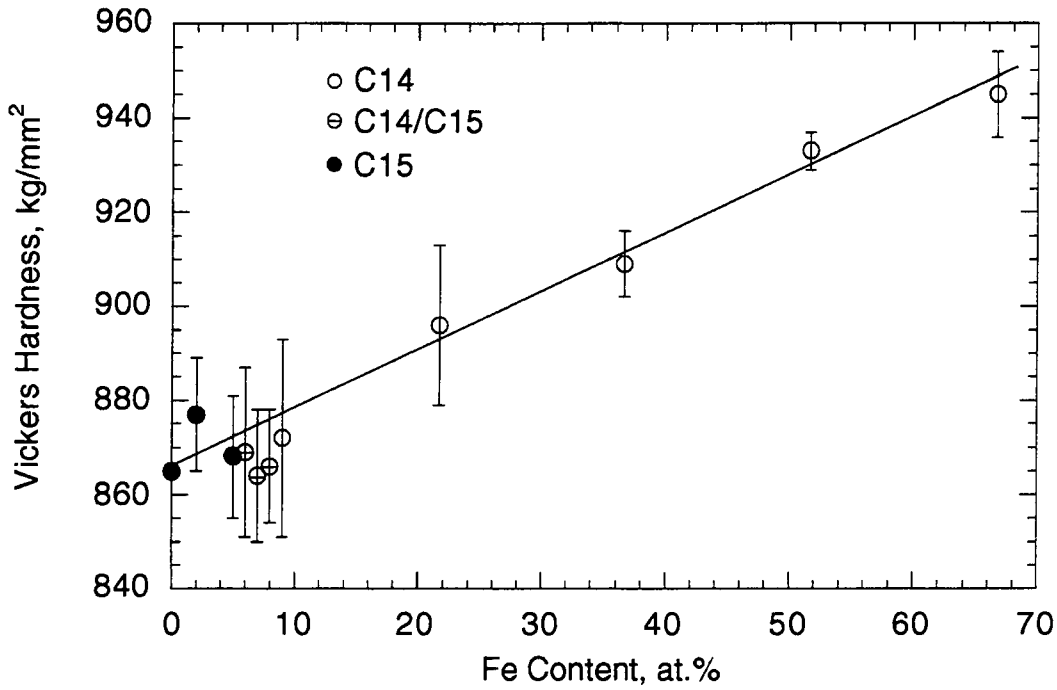


Fig. 4 The effect of Fe content on the Vickers hardness of $Nb(Cr,Fe)_2$ alloys

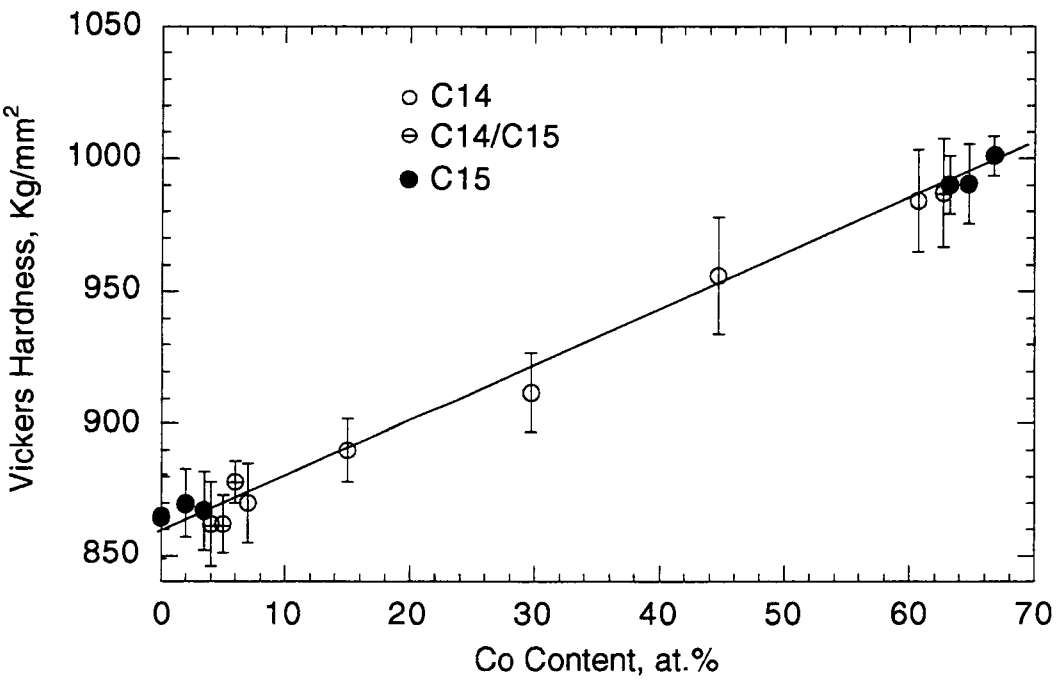
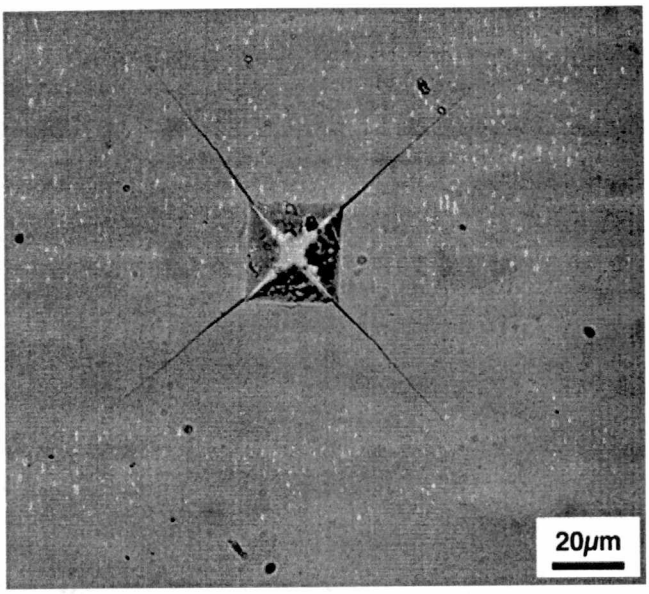


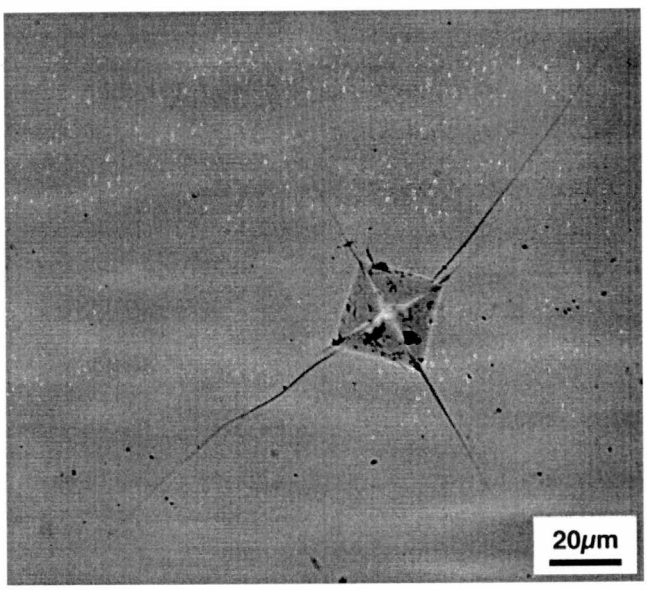
Fig. 5 The effect of Co content on the Vickers hardness of $Nb(Cr,Co)_2$ alloys

Figure 6 shows the cracking behavior after indentation with a load of 500 grams for the $NbCo_2$ and $NbFe_2$ alloys, which have C15 and C14 structures, respectively. The average crack length is shorter for the C15 $NbCo_2$ alloy [Fig. 6(a)] than for the C14 $NbFe_2$ alloys [Fig. 6(b)]. The fracture toughness calculated using Eq. (1) as a function of Fe and Co contents is presented in Figs. 7 and 8, respectively. Basically, the fracture toughness of the monolithic Laves phase is very low, about 1 $MPa\sqrt{m}$, which is a consequence of the topologically close packing manner of the structure and the subsequent difficulty in activating dislocation sources in the material. Some general trends regarding the effect of the Fe and Co contents on the fracture toughness of the Laves alloys can be deduced from Figs. 7 and 8. Basically, the fracture toughness of the C15 structure is consistently higher than that of C14 structure for the ternary systems, regardless of the X addition. This can be explained by the fact that the C15 structure is cubic, and thus, is more deformable than the hexagonal C14 structure. The toughness value for alloys in the two-phase region or near the phase boundary may increase, due to the fact that the associated structure is metastable, and it is easy to transform from one structure to another during deformation. Unfortunately, such is not the case for the present study. None of the alloys within the two-phase regions show any sign of increase in toughness. The toughness of the two-phase alloys and alloys near the phase boundary is similar to that of the C15 phase. This may be related to the small energy absorbed during the phase transformation or mechanical twinning and/or small volume change during the C15/C14 phase transition.

The future research direction, thus, will concentrate on the investigation of the point defects in the Laves phases, with the hope that certain Laves phases may have constitutional and/or thermal vacancies [28]. Toughening of the Laves phases may be facilitated through vacancy-assisted synchroshear deformation [29, 30]. This is the focus of the study in Part V.



(a)



(b)

Fig. 6 Cracking behaviors in (a) C15 $NbCo_2$ alloy and (b) C14 $NbFe_2$ alloy.

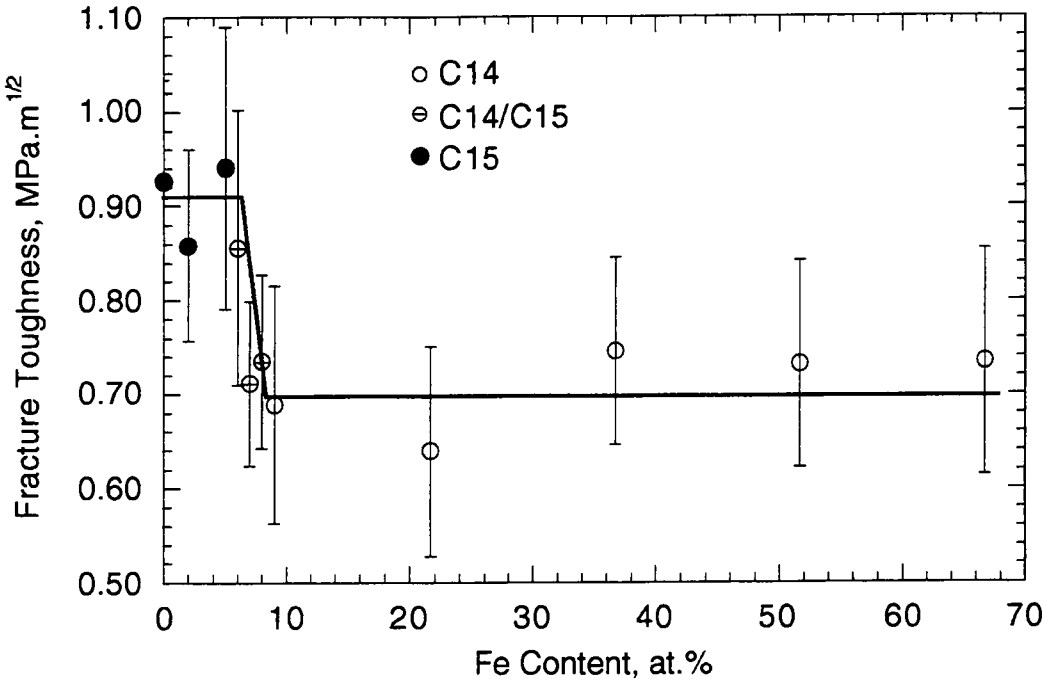


Fig. 7 Fracture toughness values of the Laves phases as a function of the Fe content

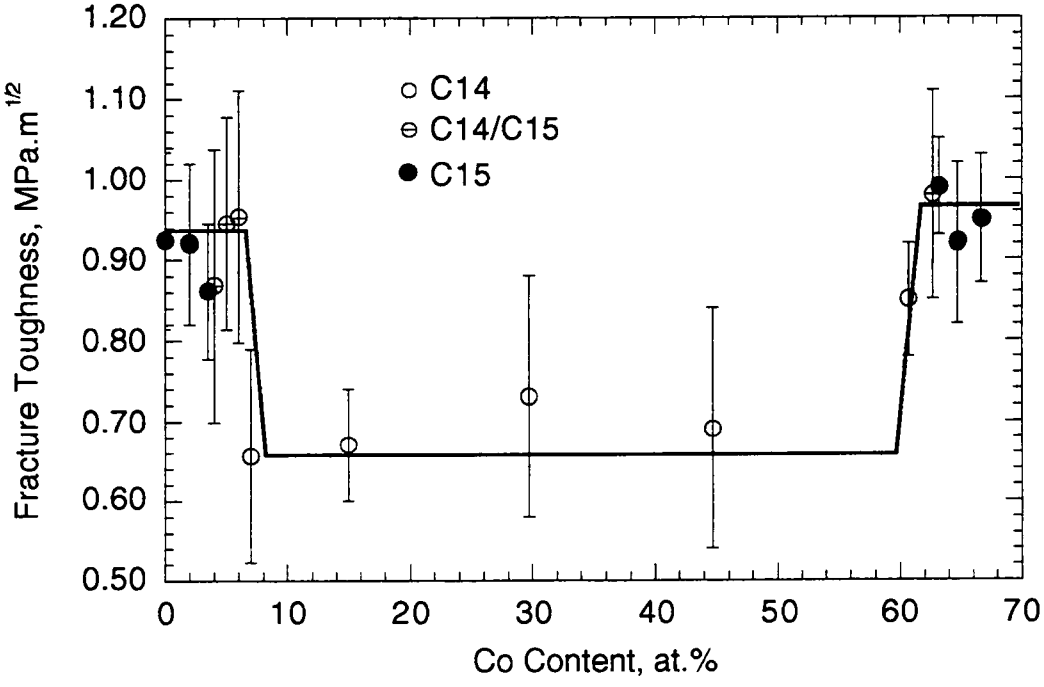


Fig. 8 Fracture toughness values of the Laves phases as a function of the Co content

4. CONCLUSIONS

It has been shown that the average electron concentration factor, e/a, is the dominating factor in controlling the phase stability of the pseudo-binary $Nb(Cr,Fe)_2$ and $Nb(Cr,Co)_2$ Laves phase systems. The substitution of Fe or Co for Cr in $NbCr_2$ increases the average electron concentration of the alloy, thus leading to the change of the crystal structures from C15 to C14 and C14 to C15. The experimentally determined critical e/a values corresponding to the C15/C14/C15 phase transition is close to those previously estimated from phase diagram information. At $e/a < 5.77$, the C15 structure is stabilized; at $5.85 < e/a < 7.5$, the C14 structure is stable; with e/a higher than 7.56, the C15 structure is stabilized again. Between the C14 and C15 phase regions, a two-phase mixture of C14 and C15 was observed, with no intermediate structures detected.

As the Fe or Co content increases, the volume of the 24-atom cell decreases for both C15 and C14 structures, while the Vickers hardness increases over the whole C15 and C14 ranges. The fracture toughness values are low for all the alloys, and the fracture toughness of the C15 structure is greater than that of the C14 structure for the pseudo-binary $Nb(Cr,Fe)_2$ and $Nb(Cr,Co)_2$ Laves phase systems.

REFERENCES

1. K. Inoue and K. Tachikawa, IEEE Trans. Magnetics 15 (1979) 635.
2. D. Ivey and D. Northwood, J. of Less- Common Met. 115 (1986) 1986.
3. F. Chu and D.P. Pope: in *High-Temperature Ordered Intermetallic Alloys V*, MRS. Symp. Proc. 288 (1993) 561.
4. K. S. Kumar and D.B. Miracle, Intermetallics 2 (1994) 257.
5. M. Takeyama and C.T. Liu, Mater. Sci. and Eng. A132 (1991) 61.
6. J.A. Cook, P.K. Liaw, and C.T. Liu: in *Fatigue and Fracture of Ordered Intermetallics*, W. O. Soboyejo, T. S. Srivatsan and R. O. Ritchie, eds., TMS, Warrendale, PA (1995) 155.
7. J.A. Cook, P.K. Liaw, C.T. Liu, and S.B. Bhaduri: in *The Johannes Weertman Symposium*, R. J. Arsenault et al., eds., TMS, Warrendale, PA (1996) 47.
8. K.S. Chan and D.L. Davidson, JOM 48 (Sept. 1996) 62.
9. D.J. Thoma and J.H. Perepezko, Mater. Sci. and Eng. A156 (1992) 97.
10. T.B. Massalski: in *Physical Metallurgy Part 1*, R. W. Cahn and P. Hassen, eds., North-Holland Physics Publishing, NY (1983) 190.
11. F. Laves and H. Witte, Metallwirschaft 14 (1935) 645.
12. F. Laves and H. Witte, Metallwirschaft 15 (1936) 840.
13. Y. Liu, J.D. Livingston, and S.M. Allen, Metall. Tran. A23 (1992) 3303.
14. M. Grujicic, S. Tangrila, O.B. Cavin, W.D. Porter, and C.R. Hubbard, Mater. Sci. and Eng. A160 (1993) 37.
15. J.H. Zhu, P.K. Liaw, and C.T. Liu, Mater. Sci. and Eng. A239-240 (1997) 260.
16. M. Sakai and R.C. Bradt, Inter, Mat. Rev. 38(2) (1993) 53.
17. G.R. Anstis, P. Chantikul, B.R. Lawn, and D.B. Marshall, J. of Amer. Ceramics. Soc. 64(9) (1981) 533.
18. H. Anton and P.C. Schmidt, Intermetallics 5 (1997) 449.

19. P. Villars, A. Prince, and H. Okamoto, *Handbook of Ternary Phase Diagrams*, ASM International, 1995.

20. Y. Komura, Acta Cryst. 15 (1962) 770.

21. Y. Komura, E. Kotera, and M. Mitarai, Acta Cryst. A25 (1969) S96.

22. Y. Komura, M. Mitarai, I. Nakatani, H. Iba, and T. Shimizu, Acta Cryst. B26 (1970) 666.

23. Y. Komura, A. Nakaue, and M. Mitarai, Acta Cryst. B28 (1972) 727.

24. Y. Komura and Y. Kitano, Acta Cryst. B33 (1977) 2496.

25. M. Grujicic, S. Tangrila, O.B. Cavin, W.D. Porter, and C.R. Hubbard, Mater. Sci. & Eng. A160 (1993) 37.

26. S. Hong and C.L. Fu, "Phase Stability and Elastic Moduli of Cr_2Nb by First-Principles Calculations", submitted to Intermetallics (1998).

27. J.H. Zhu, C.T. Liu, and P.K. Liaw, unpublished results (1998).

28. J.H. Zhu, L.M. Pike, C.T. Liu, and P.K. Liaw, "Point Defects in Binary $NbCr_2$ Laves Phase Alloys", Scripta Mater., in press (1998).

29. K.C. Chen, S.M. Allen, and J.D. Livingston, MRS Symp. Proc. 364 (1994) 1406.

30. P.M. Hazzledine and P. Pirouz, Scripta Metall. et Mater. 28 (1993) 1277.

PART IV: ENTHALPIES OF FORMATION OF LAVES PHASES

1. INTRODUCTION

On the formation of an intermetallic phase from its components, as a rule, changes of structure and of bond type and bond strength occur. An understanding of the nature of the intermetallic phase can be deduced from its thermodynamic properties. The free energy of formation gives an indication of the stability, and the enthalpy of formation is closely related to the type of bonding. The entropy of formation reflects changes in the vibrational behavior and configurational arrangement of the atoms on the formation of the compounds. The heat capacity of the solid just below the melting point and the absolute entropy also reflect the vibrational behavior. The heat capacity of the solid just below the melting point sheds light on pre-melting phenomena. The heat of fusion, the entropy of fusion, and, to a lesser extent, the level of melting point reveal some aspects of the nature of the transition from the crystalline to the liquid state. The chemical activities of the components of intermetallic compounds also give an indication of their bonding.

A decrease in free energy accompanies the formation of an intermetallic compound. A compound is stable with respect to competing neighboring phases in a multicomponent system, if its free energy is lower than that of a mixture of these phases. The enthalpy of formation of an intermetallic compound is usually also negative because the free energy change must be negative, and the entropy-temperature product is small. For this reason, the magnitude of the enthalpy of formation of a compound can be used as a measure of its stability.

Thermodynamic information on Laves phases is very limited, considering the large number of Laves phases. Much of such information can be found in the collections of Hultgren et al. [1], de Boer et al. [2] and Kubaschewski et al. [3]. The enthalpies of formation of many Laves phases, however, have been determined very recently. Such data are scattered in different journals, and no compilation of such information has been published thus far.

This chapter first briefly reviewed the measurement methods for the enthalpy of formation, bonding characteristics in Laves phases, and semiempirical prediction models for calculating the enthalpy of formation. The literature data on the enthalpies of formation in Laves phases are then surveyed and listed. Some regularities are then delineated using these surveyed data. A thermodynamic interpretation is offered to explain the atomic size ratio limitations for Laves phases.

2. MEASUREMENTS OF ENTHALPIES OF FORMATION

The enthalpies of formation of intermetallic compounds are measured by calorimetry. The main methods are direct-reaction calorimetry and solution calorimetry [3, 4]. Enthalpies of formation can also be determined indirectly from equilibrium data for several temperatures. Such equilibrium data are usually obtained by electromotive force (emf) measurements or in some cases by vapor pressure measurements [3, 4].

In direct calorimetric methods of Kubaschewski and Dench [5], Kleppa [6] and Kleppa and Topor [7], the heat evolved upon the reaction of the solid components forming a compound is measured in the calorimeter vessel, which is kept at a constant temperature. This temperature must be sufficiently high to ensure complete reaction within reasonable time. The reaction can be started by heating a (pressed) mixture of the pure powdered components.

In solution calorimetry, the enthalpies of formation are determined from the difference in the heat effects produced by dissolving additions of the compound and a mechanical mixture of its components in a solution. In general, if an acid is used as a solvent, the large heat effects limit the accuracy, but the use of liquid metals, such as tin, in which the samples have a low heat of solution, greatly improves the accuracy.

The applicability of any calorimetric method depends on the nature of the system to be investigated. The direct calorimetric method gives heats of formation for the temperature

of reaction. Enthalpies of formation obtained by solution calorimetry refer to the temperature of the addition, which may be the temperature of the bath or some other temperature, depending on the calorimeter and the method of operation.

Electromotive measurements provide equilibrium data from which free energies of formation and enthalpies of formation can be obtained. If an intermetallic compound coexists with one of its constituent elements, the following relation holds for a suitable cell:

$$\Delta H = nf(TdE/dT - E) \qquad (1)$$

where ΔH is the enthalpy of formation, n, the number of equivalents, f, Faraday's constant, T, temperature, and E, the reversible cell voltage. If the compound does not coexist with one of the constituent elements, the activity coefficient of the components may be determined from emf values. The enthalpies of formation can be calculated using certain equations. The values of enthalpies of formation obtained by this method refers to the room-temperature ones.

The enthalpies of formation of intermetallic compounds containing a volatile element, such as zinc, tellurium, or arsenic, can be determined from vapor pressure measurements by an application of the van't Hoff equation:

$$\frac{\partial \ln K_p}{\partial T} = \frac{\Delta H}{RT^2} \qquad (2)$$

where R is the gas constant and Kp is the reaction equilibrium constant.

The enthalpies of formation derived from values of the emf or vapor pressure tend to be of low accuracy, because small errors in the change of these values with temperature have a large adverse effect [3]. The enthalpies of formation may also be calculated from the following equation, if the Gibbs free energy (ΔG) and entropy of formation (ΔS) are known:

$$\Delta H = \Delta G - T \bullet \Delta S \qquad (3)$$

3. ENTHALPIES OF FORMATION AND BONDING OF INTERMETALLIC COMPOUNDS

The enthalpy of formation of a compound is the difference between the enthalpies of the compound and the component elements; the reference state of the latter is their stable state at the temperature and pressure of formation of the compound. The enthalpy of formation is related to the bond energies in the compound, but individual bond energies cannot be calculated from the thermodynamic data unless the interactions of atoms other than single nearest-neighbor pairs are neglected. If only nearest-neighbor pairs are considered, a bond energy can be obtained by dividing the energy of the compound by the number of such pairs. This approach neglects the effect of other atoms on the bond energy of the nearest-neighbor pair and also ignores any bonding between non-nearest neighbors, which could be taken into account only if the dependence of the bond energy on distance and position in the crystal were known. Wagner [8] has pointed out that for fundamental reasons, it may not be possible to calculate or measure individual bond energies in a crystal and that the concept of such energies may have to be discarded. Even without the knowledge of individual bond energies, however, it is obvious that the enthalpy of formation is closely related to the bonding of the compound.

Ionic, covalent, metallic, and van der Waals bonds and the transitions between these pure types must be considered in discussing the enthalpies of formation of intermetallic compounds. Also, in a single compound, more than one type of bond may occur. For example, in compounds with layer structures the bonding within the layers differs from that between the layers.

An intermetallic compound has a large exothermic enthalpy of formation, when the nature of its bonding is different from that in the component elements, e.g., when metallic elements form a compound in which the bonding is ionic or covalent. Robinson and Bever have analyzed the range of the enthalpy of formation of intermetallic compounds with

different bonding nature [9]. The enthalpies of formation of intermetallic compounds with ionic bonding range from approximately -125 kJ/mole to -500 kJ/mole; the numerical values of the negative enthalpy of formation (i.e., the exothermic heat of formation) increase with the degree of ionicity of the bond. The exothermic enthalpies of formation of covalent compounds are generally smaller than those of ionic compounds because the sharing of the electrons between the atoms in the covalent bond involves a smaller energy change than the electron transfer in the ionic bond. The enthalpies of formation of most covalent intermetallic compounds range from approximately -40 kJ/mole to -100 kJ/mole. The enthalpies of formation of compounds with metallic bonding are mainly due to the difference in the coordination of the atoms in the compounds. The heats of formation of most of these compounds are numerically smaller than -100 kJ/mole.

The bonding in Laves phases is generally considered to be of a metallic nature [9]. King and Kleppa [10] showed that there is no correlation between the heat of formation and the difference in electronegativity between the components of the six Laves phases investigated by them. However, these investigators found that the exothermic heat of formation decreased with positive deviations from the ideal radius ratio of 1.225 for Laves phases. This decrease has been explained by the strain energy associated with nonideal ratios, which reduces the exothermic heat of formation.

The stability of Laves phases containing a transition metal is extraordinarily higher, i.e., they have high values of (negative) enthalpies of formation. The reason for this behavior is the transfer of electrons from the other metal to the transition element, to fill up the incompletely-filled inner shell [10, 11]. This charge transfer introduces an ionic contribution to the bonding and is accompanied by an increase in the enthalpy of formation. An example of electron transfer occurs in the compound $MgNi_2$, which has a larger exothermic enthalpy of formation than those of the compounds $MgCu_2$ and $MgZn_2$, which are otherwise similar to $MgNi_2$ [10]. The energy effect of the electron transfer is opposed

to the strain energy resulting from unfavorable atomic size ratios, and thus, helps to make the formation of Laves phases possible in systems with atomic size ratios that are not ideal.

4. SEMIEMPIRICAL CALCULATION

Several approximation methods on the basis of empirical or semi-empirical models have been proposed to estimate the enthalpies of formation of binary alloys and intermetallic compounds. Dehlinger and Schulze [12] suggested that the stability of Laves phases arises from a decrease in enthalpy due to the increase in the average coordination number in these compounds with that in the component metals. Kubaschewski [13] proposed a method for calculating the heats of formation of intermetallic compounds based on the heat of sublimation of the component metals and the change in the coordination on formation, and has calculated the heats of formation of various compounds, including the Laves phases. The agreement between the calculated and experimental values is satisfactory. This indicates that their enthalpies of formation can be largely attributed to increases in the coordination.

Pasturel et al. [14, 15, 16] calculated the enthalpy of formation of transition-metal intermetallic compounds within a tight-binding scheme for the d-band, deriving as first step the partial densities of states from the knowledge of the moments of the constituents. They treated a rare earth metal as a transition metal with 1.5 to 2.0 5d electrons.

Miedema and coworkers [2, 17] developed a simple model to predict the enthalpy of formation from the work functions, molar volumes and electron densities at the boundary of the Wigner-Seitz cell of the constituents, basing their calculations on the so-called macroscopic atom picture. This model was a natural extension of Pauling's scheme for the calculation of the enthalpies of formation of alloys and compounds in their standard state [18]. In Pauling's scheme, the heat of formation of simple molecules was proposed to be proportional to the summation of the squared electronegativity differences, over all

chemical bonds. However, Pauling's scheme only included a negative contribution to the enthalpy of formation. In order to overcome this problem, Miedema and coworkers added a positive contribution, due to the electronic redistribution, proportional to the square of the cubic root of the electronic charge density difference at the Wigner-Seitz boundary, $(\Delta n_{WS}^{1/3})^2$, and an experimental work function, ∂^*, was used, instead of Pauling's electronegativity. Several other adjustments were made in order to describe accurately the heat of formation, ΔH, for every binary metallic compound of a transition metal, which was finally given by the following equation [2, 17] :

$$\Delta H = \frac{f(c)P(c_A V_A^{2/3} + c_B V_B^{2/3})}{(n_{WS}^{-1/3})_{average}} x\left[-(\Delta\partial^*)^2 + \frac{Q}{P}(\Delta n_{WS}^{1/3})^2 - \frac{R}{P}\right] + c_B \Delta H_{Btrans} \quad (4)$$

where P, Q, and R are constants derived from the examination of the phase diagram information, c_M and V_M are, respectively, the atomic concentration and the molar volume of a metal M (A or B), ΔH_{Btrans} is the energy required to convert the substance B from the non-metallic into the metallic state, $(n_{WS}^{-1/3})_{average}$ represents the averaged electrostatic screening length, and f(c) is a concentration function that, together with the $(c_A V_A^{2/3} + c_B V_B^{2/3})$ term, is a measure of the contact surface area between the two different atoms. For an ordered compound, the concentration function, f(c), was obtained empirically as given by [19]

$$f(c) = c_A^S c_B^S\left[1 + 8(c_A^S c_B^S)^2\right] \quad (5)$$

where c_A^S is the surface concentrations of the metals A and B, defined as

$$c_A^S = c_A V_A^{2/3}/(c_A V_A^{2/3} + c_B V_B^{2/3}) \quad (6)$$

This model was improved by considering the changes in atomic volumes upon alloying, due to the charge transfer between different elements [17], a correction that is usually small except in cases such as hydrides and other compounds of elements with very different electronegativity values.

In general, the enthalpies of formation of transition alloy compounds calculated by the above methods coincide well. A better agreement with experimental results can be achieved by Pasturel's methods at the cost of high computational effort. In contrast, the semi-empirical model of Miedema is relatively simple, and the computational effort is insignificant and can reasonably meet the requirements for predicting the stability or existence of an intermetallic compounds, or glass-forming possibility. The formation enthalpies for most binary alloy systems have been calculated by Miedema and co-workers themselves, but still some special binary systems have not been calculated with the model.

Niessen et al. [17] have written a simple and convenient program based on the most recent set of Miedema's parameters, and in this program a correction for the molar volume of alloy constituents has been taken into account. Using this program, the enthalpies of formation of a transition-transition metal compound and a transition-non-transition metal compound can be conveniently calculated.

5. SOME REGULARITIES IN THE ENTHALPIES OF FORMATION OF LAVES PHASES

A complete literature survey was undertaken to obtain all the available data on the enthalpies of formation of Laves phases. Table I, II and III lists all the available information for C15, C14 and C36 phases, respectively, which include the atomic size ratio (R_A/R_B), the enthalpy of formation (ΔH), entropy of formation (ΔS), the method used to evaluate the ΔH and ΔS values and the corresponding temperature, and finally the relevant references. For hexagonal C14 phases, the axial ratio, c/a, values are also included, which were calculated using the reported c and a values for the compounds.

Table I List of R_A/R_B, experimental ΔH and ΔS, the experimental temperature and method, and relevant references for binary C15 Laves phases

C15 Phase	R_A/R_B	ΔH kJ/mole	ΔS J/K.mole	Experimental Temperature & Method	Ref.
$BaPt_2$	1.617	-204	-6	990-1100K, emf	2
$BiAu_2$	1.179	-6.35		644K, solution calorimetry	1
$CaAl_2$	1.378	-240.8		298K	20
		-216.7	-12.8	298K	3, 21
		-219.7		298K	1, 22
$CaNi_2$	1.584	-57	-29.1	900-1150K, emf	2
$CeAl_2$	1.274	-163.2	-17.8	298K	22
		-175.7	-12.7	298K	21
		-146.7		298K	23
		-156.6		298K	24
		-150		298K	25
$CeCo_2$	1.458	-55.8			26
$CeIr_2$	1.345	-221.4		1473K, reaction calorim.	27
$CeNi_2$	1.465	-115.8		298K, solution calorim.	28
$CePt_2$	1.316	-51.8		1473K, reaction calorim.	27
$CeRh_2$	1.357	-199.5		1473K, reaction calorim.	27
$CeRu_2$	1.363	-85.8		1473K, reaction calorim.	27
$CuBe_2$	1.133	-47		1073K, emf, = ΔG	1
$CuBe_3$	1.133	-47.7		1073K, emf, = ΔG	1
$DyAl_2$	1.238	-158.1			24
$DyCo_2$	1.416	-52.2		1100K, solution calorim.	29
		-27.3		989K, reaction calorim.	30
$DyFe_2$	1.392	-23.1		298K, solution calorim.	31
		-87.9		1116K, reaction calorim.	30
$DyIr_2$	1.307	-209.7		1474K, reaction calorim.	33
$DyNi_2$	1.423	-115.5		985K, reaction calorim.	30
		-97.8		298K, solution calorim., 995K	29
$DyPt_2$	1.278	-294.3		1474K, reaction calorim.	33
$DyRh_2$	1.318	-186.9		1474K, reaction calorim.	33
$ErAl_2$	1.227	-147.3			23
		-108			24
		-151.5			24
$ErCo_2$	1.403	-56.4		1100K, solution calorim.	29
		-34.5		1048K, reaction calorim.	30

Table I (continued)

C15 Phase	R_A/R_B	ΔH kJ/mole	ΔS J/K.mole	Temperature & Method	Ref.
$ErFe_2$	1.379	-146.3		1163K, reaction calorim.	30
		-23.7		298K, solution calorim.	31
$ErIr_2$	1.295	-227.7		1473K, reactio calorim.	32
$ErNi_2$	1.41	-93.9		1100K, solution calorim.	29
		-147.6		1052K, reaction calorim.	30
$ErPt_2$	1.267	-323.4		1473K, reaction calorim.	32
$ErRh_2$	1.306	-209.4		1473K, reaction calorim.	32
$EuAl_2$	1.426	-108			24
$GdAl_2$	1.258	-154.2			23
		-159.6			33
$GdCo_2$	1.439	-47.4		298K, solution calorim. 998K	16
		-52.2		298K, solution calorim. 988K	34
		-32.2		1025K, reaction calorim.	35, 30
		-35.1		1100K, solution calorim.	29
$GdFe_2$	1.414	-34.8		298K, solution calorim. 998K	16, 34
		-10.5		1078K, reaction calorim.	35
		-10.5		1103K, reaction calorim.	30
$GdIr_2$	1.328	-205.5		1477K, reaction calorim.	36
$GdNi_2$	1.446	-96		1100K, solution calorim.	29
		-115.5		298K, solution calorim. 995K	16
		-75.3		954K, reaction calorim.	30
$GdPt_2$	1.299	-300		1477K, reaction calorim.	36
		-282.6		298K, solution calorim. 1091K	34
$GdRh_2$	1.34	-196.2		1477K, reaction calorim.	36
$GdRu_2$	1.346	-65.1		1477K, reaction calorim.	36
$HfCr_2$	1.232	-5.4	12	298K, assessment	2
$HoAl_2$	1.233	-157.5			24
$HoIr_2$	1.301	-227.6		1474K, reaction calorim.	37
$HoPt_2$	1.60	-319.8		1474K, reaction calorim.	37
$HoRh_2$	1.313	-211.2		1474K, reaction calorim.	37
KBi_2	1.398	-79.5		533K, vapor pressure, = ΔG	1
$LaAl_2$	1.311	-150.5		292K, acid solution calorim.	1, 2
		-149.7		298K	38
		-141.3		298K	39
		-162		298K, calorim.	2
		-201	-30	683-876K, emf	2
		-151	-14.8	298K	3, 21

Table I (continued)

C15 Phase	R_A/R_B	ΔH kJ/mole	ΔS J/K.mole	Temperature & Method	Ref.
$LaIr_2$	1.383	-183	-4.8	950-1200K, emf	2
		-188.7		1473K, calorim.	40
$LaNi_2$	1.506	-90	-2.4	298K, emf, 947-1068K	2
		-60		298K, calorim.	2
		-69		1095K, calorim.	2
$LaOs_2$	1.387	-27			
$LaPt_2$	1.353	-384	-51	1373-1673K, emf	2
		-270		1473K, calorim.	40
$LaRh_2$	1.396	-172.5		1473K, calorim.	40
$LaRu_2$	1.402	-33		1165K, calorim.	2
		-30.9		1473K, calorim.	40
$LuAl_2$	1.211	-157.8		1473K, reaction calorim.	41
$LuIr_2$	1.278	-213		1473K, reaction calorim.	27
$LuRh_2$	1.289	-204.3		1473K, reaction calorim.	27
$MgCu_2$	1.254	-35.1	-0.86	298K	21
		-33.9		298K	10
		-33.5	3.9	298K	1, 22
		-22.6	11.7	298K, vapor pressure	42
		-24.12		acid solution calorim.	43
$NbBe_2$	1.301	-60		unknown T	2
$NbCo_2$	1.173	-57	-6.3	298K, emf, 1275-1425K	2
		-51	2.1	1270-1420K, revision of above	2
		-47.7	3.9	1350K, emf, Nb=0.27	1
$NbCr_2$	1.145	-20.9	0.3	298K, vapor. pressure	2, 3, 21
		-21.2	-1.9	298K	44
$NdAl_2$	1.40	-159			45
		-160.8			24
$NdIr_2$	1.342	-202.8		1477K, reaction calorim.	46
$NdPt_2$	1.313	-293.7		1477K, reaction calorim.	46
$NdRh_2$	1.354	-179.7		1477K, reaction calorim.	46
$NdRu_2$	1.36	-56.4		1477K, reaction calorim.	46
$NdSi_2$	1.381	-236.1		1473K, reaction calorim.	41
$PbAu_2$	1.214	-1.3		298K	1, 47
$PrAl_2$	1.277	-167.4	-15.8	298K	21
		-188.4		298K	48
		-162		298K	24
$PrCo_2$	1.46	-12.9			35
		-13		803K, DTA calorim.	30

Table I (continued)

C15 Phase	R_A/R_B	ΔH kJ/mole	ΔS J/K.mole	Temperature & Method	Ref.
$PrIr_2$	1.347	-212.1		1473K, reaction calorim.	49
$PrNi_2$	1.467	-25.2		calorim.	30,35
$PrPt_2$	1.318	-280.5		1473K, reaction calorim.	49
$PrRh_2$	1.359	-181.2		1473K, reaction calorim.	49
		-181.2		1473K, reaction calorim.	49
$PrRu_2$	1.365	-50.7		1473K, reaction calorim.	49
$PuAl_2$	1.103	-141.9		298K, acid solution calorim.	1
$PuFe_2$	1.209	-27.2		298K, acid solution calori	1
		-51	-6	298K, emf, 880-1100K	2
		-42		emf, 800-1100K	2
$PuOs_2$	1.168	-14.7	6.9	298k, emf, 890-1090K	2
		-105	-29.4	298K, vapor pressure	2
$PuPt_2$	1.139	-189	-45	298K, vapor pressure	2
$PuRu_2$	1.18	-22.2	14.4	298K, emf, 880-1080K	2
		-123		298K, vapor pressure	2
		-108	-25.8	935-1069K, emf	2
$ScAl_2$	1.146	-281.9		298K, acid solution calorim.	50
$ScCo_2$	1.311	-97.5		1473K, calorim.	51
$ScFe_2$	1.288	-33.6		1473K, calorim.	51
$ScIr_2$	1.209	-198.9		1473K, calorim.	51
$ScNi_2$	1.317	-129		1473K,. calorim.	51
$SmAl_2$	1.258	-165			52
		-162.9			24
$SmCo_2$	1.439	-52.5			53
$TaCo_2$	1.172	-84	-0.6	1180-1380K, emf	2
		-82.2		assessment.	54
$TaCo_{2.7}$	1.172	-69	1.5	1270-1380K, emf	2
$TaCo_3$	1.172	-90	-19.5	1160-1275K, emf	2
		-74.4		assessment	54
$TaCr_2$	1.144	-27	-0.9	298K, assessment.	2, 22
		-27	-0.5	298K	21
		-25.6		1693K, direct reaction	1
		-27.7	1.5	1472K, vapor pressure	1
TaV_2	1.09	-3.15		assessment	54
$TbAl_2$	1.244	-157.2			24
$TbIr_2$	1.313	-211.8		1474K, reaction calorim.	55
$TbPt_2$	1.285	-290		1474K, reaction calorim.	55
$TbPt_3$	1.285	-255.6		1474K, reaction calorim.	55
$TbRh_2$	1.325	-193.2		1474K, reaction calorim.	55

Table I (continued)

C15 Phase	R_A/R_B	ΔH kJ/mole	ΔS J/K.mole	Temperature & Method	Ref.
$ThMg_2$	1.122	-31.4	-24.7	298K	21
$ThOs_2$	1.329	-162	-51	1020-1220K, emf	2
$ThRu_2$	1.343	-150	-42	1020-1170K, emf	2
$TiCo_2$	1.168	-102		1432K, calorim.	2
		-93.7	-21.5	assessment	56
$TiCr_2$	1.14	-27.9		unknown	2
		0.3		298K	3
		-9.9		1523-1653K, vapor pressure	2
$TmAl_2$	1.219	-153			24
UAl_2	1.089	-92	-0.15	298K	22
		-98.7	-0.1	298K	3, 21
UCo_2	1.246	-201	-108	1000K, emf, 873-1173K	2
UFe_2	1.224	-32.6	-0.16	298K, calorim.	2, 57
		-32.2	-0.25	298K	21, 22
		-63	0	298K, assessment	2
UIr_2	1.15	-219	-0.9	1000K, emf, 950-1140K	2
UMn_2	1.196	-39	-12	933-1130K, emf	2
UOs_2	1.153	-180	-42	1000K, emf, 950-1140K	2
YAl_2	1.258	-160.4		298K, solution calorim.	58
$YbAl_2$	1.355	-114.6			24
		-109.4			59
YCo_2	1.438	-69	-7.2	850-1200K, emf	2
YFe_2	1.414	-21.3	-3	973K, emf, 893-1271K	2
YIr_2	1.327	-178.2		1473K, reaction calorim.	60
YNi_2	1.445	-117		298K, calorim.	2
		-93	-7.5	87-1224K, emf	2
YRe_2	1.31	-135	-7.5	1000-1180K, emf	2
		-135.8	-7.4	298K	22, 21
YRh_2	1.339	-196.2		1473K, reaction calorim.	60
$ZrCo_2$	1.28	-113		298K, solution calorim.	61
		-123		1798K, calorim.	2
$ZrFe_2$	1.257	-75	21.6	1023K, solubility. in {Mg.}	1, 2
		-71		298K, solution calorim.	62
		-90		1760K, calorim.	2
$ZrIr_2$	1.181	-213.8			63
$ZrMo_2$	1.144	-27.9	-0.9	298K, assessment	2
$ZrNi_2$	1.286	-210	-0.9	1300K, emf	2
$ZrZn_2$	1.149	-159	-84	800K, assessment	1, 2
		-148	-66.7	298K	64

Table II List of R_A/R_B, c/a, experimental ΔH and ΔS, the experimental temperature and methods, and relevant references for binary C14 Laves phases

C14 Alloy	R_A/R_B	c/a	ΔH kJ/mole	ΔS, J/K.mole	Temperature and Method	Ref.
$BaMg_2$	1.4	1.604	-6.3		298K	10
$CaCd_2$	1.259	1.611	-123.3		298K, acid solution calorim.	1
$CaMg_2$	1.232	1.626	-40.17		298K	10, 22
			-39.3	-2.5	298K	3
			-38.9	-3.1	298K	21
$CdCu_2$	1.227	1.609	-6.27		298K	47
$DyRu_2$	1.324	1.684	-81.9		1474K, reaction calorim.	33
$ErRu_2$	1.312	1.679	-78.6		1473K, reaction calorim.	32
$HfAl_2$	1.103	1.654	-131.4		1473K, reaction calorim.	70
			-144	3.6	298K, assessment	2
$HoRu_2$	1.319	1.681	-80.4		1474K, reaction calorim.	37
KNa_2	1.243	1.64	-3.15		280K, Cp measurement	1
$MgCo_2$	1.28	1.629	-23.2	-5.4	800K, vapor pressure	1, 2
			-26	6.6	913-1233K, vapor pressure	2
$MgZn_2$	1.149	1.641	-32.7		298K	10
			-35.1	-8	298K	21
$MoFe_2$	1.099	1.632	-14.1		298K, assessment	2
			-24.3	-12	1160-1223K, emf	2
$NbFe_2$	1.152	1.633	-61.5	-15.5	298K	21
			-72	-13.8	1020-1330K, emf	2
			-54.6	-11.4	assessment	66
			-63	-13.8	298K, emf, 1280-1385K	2
			-164	-36	1300K, assessment	1
$NdRu_2$	1.36		-54		1473K, reaction calorim.	49
$ScMn_2$	1.258	1.645	-54		1100K, calorim.	2
			-51		1100K, calorim.	2
$SrMg_2$	1.343	1.63	-21.3		298K	1, 10
$TaFe_2$	1.151	1.633	-57.7	10.8	298K, assessment	2, 3, 21
			-75	-6.3	1250-1350K, emf	2
$TaMn_2$	1.161	1.633	-19.5		assessment	54
$TbRu_2$	1.331	1.685	-70.8		1474K, reaction calorim.	55
$ThRe_2$	1.308	1.656	-174.1	-1.2	298K	3, 21
			-174	-2.7	880-1020K, emf	2
$TiFe_2$	1.148	1.63	-87.4	-10.8	298K	3, 21
			-84		1514K, calorim.	2
			-63.9		973K, Fe bcc standard	67
			-76.2		1413K, Fe Fcc standard	67

Table II (continued)

C14 Alloy	R_A/R_B	c/a	ΔH kJ/mole	ΔS, J/K.mole	Temperature and Method	Ref.
$TiMn_2$	1.157	1.641	-21	10.5	assessment	71
UNi_2	1.252	1.662	-162	-57	1000K, emf, 1073-1173K	2
			-96		1023K, calorim.	2
WFe_2	1.105		-7.5	-0.9	298K, emf, 1200-1300K	2
			-0.3	3.9	1180-1330K, emf	2
YMg_2	1.124		-42	-9.9	800K, assessment	1, 2
YOs_2	1.331	1.657	-74.4		1473K, reaction calorim.	60
YRe_2	1.31	1.604	-135.8		298K	21
YRu_2	1.345	1.683	-58.5		1473K, reaction calorim.	60
$ZrAl_2$	1.119	1.656	-137.4		vapor pressure	68
			-138		298K, vapor pressure	2
			-170.7		free energy, ΔG	69
			-154		298K, solution calorim.	62
			-152.3		1473K, reaction calorim.	65
$ZrMn_2$	1.229		-48		1215-1381K, vapor pressure	2
$ZrRu_2$	1.196		-177		1800K, assessment	2

Table III List of R_A/R_B, experimental ΔH and ΔS, the experimental temperature and method, and relevant references for binary C36 Laves phases

Alloy	R_A/R_B	ΔH kJ/mole	ΔS kJ/K.mole	Temperature & Method	Reference
$ThMg_2$	1.122	-31.38	-26.3	298K	1, 21, 22
$MgNi_2$	1.286	-55.2	-3.7	298K	10, 22
		-55.7	-2.5	298K, vapor pressure	42
		-54		298K, calorim.	2
		-63	-12.6	923-1033K, vapor pressure	2
$NbCo_3$	1.173	-45	-3.6	298K, emf, 1275-1425K	2
		-36	6	revision of above	2
		-48	-3.9	1350K, assessment	2
		-60	-9.3	1000-1400K, emf	2
$NbZn_2$	1.053	-39	-16.2	1100K, vapor pressure	1, 2

5.1 Effect of Atomic Size Ratio on Enthalpies of Formation

The effect of atomic size ratio, R_A/R_B, on the enthalpy of formation of the C15, C14, and C36 phases is plotted in Figs. 1, 2, and 3. It is very difficult to observe any noticeable trend of the R_A/R_B effect on the enthalpies of formation. However, if we combine all the data together (Fig. 4), a R_A/R_B effect on the enthalpies of formation of Laves phase is revealed. In Fig. 4, two lines have been drawn, which set the low boundary for the enthalpies of formation at different R_A/R_B ratios, except for two data points. Surprisingly, the two lines intersect at R_A/R_B about 1.225, which is the ideal R_A/R_B for Laves phases. Furthermore, on the side where $R_A/R_B < 1.225$, the line intersects with the line, $\Delta H = 0$, at $R_A/R_B = 1.03$, which is about the observed lower limit of R_A/R_B for Laves phases (1.05); on the side where $R_A/R_B > 1.225$, the line intersects with the line, $\Delta H = 0$, at $R_A/R_B = 1.65$, which is about the observed upper limit of R_A/R_B for Laves phases (1.67). The two data points outside the limit are questionable, since they are measured with the less-accurate emf method for $BaPt_2$ [2] and acid-solution calorimetry for $ScAl_2$ [50]. For example, the enthalpy of formation $LaPt_2$ was determined to be -384 kJ/mole by the emf method [2]; however, a recent reaction calorimetric measurement [40] shows that its enthalpy of formation should be -270 kJ/mole, which is much less negative.

Clearly, Fig. 4 gives a thermodynamic interpretation for the observed size ratio limits (1.05-1.67) of Laves phases [72, 73, 74]. Since the entropy of formation is relatively low for Laves phases (see Tables I, II and III), the free energy of formation should be close to the enthalpy of formation for Laves phases, according to Eq. 3. Thus, as the atomic size ratio deviates outside the range of 1.03-1.65, ΔH, and therefore ΔG, will be positive. This means that the compound will be unstable thermodynamically. This explains why there is no Laves phase existing at $R_A/R_B < 1.05$ and $R_A/R_B > 1.67$. In this way, an explanation is offered for the size limitation of Laves phases.

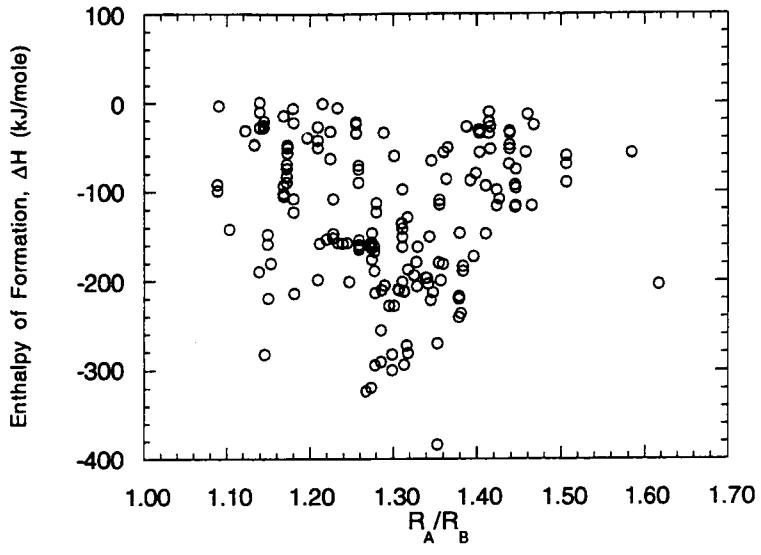


Fig. 1 Enthalpy of formation versus R_A/R_B for C15 Laves phases

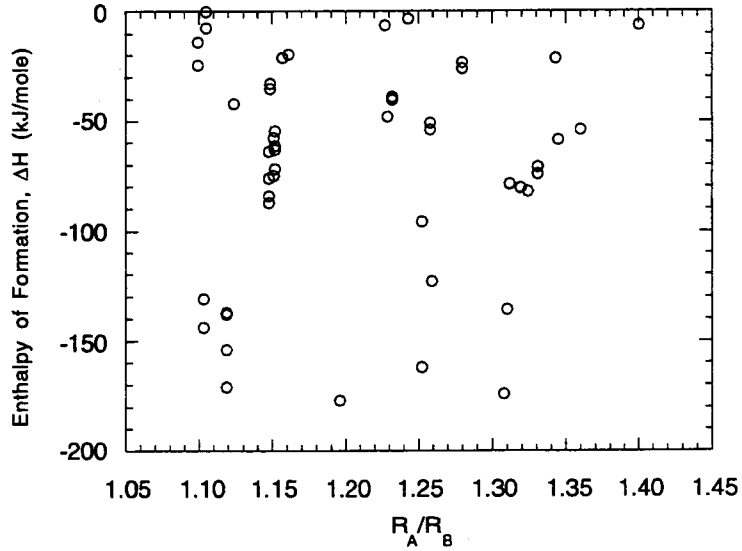


Fig. 2 Enthalpy of formation versus R_A/R_B for C14 Laves phases

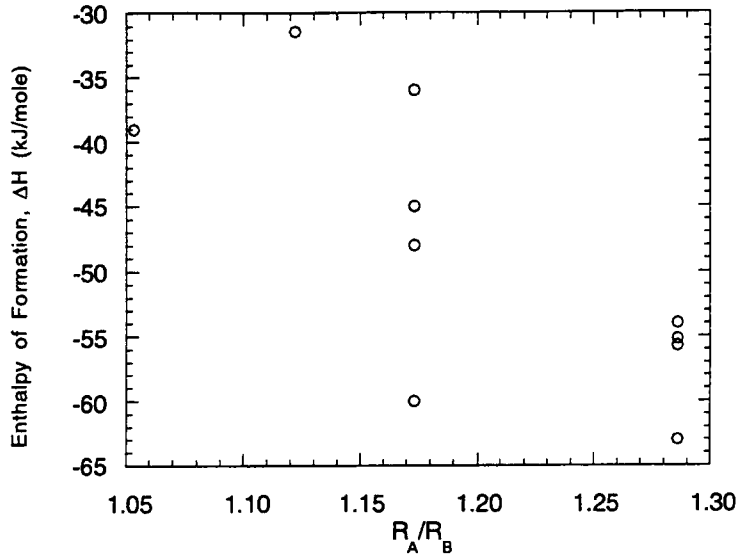


Fig. 3 Enthalpy of formation versus R_A/R_B for C36 Laves phases

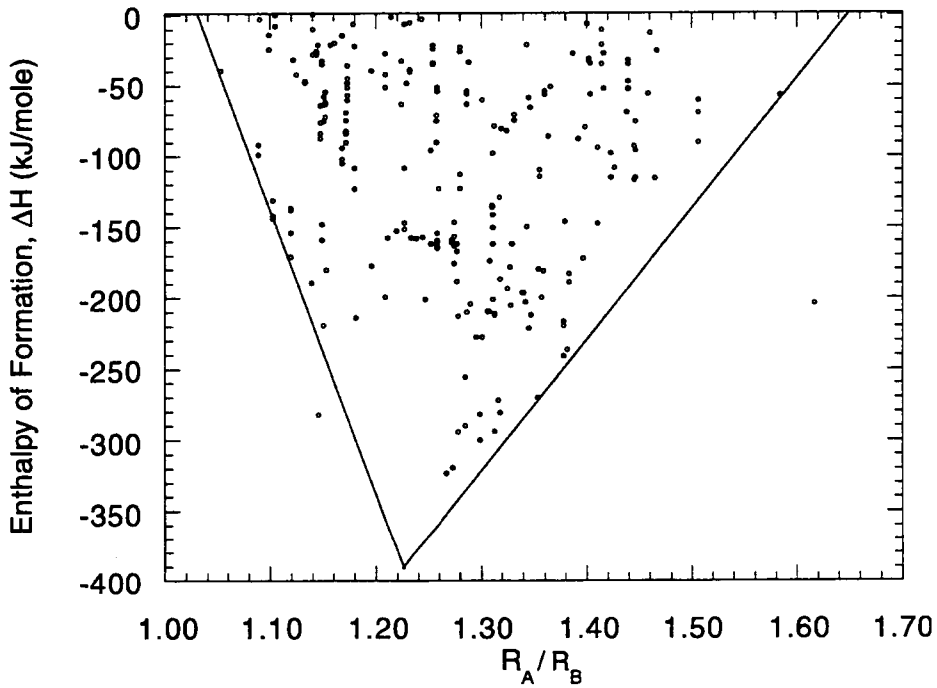


Fig. 4 Enthalpy of formation versus R_A/R_B for C15, C14 and C36 Laves phases

The two lines intersect at the ideal R_A/R_B ratio of 1.225, which means that the most stable Laves phase may be found at the ideal atomic size ratio, due to the highest negative enthalpy of formation attainable. The enthalpy of formation corresponding to the intersection is about -390 kJ/mole, which is the highest value of the negative enthalpy of formation one can obtain for Laves phases. Interestingly, if we increase the deviation for the ideal atomic ratio, the maximum negative enthalpy of formation decreases linearly on both sides with different slopes. The decrease in the maximum negative enthalpy of formation indicates that there are some energies expended for maintaining the structure, which, thus, reduced the total bonding energy. This can be explained by the fact that for Laves phase formation, the geometric facility of packing together the two components in the proportion AB_2 demands that the ratio of their radii, R_A/R_B, is equal to 1.225. If the exact atomic size ratio is different for this ratio, then the sizes of atoms in the compound need to adjust so that the ideal size ratio can be maintained. This introduces an elastic strain energy, which reduces the total bonding energy of the compound. The magnitude of the elastic strain energy increases as the size ratio deviates further from the ideal value.

The absolute values of the slopes of the two lines in Fig. 4 were calculated to be 2000 kJ/mole and 920 kJ/mole, for $R_A/R_B < 1.225$ and $R_A/R_B > 1.225$, respectively. The slope on the side where $R_A/R_B < 1.225$ is about twice that on the side where $R_A/R_B > 1.225$. It is understood from Pearson's work [74], that for atomic size ratios greater than the ideal value of 1.225, the A atoms will be compressed, and for atomic size ratios smaller than the ideal, the B atoms will be compressed. Since there are two B atoms and one A atom per formula unit, the elastic strain energy will be twice for atomic size ratios smaller than ideal, as compared to that for the atomic size ratio greater than ideal. Thus, the negative enthalpy of formation decreases faster on the side where $R_A/R_B < 1.225$ than on the side where $R_A/R_B > 1.225$ and the slope difference is thus explained. From the data in Fig. 4, the strain energy to compress atoms can be calculated to be around 10 kJ/mole.%.

Ellner and Predel [4] found that the value of the negative enthalpy of formation increases with increasing deviation from the "ideal" axial ratio c/a = 8/3, i.e., larger hexagonal distortions cause higher stability of the phase isotypical with $MgZn_2$. Their observation is based on a very limited number of the C14 phases. To verify if this observation is correct generally or just an artifact due to limited number of data they used, we plotted the enthalpy of formation versus axial ratio, c/a, for all the C14 phases listed in Table II, as shown in Fig. 5. No general trend regarding the effect of c/a on the enthalpy of formation can be discerned from this plot. It is clear that the observation by Ellner and Predel is just an artifact due to the limited formation enthalpy data used in their plot. Actually, there is no reason why larger hexagonal distortions should cause higher stability of the C14 phases. The large hexagonal distortions will introduce elastic energies in the compounds, leading to the reduction in the bond strength and enthalpy of formation in the Laves phases, as discussed above.

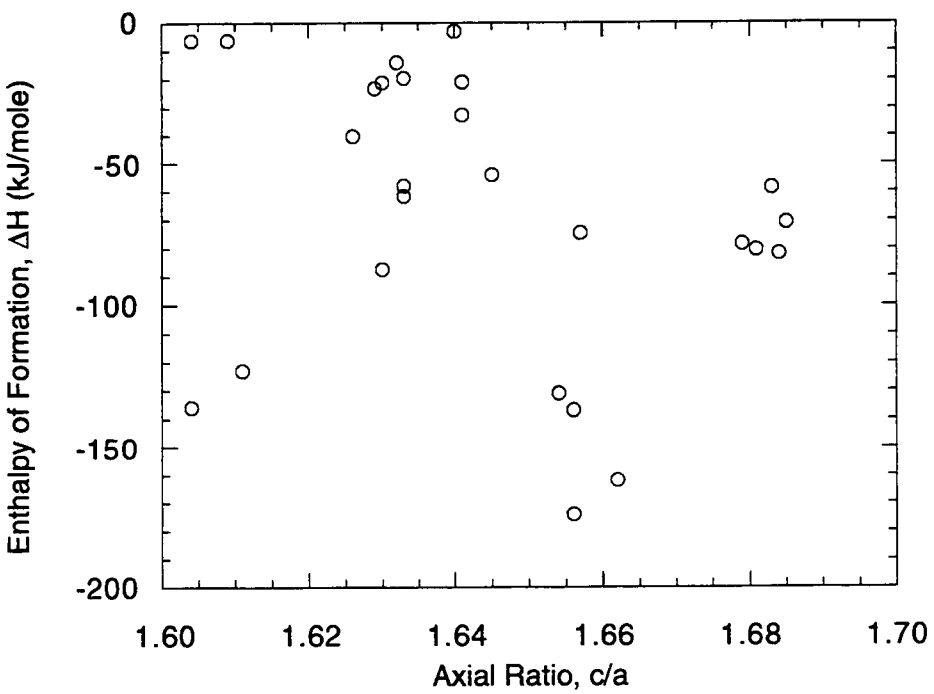


Fig. 5 Enthalpy of formation versus the axial ratio c/a for C14 Laves phases

According to the classification of the bond strength for different bonds [9], it is clear that the bond in Laves phases is not necessarily metallic in nature. Since the observed enthalpies of formation varied from 0 to about -350 kJ/mole, metallic, covalent, and ionic bonds may be present in different Laves phases. Actually, ionic bond has been suggested to increase the stability of transition-metal containing Laves phases [10, 11], while several researchers have provided a covalent view of chemical bond [75, 76] in some Laves phases. Thus, it can be concluded that, most likely, the bond characteristics in Laves phases are very complicated, and should be a mixed metallic-covalent-ionic bond in nature.

5.2 Enthalpies of Formation in Non-Transition Metal Laves Phases

Usually, Laves phases that contain transition metals have extraordinarily high values (negative) of enthalpies of formation. The reason for this behavior is the transfer of electrons from the second component to the transition element, to fill up the incompletely filled inner shells, as King and Kleppa [10] and Wernick et al. [11] originally proposed. Owing to this charge transfer, Coulomb interactions were realized, which raised the stability. On the other hand, if a non-transition metal is involved in the Laves phase, it was observed that the bonding strength and enthalpy of formation of the Laves phases will be relatively low [10], due to the fact that no electron transfer happens and the bonding is metallic in nature.

We reevaluated the bond characteristics using the enthalpy of formation data listed in Table I, II and III. Figure 6 shows the enthalpy of formation versus atomic size ratio, R_A/R_B, for the Laves phases which involve non-transition metals only. First, it is noted that the enthalpy of formation is not necessarily low in the non-transition metal Laves phases. The enthalpy of formation ranges from 0 to -250 kJ/mole. This indicates that there are other bonds existing beside the metallic bond. There is no clear indication that as the R_A/R_B deviates from the ideal value, the enthalpy of formation decreases, as noted by King and

Kleppa [10]. If there are only metallic bond in the Laves phases, the enthalpy of formation will decrease, as the R_A/R_B deviates form the ideal one, due to the increased elastic strain energy, as we discussed above and also by King and Kleppa [10].

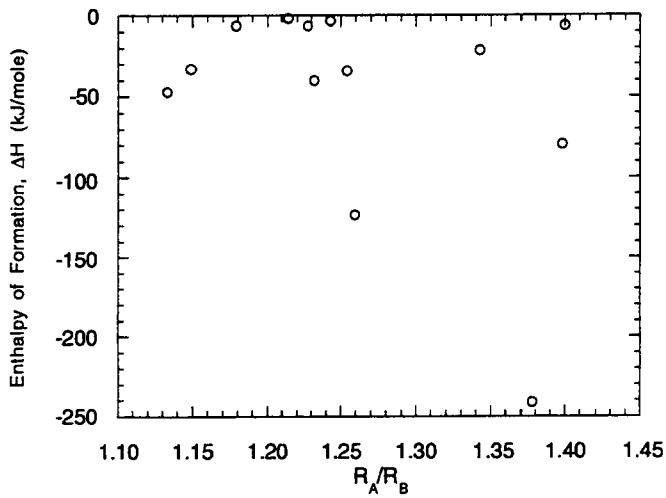


Fig. 6 Enthalpy of formation versus R_A/R_B for non-transition metal Laves phases

Clearly, the bond characteristics in non-transition metal Laves phases are not as simple as originally thought. There are also ionic and/or covalent bonds existing in the Laves phases. If their bonds are mainly ionic in nature, one would expect a relationship between the enthalpy of formation and the electronegativity difference between the two components in the Laves phase. Figure 7 plots the enthalpy of formation versus the Pauling electronegativity difference. No clear trend can be discerned from this plot. Obviously, for non-transition metal Laves phases, the covalent bond is also important for those Laves phases with large enthalpy of formation. Actually, Nesper and Miller [76] calculated the electronic band structure of $CaLi_xAl_{2-x}$ Laves phase system using the extended Hückel theory within the framework of the tight-binding approximation to examine the local chemical bonding effects. They provided a covalent view of the chemical bonding in the $CaLi_xAl_{2-x}$ Laves phases.

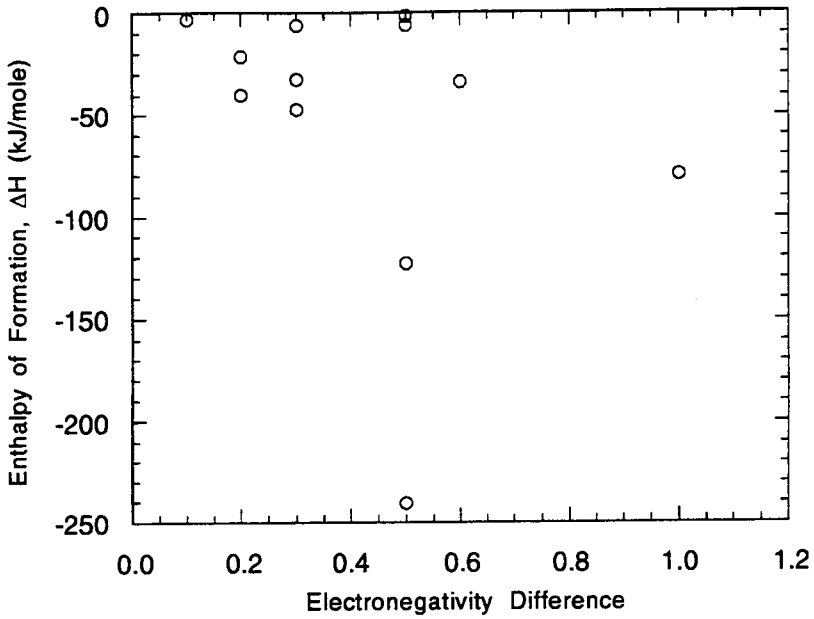


Fig. 7 Enthalpy of formation versus the difference in electronegativity of the two components for non-transition metal Laves phases

5.3 Enthalpies of Formation in Transition-Metal Laves Phases

As mentioned in the previous section, electron transfer is possible in transition metal containing Laves phases, leading to the formation of ionic bond. However, this possibility does not mean that an ionic bond necessarily exists in the Laves phases. Some other requirements must also be met for ionic bond to form in the transition-metal Laves phases.

This can be understood from the fact the enthalpy of formation of transition-metal Laves phases can be as low as -5.4 kJ/mole for $HfCr_2$, see Table I. Even though the elastic strain energy from the atom-size adjustment may reduce the enthalpy of formation, the Laves phases, such as $HfCr_2$, have a R_A/R_B ratio of 1.23, which does not deviate much from the ideal one. Therefore, depending on the actual systems, the bonding characteristics can be metallic, covalent, and ionic again.

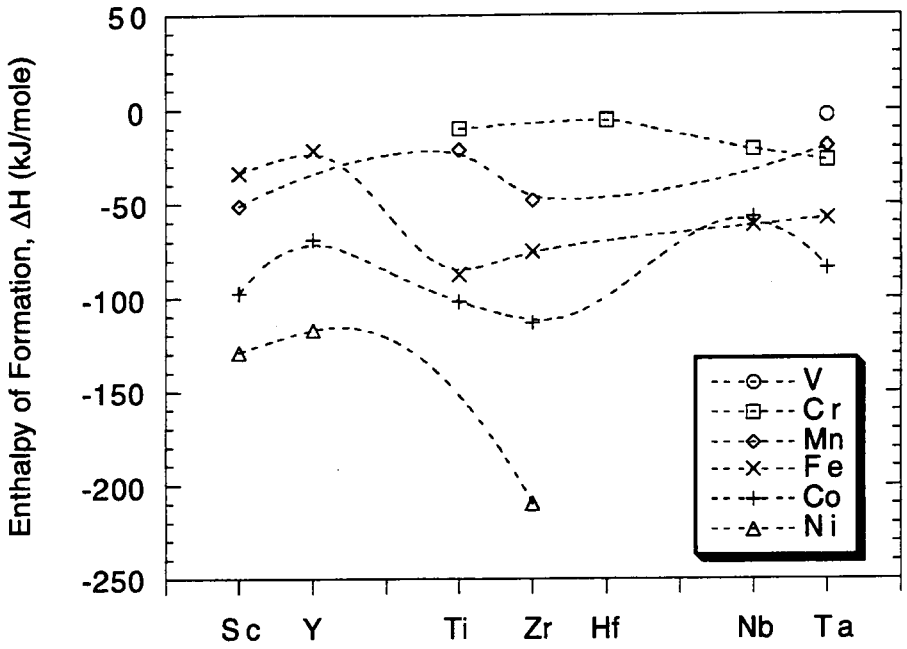


Fig. 8 Enthalpy of formation in transition-metal Laves phases

Some general trends in the enthalpy of formation can be found in Laves phases formed between early transition metals and later transition metals, as indicated in Fig. 8. When the atomic number increases for the later transition metal, the enthalpies of formation increase in the order of V > Cr > Mn > Fe > Co > Ni, for Laves phases formed between early transition metals and these elements. As the atomic number increases from V to Ni, the d-band electrons and the average electron concentration in the Laves phases increase correspondingly. This may indicate that the enthalpy of formation may also be related to the average electron concentration in the Laves phases.

5.4 Enthalpies of Formation in Laves Phases Involving Rare Earth Elements

The transition-metal lanthanide Laves phases and Al lanthanide Laves phases, usually having the C15 structure, are receiving more attention recently. The transition-

metal lanthanide Laves phases have unique magnetic properties. In particular, the alloy Terfenol-D, which is essentially a Laves phase having the composition $Tb_{0.27}Dy_{0.73}Fe_2$, has large magnetostriction [77, 78]. The lanthanide aluminum Laves phases are being developed for hydrogen storage materials [79]. Hydrogen-induced amorphization of the rare earth lanthanide-containing Laves phases has also been studied as a method to develop amorphous alloys [80, 81, 82]. Despite their interesting properties of these alloys, the basic thermodynamic properties and phase diagram information are very scare or incomplete owing to experimental difficulties. Sommer and Keita observed that the glass-forming ability of rare earth lanthanide-containing alloys may be related to thermodynamic behavior of the stable phases [23]. Obviously, the thermodynamic data are of great importance in calculations of binary or ternary phase diagrams and in theoretical predictions of the glass-forming ability.

The enthalpies of formation of the Laves phases depend more on the transition metal than on the lanthanide. Figure 9 shows the experimental enthalpies of formation for 3d transition metal lanthanide Laves phases RFe_2, RCo_2, and RNi_2 as a function of lanthanide atomic number. Figure 10 presents the experimental enthalpies of formation for 4d transition metal lanthanide Laves phases RRu_2 and RRh_2 as a function of lanthanide atomic number. Figure 11 shows the experimental enthalpies of formation for 5d transition metal lanthanide Laves phases ROs_2, RIr_2 and RPt_2 as a function of lanthanide atomic number. Obviously, the enthalpies of formation of the Laves phases decrease slightly from La to Lu, i.e., as the atomic number of lanthanide increases. As the d-electron number increases, the enthalpies of formation of the Laves phases become more negative, i.e. the laves phases are more stable. For the same column VIII transition metal lanthanide Laves phases, the enthalpies of formation increases from 3d to 4d to 5d transition metal Laves phases, as shown in Figs. 12-14.

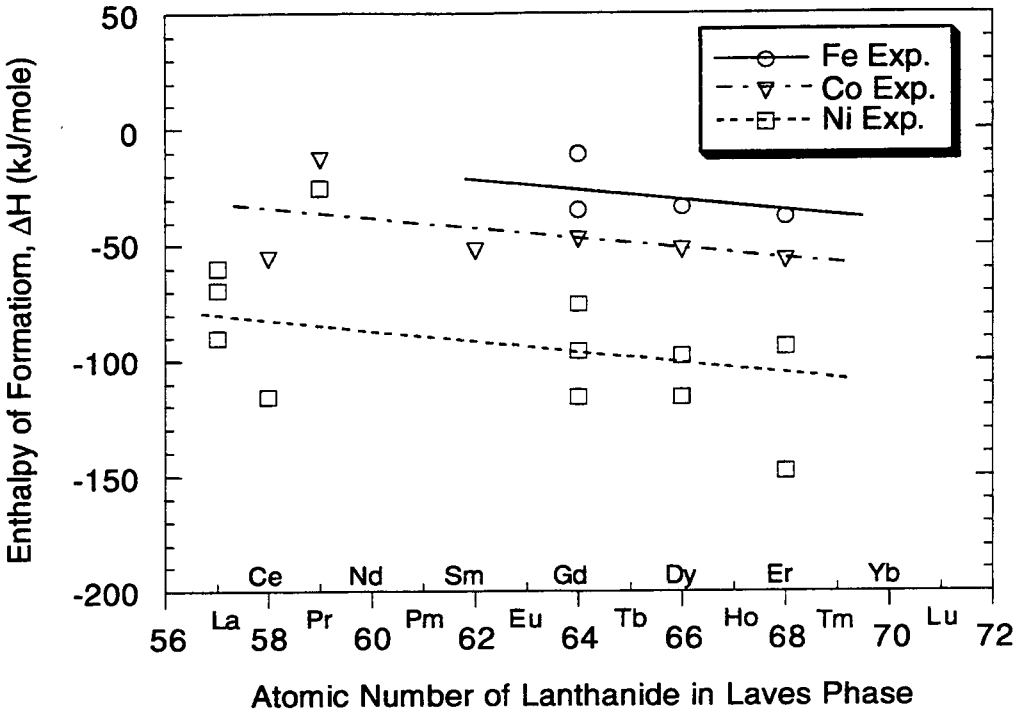


Fig. 9 Experimental enthalpy of formation for 3d transition metal lanthanide Laves phases as a function of lanthanide atomic number

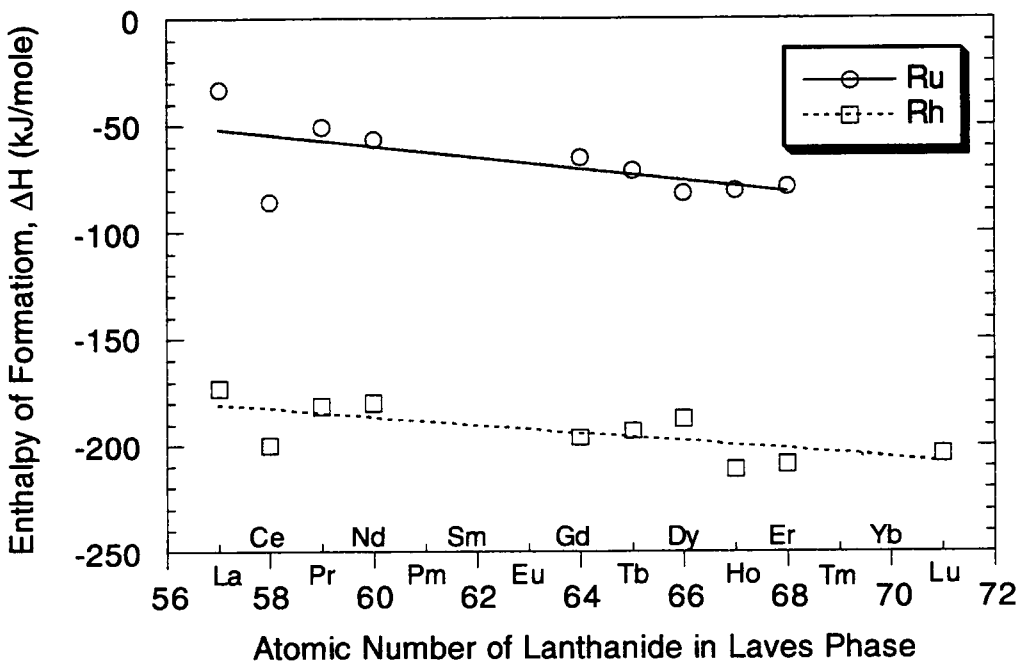


Fig. 10 Experimental enthalpy of formation for 4d transition metal lanthanide Laves phases as a function of lanthanide atomic number

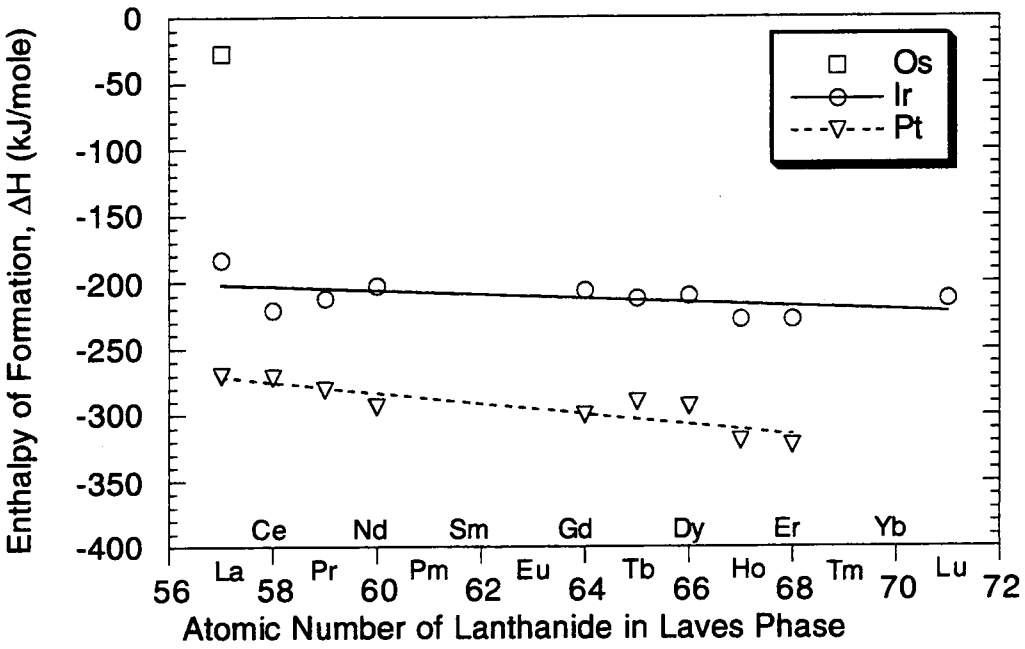


Fig. 11 Experimental enthalpy of formation for 5d transition metal lanthanide Laves phases as a function of lanthanide atomic number

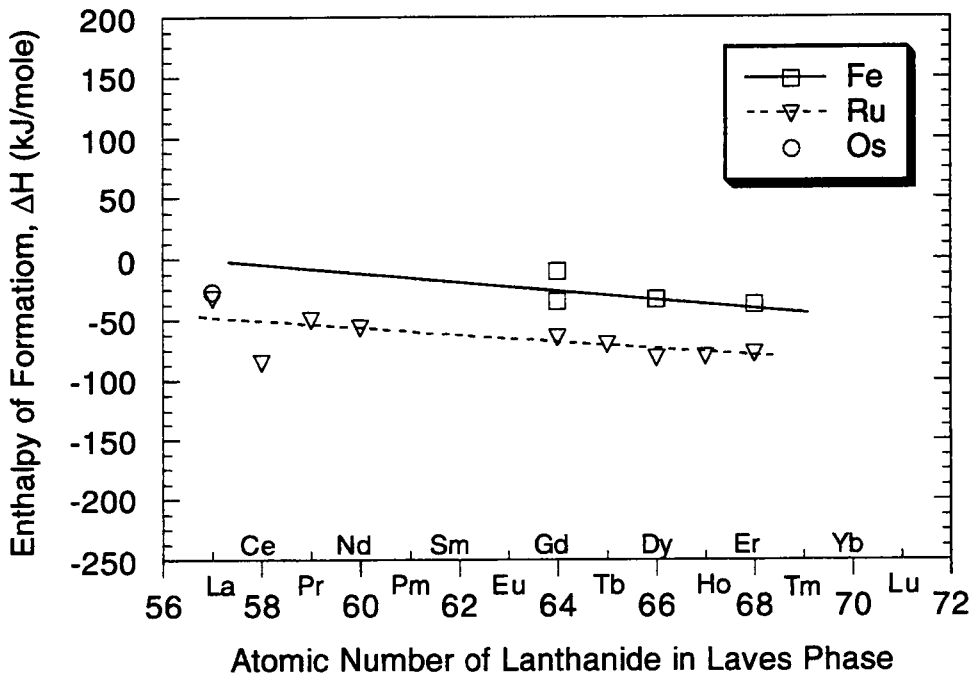


Fig. 12 Experimental enthalpy of formation for VIII transition metal (Fe, Ru, and Os) lanthanide Laves phases as a function of lanthanide atomic number

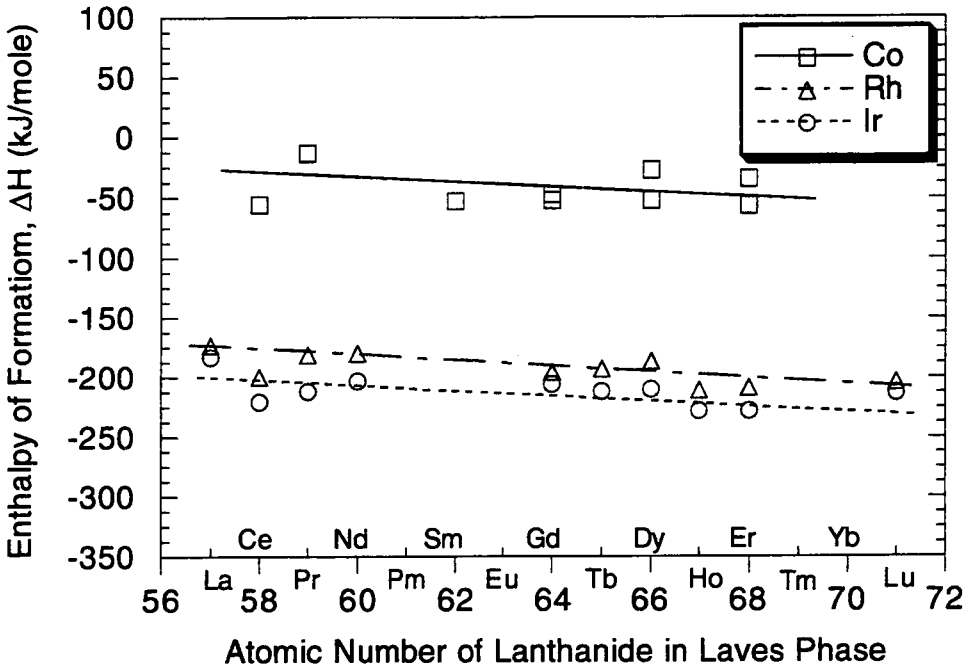


Fig. 13 Experimental enthalpy of formation for VIII transition metal (Co, Rh, and Ir) lanthanide Laves phases as a function of lanthanide atomic number

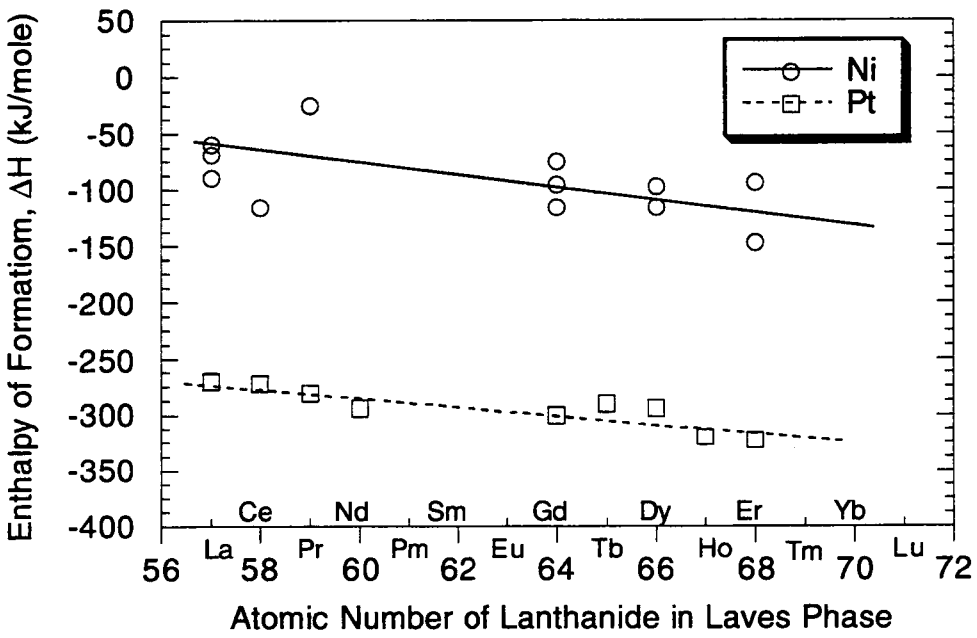


Fig. 14 Experimental enthalpy of formation for VIII transition metal (Ni and Pt) lanthanide Laves phases as a function of lanthanide atomic number

The predicted enthalpies of formation for the RFe_2, RCo_2, and RNi_2 Laves phases were calculated using the semiempirical Miedema method [2, 16], Eqs. 4 - 6 and are plotted in Fig. 15. It can be seen that calculated enthalpies of formation are generally in agreement with the experimental data (see Fig. 9), i.e., the enthalpy of formation becomes more negative from RFe_2 to RNi_2. However, the calculated data are generally more negative than the experimental data. It is interesting to note that for Eu and Yb containing Laves phases, there is a peak in the predicted curve, i.e., the enthalpies of formation for these Laves phases is much less negative than other Laves phases. This can be understood by the fact that these two elements are preferentially divalent in compounds and, thus, some additional energy would be needed to make it trivalent, which is necessary in the Laves phase. This reduced the enthalpies of formation for these Laves phases. Unfortunately, no experimental data are available to verify this prediction.

Figure 16 shows the enthalpies of formation of RAl_2 Laves phases. Both experimental data and predicted data using Miedema's model [83] are included. Both the experimental and predicted values keep constant, as the atomic number of lanthanide in Laves phase increases. Furthermore, both the experimental and predicted curves show peaks for Eu and Yb containing Laves phases, which is due to the valency of these two elements. These indicates that Miedama's model captures the main feature of the enthalpy of formation of RAl_2 Laves phases. However, the predicted values are more negative than the experimental ones.

All the above results demonstrate that the bond characteristics in forming lanthanide-aluminum and lanthanide-transition metal Laves phases are independent on the rare earth elements, except for Eu and Yb containing Laves phases. This can be used to predict the unknown enthalpies of formation for Laves phases containing lanthanide elements.

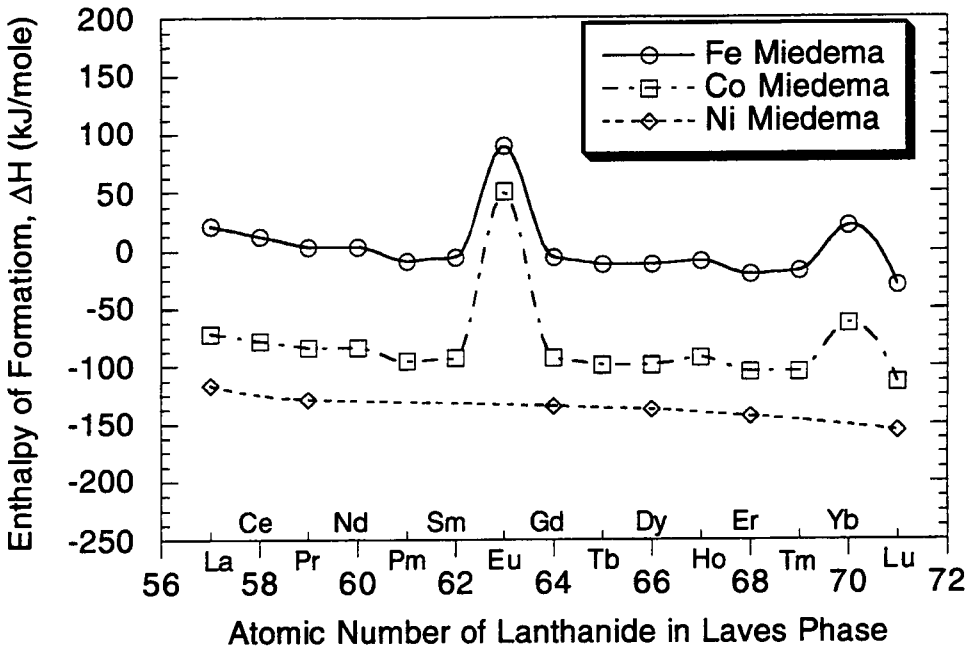


Fig. 15 Predicted enthalpy of formation for 3d transition metal lanthanide Laves phases as a function of lanthanide atomic number by Miedema's method

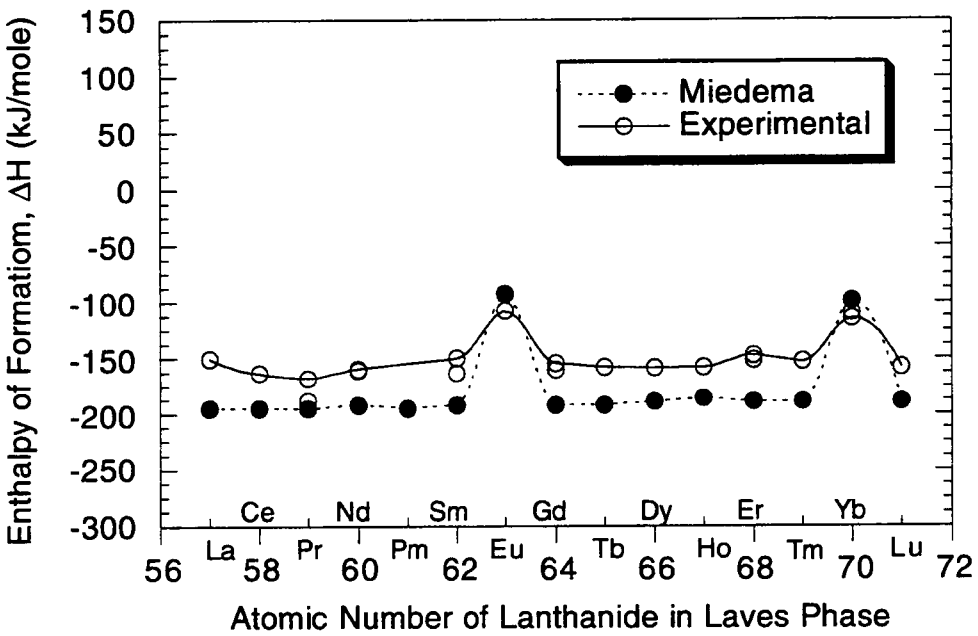


Fig. 16 Predicted enthalpy of formation for aluminum lanthanide Laves phases as a function of lanthanide atomic number by Miedema's method

6. SUMMARY

Enthalpies of formation of Laves phases have been critically surveyed and reviewed. It was found that the bond characteristics in Laves phases are not necessarily metallic in nature for both non-transition metal Laves phases and Laves phases containing transition metals. There are metallic, covalent and ionic bonds, or a mixed metallic-covalent-ionic bond. A thermodynamic interpretation is offered to explain the size ratio limits for Laves phase formation. As the deviation from the ideal size ratio increases, the maximum negative enthalpy of formation decreases linearly, which is assumed to be due to the elastic strain energy expended in compressing the atoms. At R_A/R_B =1.03 and 1.65, the enthalpy of formation reaches zero. Further deviation in the R_A/R_B ratio will lead to the enthalpy of formation positive. Thus, the free energy of formation becomes positive, due to the negligible entropy of formation term. Therefore, Laves phases can only be stabilized in certain atomic size, R_A/R_B, ratios.

The enthalpies of formation calculated by the semiempirical Miedema model is in good agreement with the available experimental data for transition-metal and Al lanthanide Laves phases. This means that Miedema's theory can be used to predict quantitatively, at least qualitatively, the enthalpies of formation of transition-metal and Al lanthanide Laves phase systems.

REFERENCES

1. R. Hultgren, P.D. Desai, D.T. Hawkins, M. Gleiser and K.K. Kelly, *Selected Values of the Thermodynamic Properties of Binary Alloys*, ASM, Metals Park, OH (1973).
2. F.R. de Boer, R. Boom, W.C. M. Mattens, A.R. Miedema, and A.K. Niessen, *Cohesion in Metals Transition Metal Alloys*, F. R. de Boer and D. G. Pettifor, eds., vol. 1, Second Corrected Printing, North Holland Physics Publishing, Amsterdam (1989).
3. O. Kubaschewski, C.B. Alcock, and P.J. Spencer, *Material Thermochemistry*, Sixth Edition, Pergamon Press, Oxford (1993).
4. M. Ellner and B. Predel, in *Intermetallic Compounds: Vol. 1, Principles*, J. H. Westbrook and R. L. Fleischer, eds., John Wiley & Sons Ltd. (1994) 91.
5. O. Kubaschewski and W.A. Dench, Acta Metall. 3 (1955) 338.
6. O.J. Kleppa, J. Phys. Chem. 59 (1955) 175.
7. O.J. Kleppa and L. Topor, Thermochim. Acta 139 (1989) 291.
8. C. Wagner, in *The Physical Chemistry of Metallic Solutions and Intermetallic Compounds*, N.P.L. Symposium No. 9, 1, 3K, 14, H.M.S.O., London (1959).
9. P.M. Robinson and M.B. Bever, in *Intermetallic Compounds*, J. H. Westbrook, ed., John Wiley & Sons, Inc. (1967) 38.
10. R.C. King and O.J. Kleppa, Acta Metall. 12 (1964) 87.
11. J.H. Wernick, S.E. Haszko, and D. Dorsi, J. Phys. Chem. Solids 23 (1962) 567.
12. U. Dehlinger and G.E.R. Schulze, Z. Metallkd. 33 (1941) 157.

13. O. Kubaschewski, in *The Physical Chemistry of Metallic Solutions and Intermetallic Compounds*, N.P.L. Symposium No. 9, 1, 3C, 2, H.M.S.O., London (1959).

14. A. Pasturel, P. Hicter, and F. Cyrot-Lackmann, Solid State Commun. 48 (1993) 561.

15. C. Colinet and A. Pasturel, CALPHAD 11 (1987) 335.

16. C. Colinet and A. Pasturel, J. Less-Common Met. 119 (1986) 167.

17. A.K. Niessen, F.R. de Boer, R. Boom, P.F. de Chatel, W.C.M. Mattens, and A.R. Miedema, CALPHAD 7 (1983) 51.

18. L. Pauling, *The Nature of the Chemical Bond*, 3rd Ed., Cornell Univ. Press, New York (1960).

19. A.R. Miedema, R. Boom, and F.R. de Boer, J. Less-Common Met. 41 (1975) 283.

20. O. Kubaschewski and G. Heymer, Trans. Farad. Soc. 56 (1960) 473.

21. Thermo-Calc Database, (1998).

22. I. Barin, *Thermochemical Data of Pure Substances*, 2nd Edition, VCH, New York (1993).

23. F. Sommer and M. Keita, J. of Less-Common Met. 136 (1987) 95.

24. C. Colinet, A. Pasturel, K.H.J. Buschow, J. Chem. Thermodyn. 17 (1985) 1133.

25. G. Borzone, A.M. Cardinale, G. Cacciamani, R. Ferro, Metall. Trans. 22A (1991) 2119.

26. K.N. Semenenko, R.A. Sirotina, A.P. Savchenkova, and T.S. Ill'ma, Russ. J. Phys. Chem. 56 (1982) 1564.

27. N. Selhaoui and O.J. Kleppa, Z. Metallkd. 84 (1993) 11.

28. B.P. Reddy, R. Babu, K. Nagarajan, P.R.V. Rao, J. of Nuclear Materials 247 (1997) 235.

29. J. Schott and F. Sommer, J. of Less-Commom Met. 119 (1986) 307.

30. S.S. Deodhar and P.J. Ficalora, High Temp. Sci. 8 (1976) 185.

31. S. Norgren, F. Hodaj, P. Azay, and C. Colinet, Metall. Mater. Trans. 29A (1998) 1367.

32. Qiti Guo and O.J. Kleppa, Z. Metallkd. 87 (1996) 10.

33. C. Colinet, A. Pasturel, K.H.J. Buschow, Physica B 150 (1988) 397.

34. C. Colinet, A. Pasturel, K.H.J. Buschow, Metall. Trans. 18A (1987) 903.

35. S.S. Deodhar and P.J. Ficalora, Metall. Trans. 6A (1975) 1909.

36. Qiti Guo and O.J. Kleppa, J. of Alloys and Compounds 221 (1995) 45.

37. Qiti Guo and O.J. Kleppa, J. of Alloys and Compounds 234 (1996) 280.

38. W.-G. Jung, O.J. Kleppa, and L. Topor, J. of Alloys and Compounds 176 (1991) 309.

39. F. Sommer, M. Keita, H.G. Krull, B. Predel, J. of Less-Common Met. 137 (1988) 267.

40. N. Selhaoui and O.J. Kleppa, J. of Alloys and Compounds 191 (1993) 155.

41. S.V. Meschel and O.J. Kleppa, J. of Alloys and Compounds 217 (1995) 235.

42. J.F. Smith and J.L. Christian, Acta Metall. 8 (1960) 249.

43. B. Predel and H. Ruge, Mater. Sci. Eng. 9 (1972) 333.

44. J.F. Martin, F. Mueller, and O. Kubaschewski, Trans. Faraday Soc. 66 (1970) 1065.

45. G. Borzone, A.M. Cardinale, G. Cacciamani, R. Ferro, Z. Metallkd. 84 (1993) 635.

46. Qiti Guo and O.J. Kleppa, Metall. Mater. Trans. 26B (1995) 275.

47. O.J. Kleppa, J. Phys. Chem. 60 (1956) 852.

48. G. Canneri and A. Rossi, Gazz. Chim. Ital. 63 (1933) 182.

49. Qiti Guo and O.J. Kleppa, Metall. Mater. Trans. 25B (1994) 73.

50. I.N. Pyagai and A.V. Vakhobov, Russian Metallurgy 5 (1990) 50.

51. N. Selhaoui and O.J. Kleppa, J. of Alloys and Compounds 191 (1993) 145.

52. G. Borzone, A.M. Cardinale, G. Cacciamani, R. Ferro, J. of Alloys and Compounds 220 (1995) 122.

53. A.L. Shilov, Russ. J. Phys. Chem. 61 (1987) 719.

54. L. Kaufman, CALPHAD 15 (1991) 243.

55. Qiti Guo and O. J. Kleppa, J. of Alloys and Compounds 221 (1995) 50.

56. L. Kaufman and H. Nesor, CALPHAD 2 (1978) 81.

57. V.V. Akhachinski, L.M. Kopitin, M.I. Ivanov, and N.S. Podolskaya, *Thermodynamics of Nuclear Materials*, International Atomic Energy Agency, Vienna, (1962).

58. V.S. Timofeev, A.A. Turchanin, A.A. Zubkov, I.A. Tomilin, Thermochimica Acta 299 (1997) 37.

59. A. Pasturel, C. Chatillon-Colinet, A. Percheron-Guegen, and J.C. Achard, J. of Less-Common Met. 90 (1983) 21.

60. N. Selhaoui and O.J. Kleppa, J. Chim. Phys. 90 (1993) 435.

61. R. Klein, P.A.G. O'Hare, and I. Jacob, J. of Alloys and Compounds 261 (1997) 204.

62. R. Klein, I. Jacob, P.A.G. O'Hare, and R.N. Goldberg, J. Chem. Thermodyn. 26 (1994) 599.

63. J.C. Gachon, J. Charles, and J. Hertz, CALPHAD 9 (1985), 29.

64. P. Chiotti and G.R. Kilp, Trans. Met. Soc. AIME 218 (1960) 41.

65. S.V. Meschel and O.J. Kleppa, J. of Alloys and Compounds 191 (1993) 111.

66. L. Kaufman and H. Nesor, CALPHAD 2 (1978) 55.

67. K.C.H. Kumar, P. Woollants, and L. Delaey, CALPHAD 18 (1994) 223.

68. R.J. Kematic and H. Franzen, J. Solid State Chem. 54 (1984) 226.

69. A. Schneider, H. Klotz, J. Stendel, and G. Straus, Pure Appl. Chem. 2 (1961) 13.

70. S.V. Meschel and O.J. Kleppa, J. of Alloys and Compounds 197 (1993) 75.

71. L. Kaufman, CALPHAD 2 (1978) 117.

72. A.E. Dwight, Trans. Amer. Soc. Met. 53 (1961), 479.

73. M.V. Nevitt, in *Electronic Structure and Alloy Chemistry of the Transition Elements*, P.A. Beck, ed., Interscience Publishers, New York (1963) 101.

74. W.B. Pearson, Acta Cryst. B24 (1968) 7.

75. J. Hafner, *From Hamiltonians to Phase Diagrams*, Springer, Heidelberg (1987).

76. R. Nesper and G.J. Miller, J. of Alloys and Compounds 197 (1993) 109.

77. D.C. Jiles, J. Phys. D.: Appl. Phys. 27 (1994) 1.

78. J.D. Verhoeven, E.D. Gibson, O.D. McMasters, and H.H. Baker, Metall. Trans. 18A (1987) 223.

79. K.H.J. Buschow, Mater. Res. Bull. 19 (1984) 935.

80. X.L. Yeh, K. Samwer, and W.L. Johnson, Appl. Phys. Lett. 42 (1983) 242.

81. K. Aoki, T. Yamamoto, and T. Masumoto, Scripta Metall. 21 (1987) 27.

82. Y.G. Kim, S.M. Lee, and J.Y. Lee, J. Less-Common Met. 169 (1991) 245.

83. Y. Ouyang, B. Zhang, Z. Jin, and S. Liao, Z. Metallkd. 87 (1996) 10.

PART V: POINT DEFECTS IN BINARY LAVES-PHASE ALLOYS

1. INTRODUCTION

1.1 Point Defects in B2 Compounds

Intermetallic phases formed from two or more component elements rarely exist as line compounds, i.e., at a single stoichiometric composition. Since a perfectly ordered structure may be obtained only at a temperature of 0°K, any intermediate phase even with a narrow homogeneity range must possess thermally activated structural defects at any finite temperature [1]. Furthermore, the existence of intermetallic phases at non-stoichiometric compositions must also be accompanied by the formation of defects which are called constitutional defects.

There have been many studies conducted to elucidate point defects in B2 compounds. Available experimental evidence shows that two types of defects occur in B2 phases as a function of stoichiometry: triple defects and anti-site defects.

When two component elements, A and B, interact in equiatomic amounts to form an ordered phase AB (where B is the larger atom) with the B2 structure, all A atoms occupy the α-sites [0, 0, 0] and all B atoms occupy the β-sites [1/2, 1/2, 1/2]. In triple-defect B2 phases, for each A atom occupying a β-site (the wrong site), two vacancies are formed on α-sites; in anti-site defect B2 phases, for each A atom occupying a β-site, one B atom occupies an α-site. These defects are termed thermal or intrinsic defects of the lattice. However, many of the B2 phases with either type of defect exist over wide ranges of composition. Deviations from the stoichiometric composition are achieved by the formation of additional constitutional or extrinsic defects. In triple-defect B2 phases, with an excess of B atoms over the stoichiometric composition, additional vacancies are formed on the α-sites; with an excess of A atoms over the stoichiometric composition, additional A

atoms occupy the β-sites. Some examples of phases which exhibit the triple defect structure include NiAl, CoAl, FeAl, NiGa, and CoGa. In anti-site defect B2 phases, deviations from the stoichiometric compositions are accompanied by the incorporation of additional A or B atoms on the β-sites or α-sites, respectively. Some examples of phases which exhibit the anti-site defect structure include AgMg, AuZn, CuZn, and FeCo.

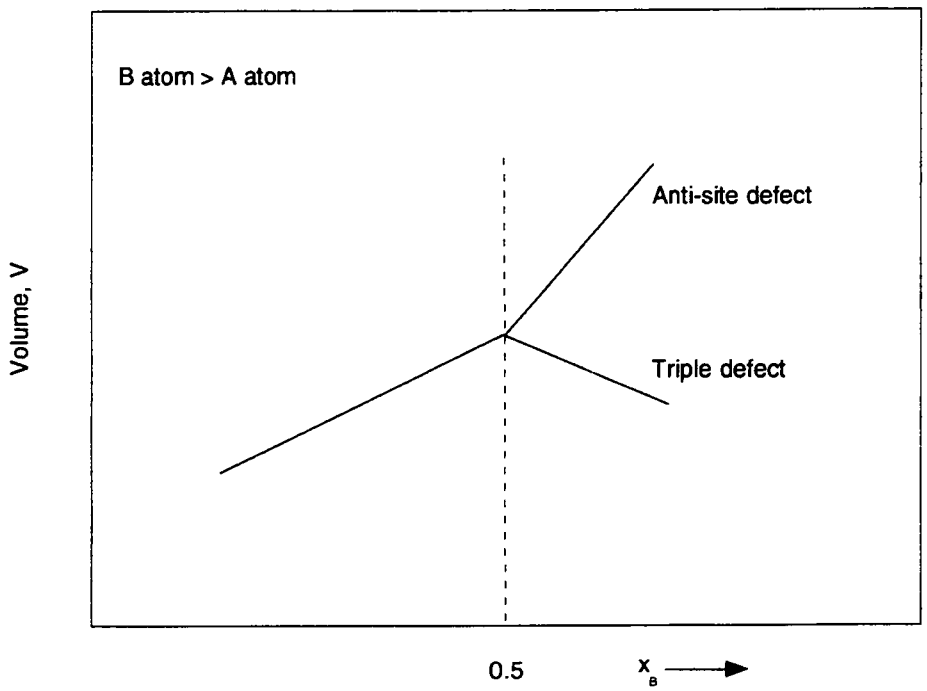


Fig. 1 The difference in the shapes of the unit cell volume vs. composition curves between anti-site defect and triple defect B2 compounds [1]

The defect structure can be predicted from the consideration of the lattice parameter and volume of the compound as a function of composition. The compositional variation of the atomic volume, V, of the intermetallic phases, shown schematically in Fig. 1, demonstrates unambiguously the two different types of defects. The example shown in Fig. 1 is for the case when $V_B > V_A$. For both types of defects, V increases smoothly with the composition up to $x_B = 0.5$. However, for $x_B > 0.5$, the slope will be larger in the case

of anti-site defects, but it will be smaller in the case of triple-defects due to the formation of vacancies.

The vacancy concentration of a given compound, c_V, which is defined as the ratio of the total number of vacancies to the total number of atoms, can be obtained from the following equation [1]:

$$c_V = \frac{\rho_X - \rho_B}{\rho_B} \qquad (1)$$

where ρ_X and ρ_B are the X-ray density and the bulk density, respectively. The X-ray density is calculated from the lattice parameter by assuming all lattice sites are occupied. The bulk density is usually measured by hydrostatic or pycnometric methods. In addition to being relatively simple to perform, this technique has the added benefit of being straightforward to interpret. Other techniques, such as electrical resistivity, dilatometry, perturbed angular correlation (PAC), X-ray diffraction, positron annihilation, magnetic susceptibility, and others, can also provide useful information, even though no quantitative information concerning the vacancy concentration can be obtained from these studies.

1.2 Point Defects in Laves Phases and the Objective of This Study

Laves phases are a common type of topologically close-packed (TCP) structures [2-4]. They are generally considered to be line compounds at a strict AB_2 composition. However, solubility ranges exist for about 25% of the known binary Laves phases [5]. For non-stoichiometric compositions, constitutional defects are incorporated into intermetallic compounds, as discussed in Section 1.1. However, for the Laves phases, little is known about the possible defect structures that may be associated with the solubility at off-stoichiometric compositions. It has been postulated that the A-rich side is accommodated by vacancies, while the B-rich compositions result from the anti-site substitution [5]. Since the A atom is much larger than B atom, at the A-rich side, the extra

A atoms will tend to stay on their own sublattice sites, thus creating vacancies on the B atom sublattice; at the B-rich side, the extra B atoms will be able to occupy the A atom sublattice sites, leading to the formation of anti-site defects.

The types of constitutional defects may affect physical, mechanical and functional properties of Laves phases. Vacancies have been proposed to assist the movement of synchro-Shockley dislocations [6], thus possibly facilitating the synchroshear deformation mechanism and increasing the toughness of Laves phases [7]. Off-stoichiometry was also found to affect the hydride stability of $ZrMn_2$ [8] and the hydrogen storage capability of $TiMn_2$ alloys [9].

The $NbCr_2$ Laves phase has received considerable attention recently as a potential high-temperature structural material [10-14], due to its high melting temperature (1730°C), appreciable creep resistance, high strength, relatively low density (7.7 g/cm^3), and good oxidation resistance below 1100°C. It has a limited range of solubility on both sides of stoichiometry. The geometric factor [5] and electronic factor [15] have been cited to contribute to such a solubility range. However, so far no systematic study has been undertaken to investigate the off-stoichiometric defects in this binary system, even though such information is imperative in understanding the phase stability, deformation characteristics, and alloying behavior of the Laves phase alloy.

The $NbCo_2$ Laves phase has been a model material for studying the off-stoichiometric defects. Saito and Beck [16] performed a comparison of the X-ray density with gravimetrically measured densities for the Co-rich $NbCo_2$ Laves phase system. Their measurements show that the variable stoichiometry of the $NbCo_2$ Laves phase is the result of the progressive occupation of Nb sites by Co atoms, and not the result of constitutional vacancies in the Nb sublattice. However, only the Co-rich side was studied previously and only qualitative information regarding the defect mechanism is available. From the previous discussion, such anti-site substitution is expected for the Co-rich side. However,

previous discussion, such anti-site substitution is expected for the Co-rich side. However, a more interesting study will be to clarify the constitutional defect mechanisms on the Nb-rich side, which may be constitutional vacancies according to the previous reasoning. So far, no work has been done to carefully determine the homogeneity range of this Laves phase, especially the Nb-rich side. No solubility has been indicated on the Nb-rich side of this Laves phase system from the Nb-Co phase diagram [17]. The solubility range and the possible defect mechanisms on the Nb-rich side in this system will be carefully determined in this study.

While the $NbCr_2$ and $NbCo_2$ Laves phases are of a C15 structure, the third Laves phase system, $NbFe_2$, to be studied has a C14 structure. The homogeneity range of this Laves phase has been studied by Smith, Rogers and Rawlings [18], Paul and Swartzendruber [19] and more recently by Bejarano et al. [20]. The homogeneity range was originally thought to be from 27 to 38 at.% Nb [19] and should be much narrower, i.e., from 32 to 37 at.% Nb, according to a recent study [20]. From the lattice parameter measurements, the defect mechanism has been postulated to be anti-site substitution for both the Fe-rich and Nb-rich sides [18]. Furthermore, the authors postulated that there may be thermal vacancies existing in the stoichiometric compound. However, no direct measurement of the vacancy concentration in this Laves phase has been undertaken so far.

We have attempted to clarify the point defect mechanisms on both sides of stoichiometry in these three binary systems, by measuring the lattice parameters, bulk densities, and therefore, vacancy concentrations of binary $NbCr_2$, $NbCo_2$, and $NbFe_2$ alloys of various compositions after quenching from 1000°C. For the $NbCr_2$ alloys, the vacancy concentrations after quenching from 1400°C were also determined to see if thermal vacancies can be introduced by quenching from elevated temperatures.

The hardness of the above alloys with various point defect concentrations was also determined for understanding the solid solution hardening behavior in the Laves phases.

The fracture toughness was also determined to investigate if the point defects will affect the toughness of the alloys, and especially, if it is possible to facilitate synchroshear deformation through vacancy incorporation.

2. EXPERIMENTAL PROCEDURES

The alloy compositions investigated in this study are listed in Table I, II, and III. A total of 19 binary alloys was prepared: 6 for the $NbCr_2$ system, 6 for the $NbCo_2$ system, and 7 for the $NbFe_2$ system. For each alloy system, as the code number of the alloys increases, the Nb content in the alloy increases correspondingly. The selected compositions covered a wide range of stoichiometry: for $NbCr_2$ and $NbCo_2$ systems, alloys #1 - # 3 are Cr-rich or Co-rich, and #4 is the stoichiometric alloy, while alloys #5 and #6 are Nb-rich; for the $NbFe_2$ system, alloys #1 - #2 are Fe-rich and #3 is the stoichiometric one, while alloys #4 - #7 are Nb-rich. Ingots of about 50 grams were prepared by arc-melting techniques using high-purity starting materials. An excess amount (typically 0.05 gram) of Cr was added to compensate for the evaporation loss of Cr during melting for the $NbCr_2$ alloys. Each ingot was inverted and remelted 5 times to ensure compositional homogeneity.

The alloys #1 and #2 of the $NbCo_2$ system were homogenized at 1200°C for 24 hours in vacuum. All the other alloys were given a homogenization anneal of 1300°C for 10 hours in vacuum. After the homogenization anneal, all the alloys were sectioned into two halves. One half was encapsulated in quartz, which was evacuated and backfilled with helium and heat-treated at 1000°C for 7 days, followed by water quenching. The other half of the 6 alloys in the binary $NbCr_2$ system was heat-treated at 1400°C for 1 hour in a vertical flowing-argon furnace, then water quenched. All the alloys were fully homogenized following the above heat treatments, except the alloys #1 and #2 for the $NbCo_2$ system. Therefore, density and vacancy concentration measurements were not conducted for these two alloys.

Table I Composition, lattice parameter, X-ray density, bulk density and vacancy concentration (c_v) of the $NbCr_2$ alloys quenched from 1400 and 1000°C

Alloy Code	Nb (at.%)	Lattice Parameter (Å)		X-Ray Density (g/cm^3)		Bulk Density (g/cm^3)		c_v (%)	
		1400°C	1000°C	1400°C	1000°C	1400°C	1000°C	1400°C	1000°C
#1	31.8	6.9843*	6.9861*	---	---	7.613	7.621	---	---
#2	32.3	6.9861	6.9862*	7.619	---	7.617	7.623	0.03	---
#3	32.8	6.9882	6.9884	7.636	7.635	7.623	7.636	0.17	0.03
#4	33.3	6.9904	6.9908	7.652	7.651	7.627	7.646	0.33	0.07
#5	33.8	6.9956	6.9954	7.659	7.660	7.646	7.655	0.17	0.06
#6	34.8	7.0063	7.0063	7.671	7.671	7.664	7.672	0.10	0.00

* Two-phase alloys with the lattice parameter of the $NbCr_2$ phase listed here

Table II Composition, lattice parameter, X-ray density, bulk density and vacancy concentration (c_v) of the $NbCo_2$ alloys quenched from 1000°C

Alloy Code	Nb (at.%)	Lattice Parameter (Å)	X-Ray Density (g/cm^3)	Bulk Density (g/cm^3)	c_v (%)
#1	27.3	6.7265	---	---	---
#2	29.3	6.7450	---	---	---
#3	31.3	6.7641	8.951	8.950	0.02
#4	33.3	6.7824	8.966	8.967	-0.01
#5	33.8	6.7884	8.964	8.963	0
#6	34.3	6.7917*	---	---	---

* Two-phase alloys with the lattice parameter of the $NbCo_2$ phase listed here

Table III Composition, lattice parameter, X-ray density, bulk density and vacancy concentration (c_V) of the $NbFe_2$ alloys quenched from 1000°C

Alloy Code	Nb (at.%)	Lattice Parameter (Å)		X-Ray Density (g/cm^3)	Bulk Density (g/cm^3)	c_V (%)
		a	c			
#1	32.3	4.8363	7.8919	8.449	8.444	0.07
#2	32.8	4.8378	7.8936	8.465	8.462	0.04
#3	33.3	4.8406	7.8966	8.47	8.470	0.06
#4	33.8	4.8446	7.9030	8.478	8.472	0.07
#5	34.3	4.8504	7.9093	8.473	8.469	0.06
#6	36.3	4.8601*	7.9147*	---	---	---
#7	37.3	4.8602*	7.9146*	---	---	---

* Two-phase alloys with the lattice parameter of the $NbFe_2$ phase listed here

Small fractions of the quenched samples were mounted for microstructural observations, and chemical composition analyses of the various phases in the heat-treated condition, using an optical microscope and a field-emission-gun scanning electron microscope (SEM) equipped with an energy dispersive X-ray spectroscope (EDS).

The remaining parts of the samples were crushed in an agate mortar into powders with particle sizes smaller than 40 mesh. Powders with a mesh size of -40+80 were used for density measurements, and powders smaller than 320 mesh were used for X-ray analyses. The bulk density was measured using a helium pycnometer with an accuracy of around 0.01 vol.%. The use of powdered samples was intended to eliminate the micropores generated during solidification, and thus, will lead to more accurate density measurements. The vacancy concentration was calculated using Eq. 1.

X-ray diffraction measurements were made using a Scintag XD2000 diffractometer with Cu K_a radiation. The lattice parameter was determined from 13-15 peaks. The X-ray density was calculated using the measured lattice parameter. The accuracy of the vacancy concentration using our method is about 0.08%, which is mainly due to the compositional uncertainty of the alloys.

The microhardness was measured on a Buehler microhardness tester using a load of 50 grams with a holding time of 15 seconds. Due to the extremely brittle nature of the Laves phases, it is challenging to determine the hardness and discern the hardness difference for the Laves phases with small compositional variations. The use of 500 grams load is not so desirable, due to the extensive cracking near the corners of the indented region, which makes the determination of the diagonal length less accurate. Therefore, we use a small load of 50 grams for indentation, which tends to reduce the cracking problem and make the measurement of the diagonal length more accurate. However, the indented area is much smaller for the 50 grams load than for the 500 grams load. As a consequence, SEM has to be used for imaging with a high magnification (10,000x), which gives us a more accurate measurement of the diagonal length, and thus, the hardness values. The magnification of the SEM was calibrated with a calibration grating. The Vickers hardness number (VHN) is determined by the following equation [21]:

$$VHN = \frac{1.854P}{L^2} \qquad (2)$$

where P = applied load (kg) and L = average length of diagonals (mm).

The fracture toughness of the alloys was calculated from the crack length values after the indentation using a load of 500 g with a holding time of 15 seconds. The crack lengths were measured immediately after the indentation to eliminate the possibility of slow crack propagation following the removal of the indenter. The following equation was used to calculate the fracture toughness of the alloy [22, 23]:

$$K_{IC} = A\left(\frac{E}{H}\right)^{n} \frac{P}{L^{3/2}} \qquad (3)$$

where K_{IC} = fracture toughness ($MPa\sqrt{m}$), E = Young's modulus (GPa), which is assumed to be 218 GPa for all of the investigated alloys, H = Vickers hardness (GPa), P = load (N), and L = average length of the four radial cracks from the center of the indent to the crack tip. A and n are constants, which are taken as 0.016 and 0.5, respectively, for relatively brittle materials [22].

3. RESULTS

3.1 Microscopic Observation

Optical microstructural observations show that for the $NbCr_2$ Laves phase system the alloys #2 - #6 listed in Table 1 are in the single Laves phase region, and alloy #1 is in the two-phase region after quenching from 1400°C. After quenching from 1000°C, the alloys #3 - #6 are in the single Laves phase region and alloys #1 and #2 are in the two-phase region. Alloy #1 after quenching from 1400°C and alloy #2 after quenching from 1000°C start to precipitate small amounts of a second phase. Such observations are further supported by the lattice parameter results, as shown later. Typical microstructures of single Laves phase alloys, which were etched with a solution of $HF:HNO_3:H_2O$ = 1:1:3, are shown in Fig. 2. There are many annealing twins in the alloy, indicating that the C15 structure is easily twinned, i.e., it has a low stacking fault energy. The second phase in alloys #1 and #2 was analyzed with EDS in an SEM, and determined to be a Cr solid solution with a small amount of Nb. Figure 3 presents an SEM micrograph of the alloy #1 after quenching from 1000°C, with a two-phase microstructure. The dark phase and the matrix are the Cr precipitate and $NbCr_2$ Laves phase, respectively, as is clear form the EDS results shown in Fig. 4. The maximum solubility of Cr in $NbCr_2$ at 1000°C in this study is found to be similar to the value reported in the recent binary Cr-Nb phase diagram [14].

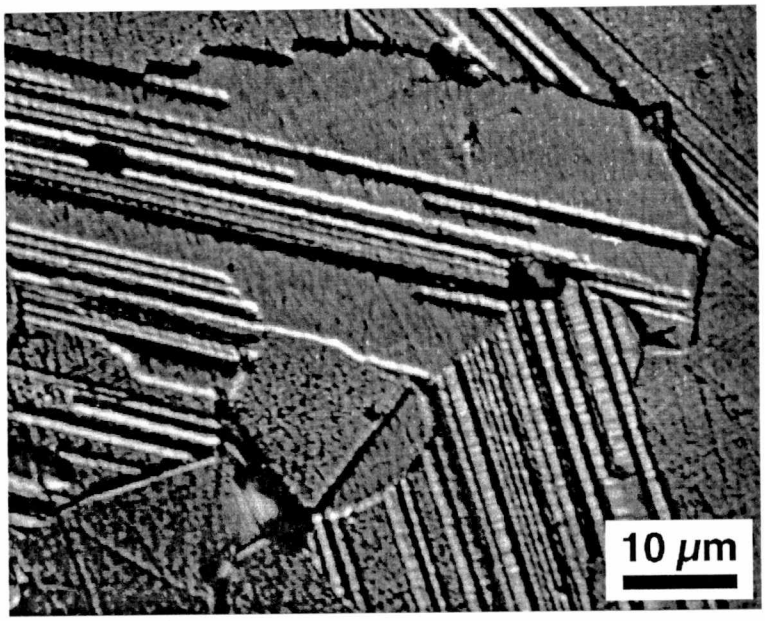


Fig. 2 Optical microstructure of the stoichiometric $NbCr_2$ alloy after quenching from 1000°C (in etched condition)

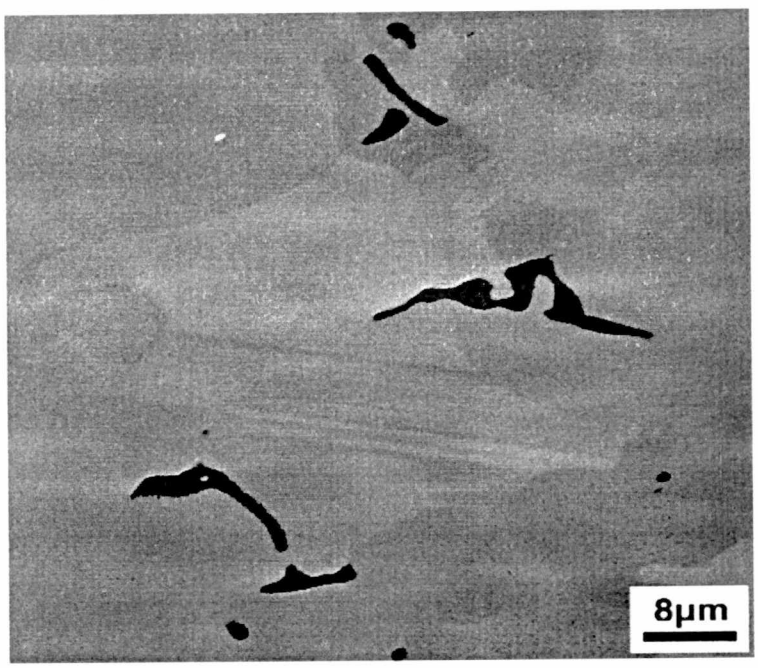


Fig. 3 SEM micrograph of the $NbCr_2$ alloy #1 after quenching from 1000°C (in as-polished condition)

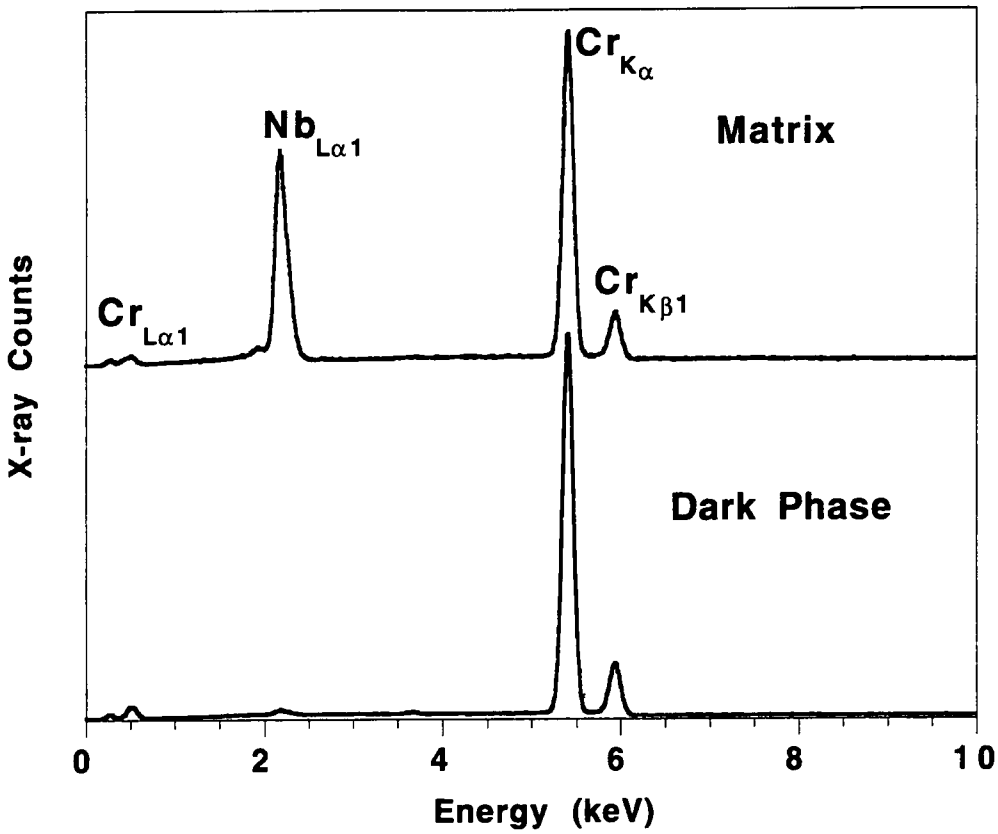


Fig.4 EDS spectra of the matrix and the dark phase indicated in Fig. 3, which were $NbCr_2$ Laves phases and Cr precipitate, respectively

For the $NbCo_2$ system, all the alloys except #6 are within the homogeneity range, and there are few annealing twins in the alloys compared to the $NbCr_2$ alloys, indicating the stacking fault energy is high in this $NbCo_2$ phase. Fig. 5 shows the optical microstructure of the stoichiomteric $NbCo_2$ alloy, etched with a solution of 60% glycerine + 20% HNO_3 + 10% HF +10%H_2O. The alloys #1 and #2 are not fully homogenized. The alloy #6 is in the two-phase range, i.e., there are small amounts of second phase, especially near grain boundaries, see Fig. 6. The second phase is β Nb_6Co_7 phase, with a $D8_5$ structure, according to the binary Nb-Co phase diagram [17]. Consistent with the phase diagram, the EDS results show that this phase is richer in Nb content than the matrix, see Fig. 7.

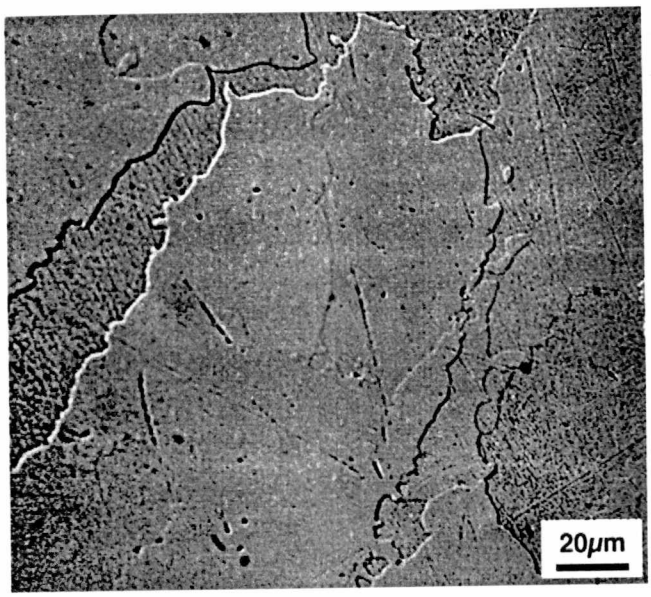


Fig. 5 Optical microstructure of the stoichiometric $NbCo_2$ alloy

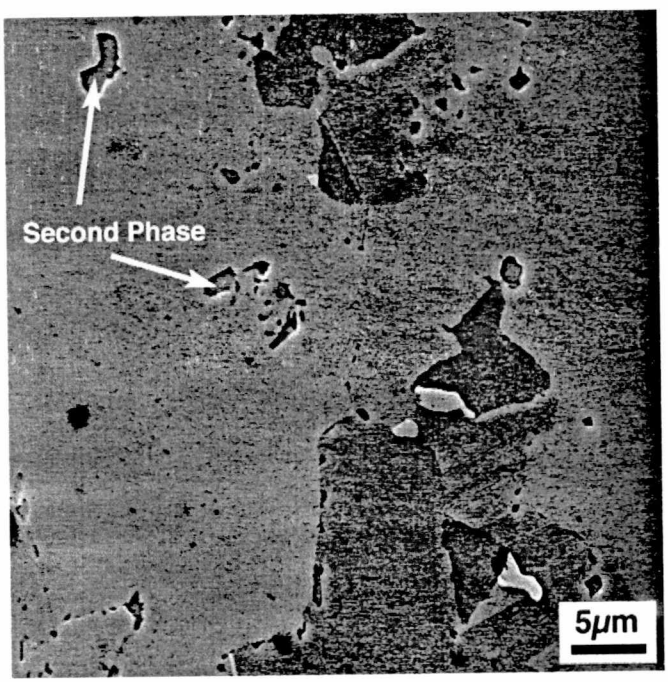


Fig. 6 SEM micrograph of the $NbCo_2$ alloy #6

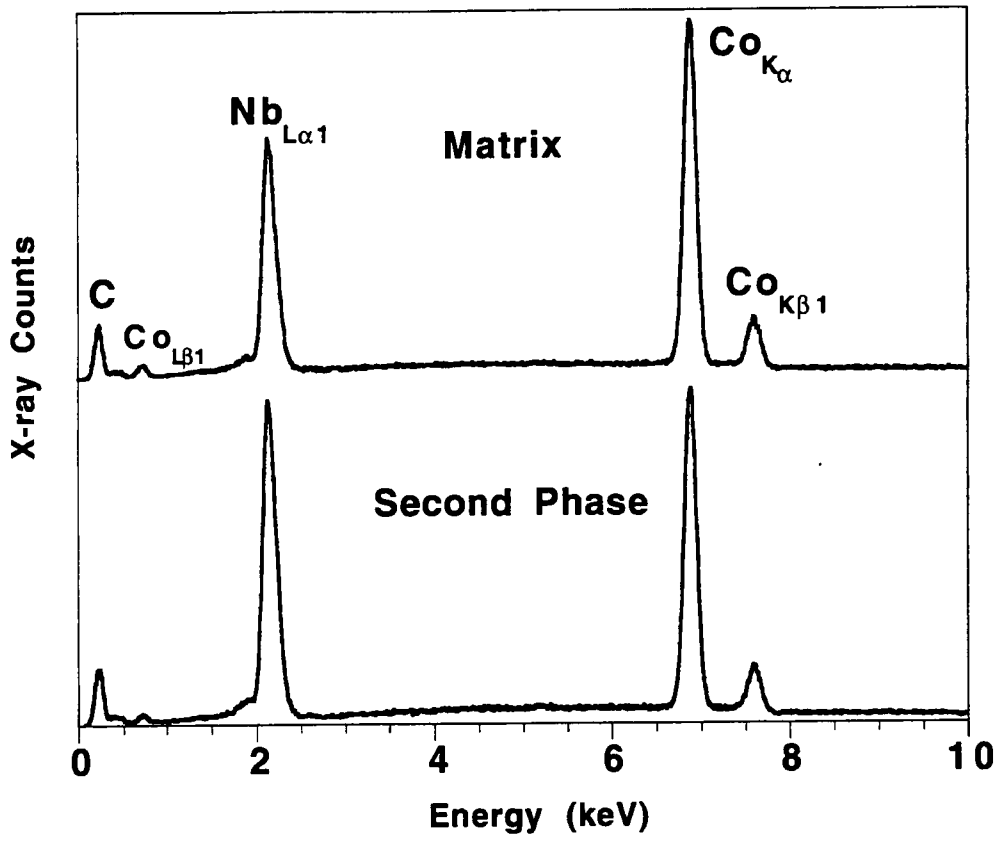


Fig.7 EDS spectra of the matrix and the second phase indicated in Fig. 6, which were $NbCo_2$ Laves phase andβ Nb_6Co_7 phase, respectively

Compared to the binary Nb-Co phase diagram where no solubility on the Nb-rich side is indicated, it is found that the solubility of Nb in the $NbCo_2$ Laves phase is higher than 0.5 at.%, but less than 1 at.% from this study.

For the $NbFe_2$ system, the alloys #1-#5 are within the homogeneity range, and alloys #6 and #7 are in the two-phase region, a Laves phase of $NbFe_2$ and a μ phase of NbFe [20]. Fig. 8 shows the microstructure of the single-phase stoichiomteric $NbFe_2$ alloy, with large grains and no annealing twin. Fig. 9 shows the two-phase structures in alloy #7, and the EDS results (Fig. 10) indicate the second phase is richer in Nb than the matrix. Compared to the binary Nb-Fe phase diagram [20], the maximum solubility of Nb in $NbFe_2$ at 1000°C in this study is found to be lower than the reported one (37 at.% Nb).

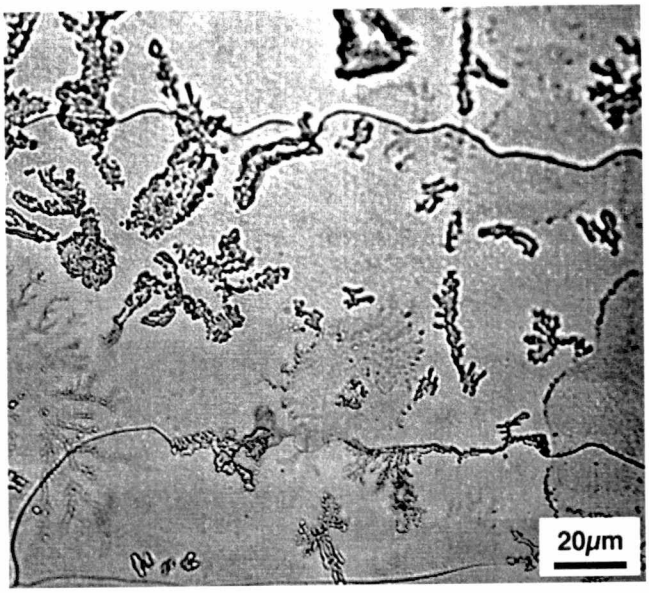


Fig. 8 Optical microstructure of the stoichiometric $NbFe_2$ alloy

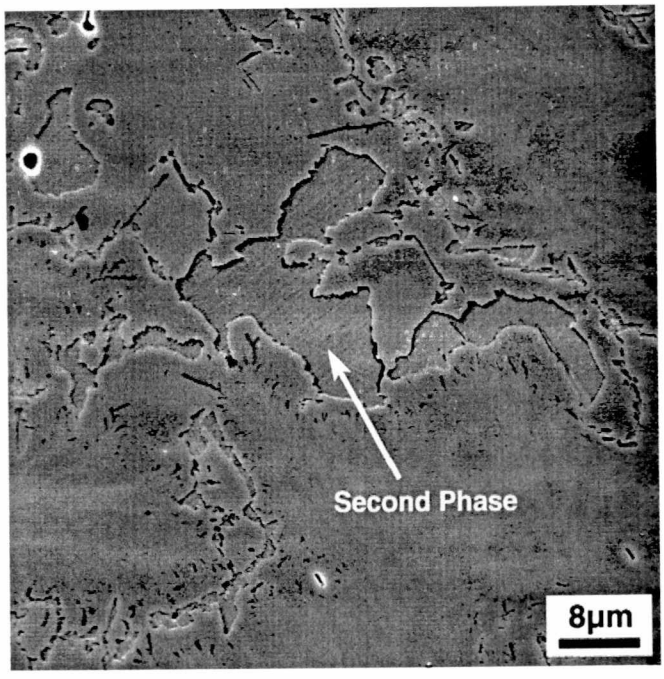


Fig. 9 SEM micrograph of the $NbFe_2$ alloy #7

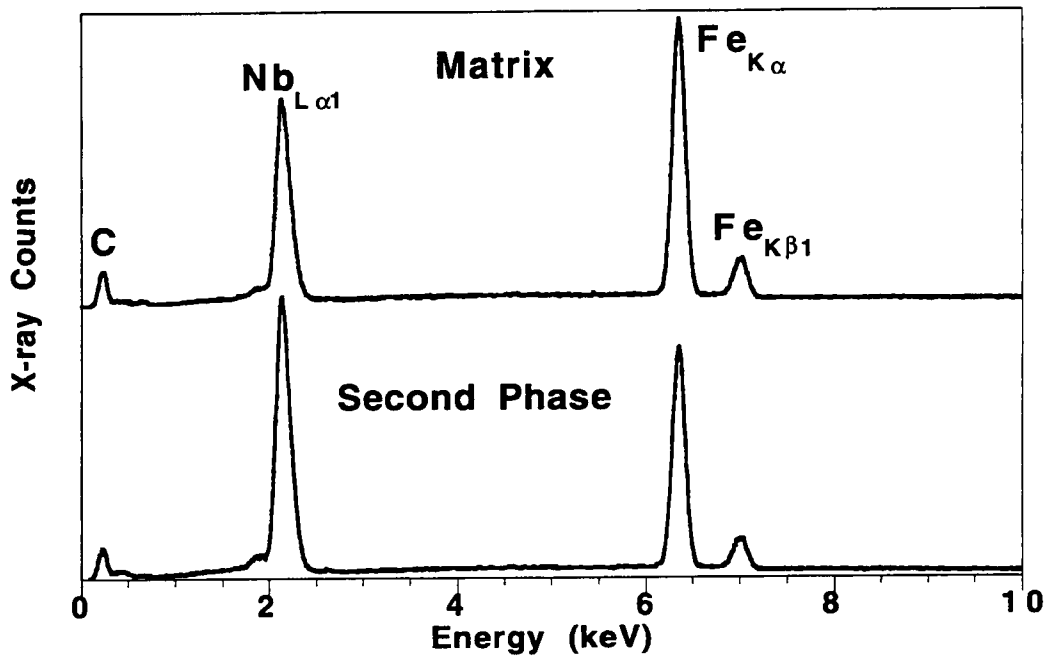


Fig. 10 EDS spectra of the matrix and the second phase indicated in Fig. 9, which were $NbFe_2$ Laves phase and μ NbFe phase, respectively

3.2 Lattice Parameter, Density, and Vacancy Concentration

3.2.1 Binary $NbCr_2$ Alloys

The lattice parameters of the alloys listed in Table I are plotted in Fig. 11 as a function of stoichiometry for all the samples quenched from both 1400°C and 1000°C. Basically, as the Nb content increases, the lattice parameter of the $NbCr_2$ compound also increases. For the alloys quenched from 1400°C, the data points for the Cr-rich side fit along a straight line; similarly, for the Nb-rich side, the data points also fit along a straight line, with a slope greater than that of the line on the Cr-rich side. For the alloys quenched from 1000°C, similar trends are observed, except that on the Cr-rich side the lattice constants are identical for alloys #1 and #2, which indicates the composition of the Laves phase is the same in the two alloys. This is to be expected, since these alloys were found to be of a two-phase microstructure. Except for alloy #1, the lattice parameters after quenching from 1000°C are similar to those after quenching from 1400°C.

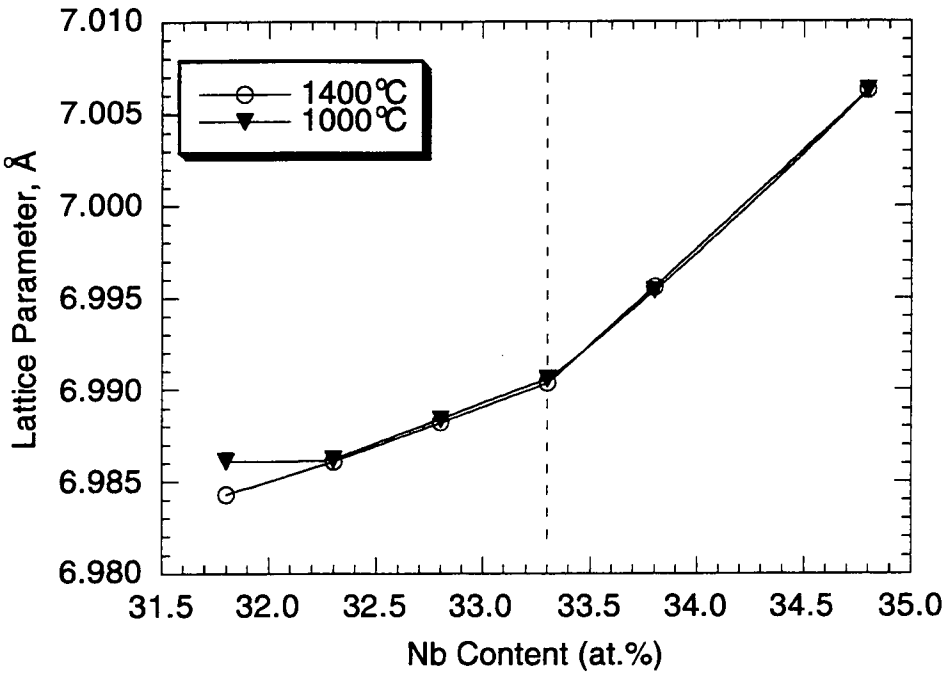


Fig. 11 Lattice parameter as a function of the Nb content for $NbCr_2$ alloys

The X-ray and bulk density results after quenching from both 1400°C and 1000°C are presented in Table I and Fig. 12. The density of the alloys increases, as the Nb content increases. Also, the bulk densities after quenching from 1000°C are consistently higher than those after quenching from 1400°C. Using Eq. 1 and the data presented in Table I and Fig. 12, the vacancy concentrations were calculated, and are also listed in Table I. Due to the precipitation of the second phase, the vacancy concentration could not be determined for alloy #1 after quenching from 1400°C and alloys #1 and #2 after quenching from 1000°C. Figure 13 is a plot of the vacancy concentration as a function of the Nb content for the single-phase alloys after quenching from both 1400°C and 1000°C. It is interesting to note that the vacancy concentration in the alloys is quite high (~ 0.33 %) after quenching from 1400°C, reaches a peak at the stoichiometric composition, and decreases on both sides of stoichiometry. After annealing at 1000°C, the vacancies are annealed out and the vacancy concentrations are near zero, considering the accuracy of the vacancy concentration measurements. However, a slight peak at the stoichiometric composition can be detected.

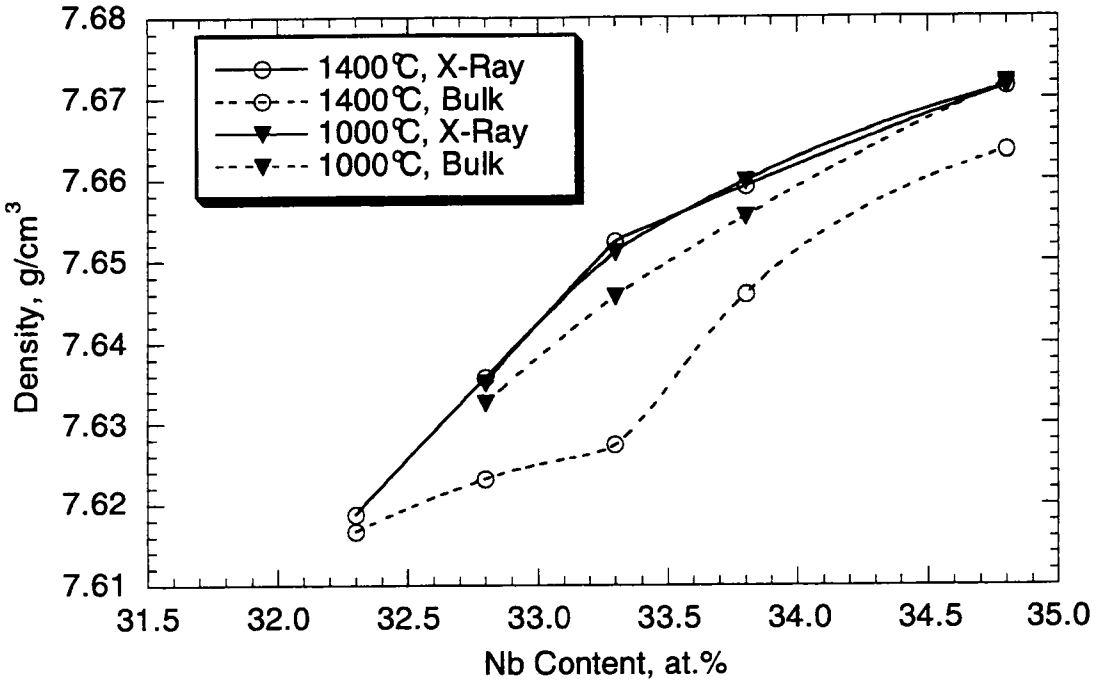


Fig. 12 X-ray and bulk densities as a function of the Nb content for $NbCr_2$ alloys after quenching from 1400 and 1000°C

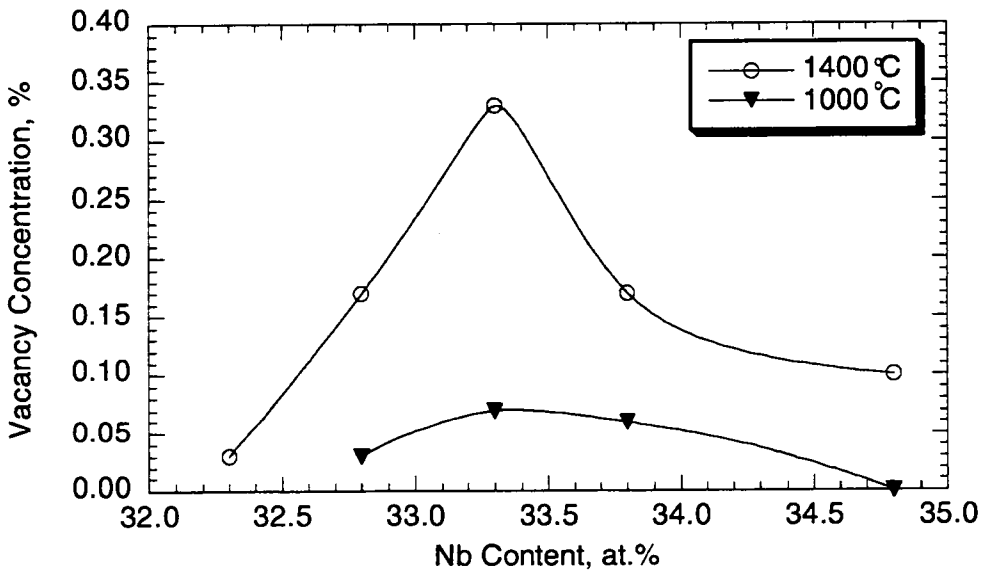


Fig. 13 Vacancy concentration as a function of the Nb content for $NbCr_2$ alloys after quenching from 1400 and 1000°C

3.2.2 Binary $NbCo_2$ Alloys

The lattice parameters of the alloys listed in Table II are plotted in Fig. 14 as a function of stoichiometry for all the $NbCo_2$ alloys quenched from 1000°C. As the Nb content increases, the lattice parameter of the $NbCo_2$ compound also increases. The data points for the Cr-rich side fit along a straight line; for the Nb-rich side, the initial data points also fit along a straight line, with a slope greater than that of the line on the Cr-rich side, similar to the result observed in $NbCr_2$ alloys (Fig. 11). For the alloy #6, its lattice parameter can not be fit into the line, due to the two-phase nature of this alloy. The solubility of Nb in $NbCo_2$ is about 34 at.%, see Fig. 14.

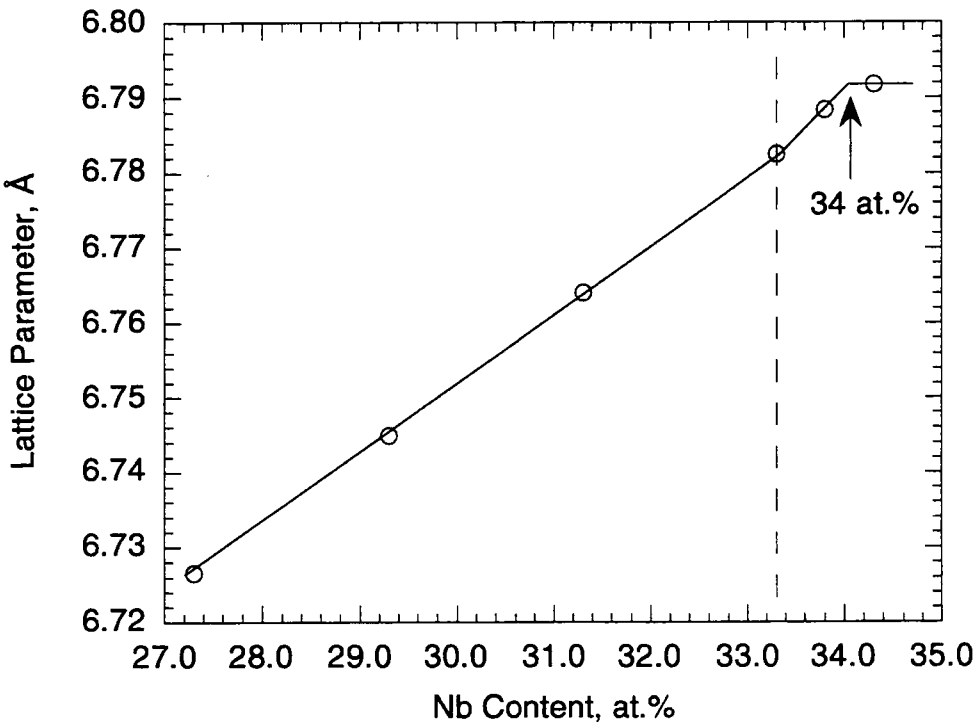


Fig. 14 Lattice parameter as a function of the Nb content for $NbCo_2$ alloys

The X-ray and bulk density results for the $NbCo_2$ alloys after quenching from 1000°C are presented in Table II and Fig. 15. Both the X-ray and bulk densities of the alloys increase initially as the Nb content increases; however, on the Nb-rich side, the X-ray and bulk densities of the alloys decrease as the Nb content increases. This trend seems to indicate that there may be a great amount of vacancies in these alloys, which reduce the density of the alloys. Using Eq. 1 and the data presented in Table II and Fig. 15, the vacancy concentrations were calculated, and are also listed in Table II and plotted in Fig. 16 as a function of the Nb content. The results indicate that the vacancy concentration in the alloys is quite low, i.e. essentially zero, considering the accuracy of the vacancy concentration measurement. It is interesting to note that the decrease of the bulk density, as the content of the heavy element Nb in the alloy increases, does not necessarily mean that there are vacancies in the alloys. No peak at the stoichiometric composition in the vacancy concentration curve can be detected in Fig. 16.

3.2.3 Binary $NbFe_2$ Alloys

The lattice parameters of the $NbFe_2$ alloys listed in Table III are plotted in Fig. 17 as a function of stoichiometry for all the $NbFe_2$ alloys quenched from 1000°C. Basically, as the Nb content increases, the lattice parameters, a and c, of the C14 $NbFe_2$ compound also increase. The data points for the Fe-rich side fit along a line; similarly, for the Nb-rich side, the initial data points also fit along a line, with a slope greater than that of the line on the Fe-rich side, with the exception for the last two data points where the lattice parameters, a and c, are both identical for alloys #6 and #7, which indicates the composition of the Laves phase is the same in the two alloys. This is to be expected, since these alloys were found to be two-phase. If we extrapolate the lines on the Nb-rich side to the a and c values for the alloys #6 and #7, the maximum solubility of Nb in $NbFe_2$ Laves phase is obtained, which is close to 35 at.%. This is lower than the reported one (37 at.% Nb) [20].

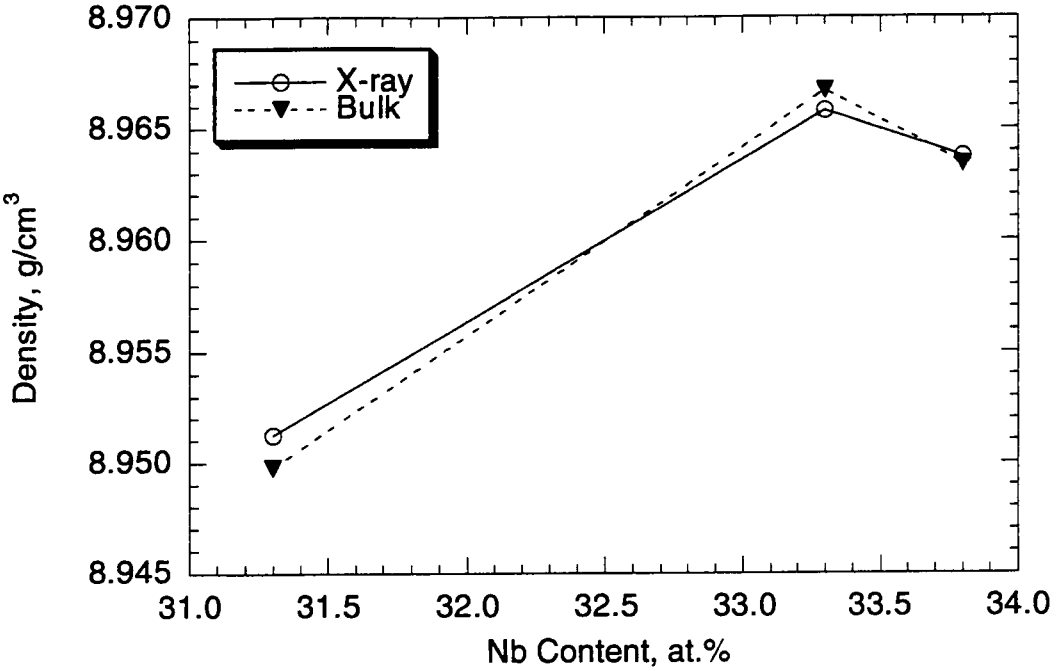


Fig. 15 X-ray and bulk densities as a function of Nb content for $NbCo_2$ alloys

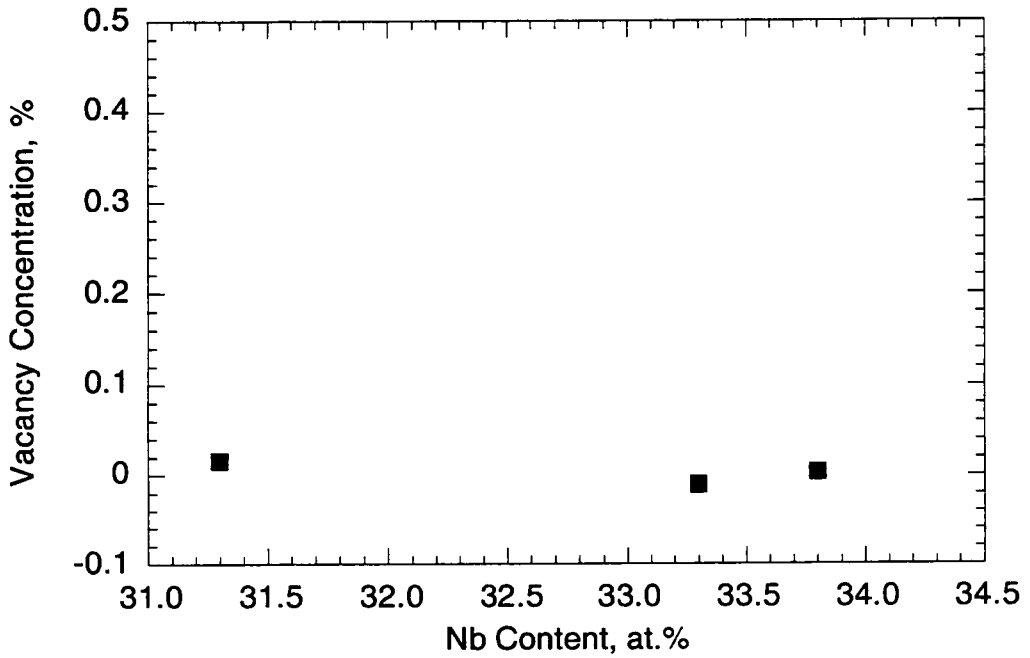


Fig. 16 Vacancy concentration as a function of Nb content for $NbCo_2$ alloys

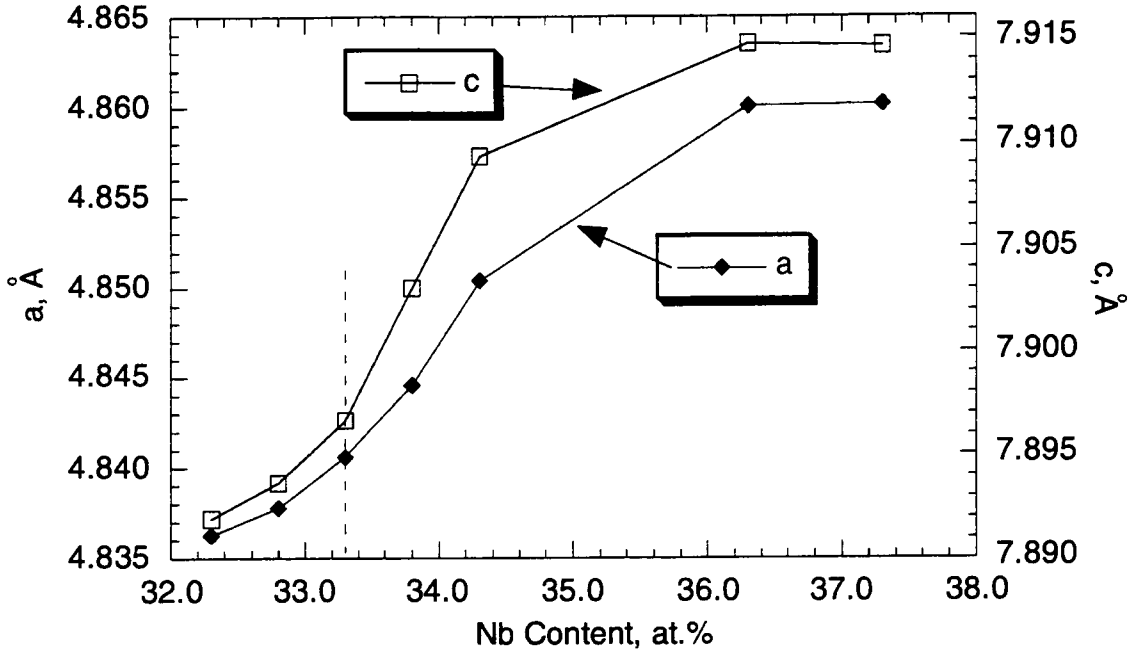


Fig. 17 Lattice parameters, a and c, as a function of Nb content for $NbFe_2$ alloys

The X-ray and bulk density results for the $NbFe_2$ Laves phases after quenching from 1000°C are presented in Table III and plotted in Fig. 18. The density of the alloys increases, as the Nb content increases initially; however, after the Nb content reaches 33.8 at.%, the density decreases with a further increase in the Nb content. Also, the bulk densities after quenching from 1000°C are consistently higher than the X-ray densities. Using Eq. 1 and the data presented in Table III and Fig. 18, the vacancy concentrations were calculated, and are also listed in Table III. Due to the precipitation of the second phase, the vacancy concentration could not be determined for alloys #6 and #7. Figure 19 is a plot of the vacancy concentration as a function of the Nb content for the single-phase $NbFe_2$ alloys after quenching from 1000°C. The vacancy concentrations are essentially zero, considering the accuracy of the vacancy concentration measurement. No peak at the stoichiometric composition in the vacancy concentration curve can be detected in Fig. 19.

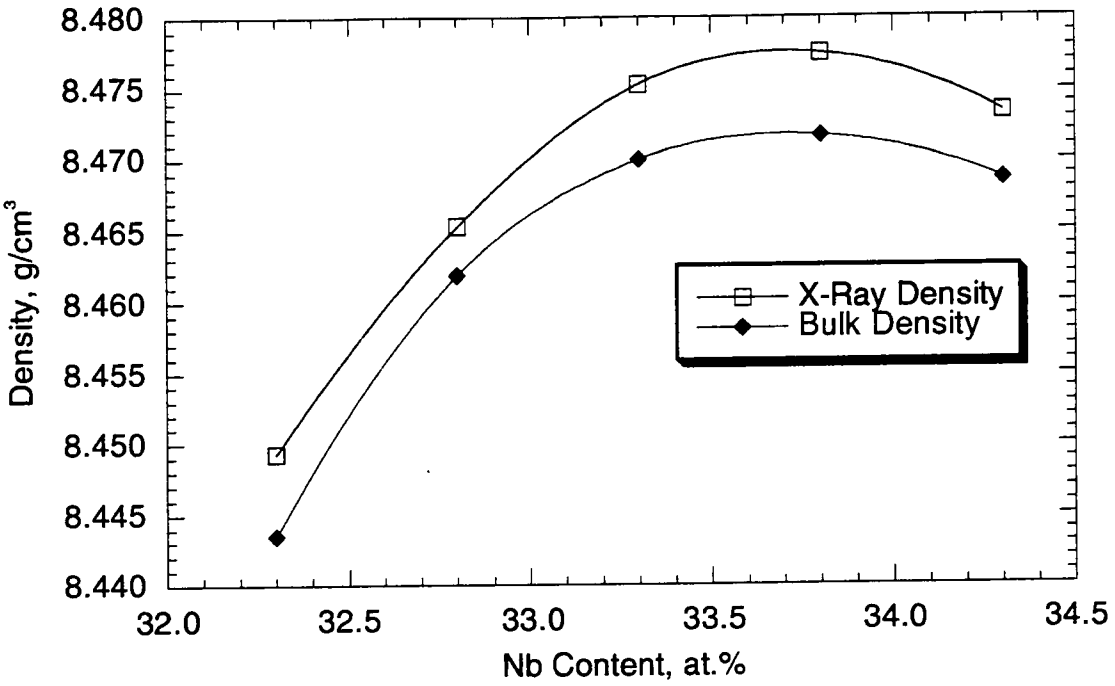


Fig. 18 X-ray and bulk densities as a function of Nb content for $NbFe_2$ alloys

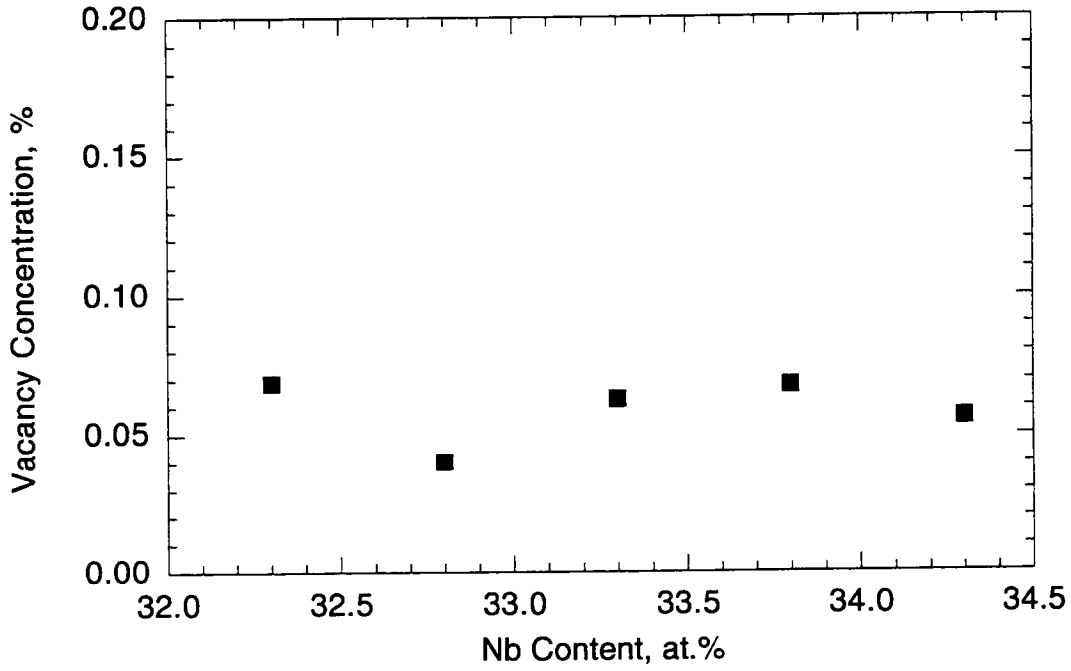


Fig. 19 Vacancy concentration as a function of Nb content for $NbFe_2$ alloys

3.3 Hardness and Fracture Toughness Behaviors

The hardness as a function of the stoichiometry for the $NbCr_2$ alloys after quenching from 1400 and 1000°C is plotted in Fig. 20. It can be seen that as the composition deviates from the stoichiometry, the hardness of the Laves phase increases on both sides of stoichiometry. Since constitutional anti-site defects are the defect mechanisms on both Cr-rich and Nb-rich sides, anti-site substitution hardening was observed. Furthermore, the hardness of the alloys quenched from 1400°C is consistently lower than that of the alloys quenched from 1000°C, due to the presence of thermal vacancies. Such vacancy-induced softening of the materials is different from what was observed in B2 interemetallics, where the vacancy is a stronger hardener than the anti-site defect.

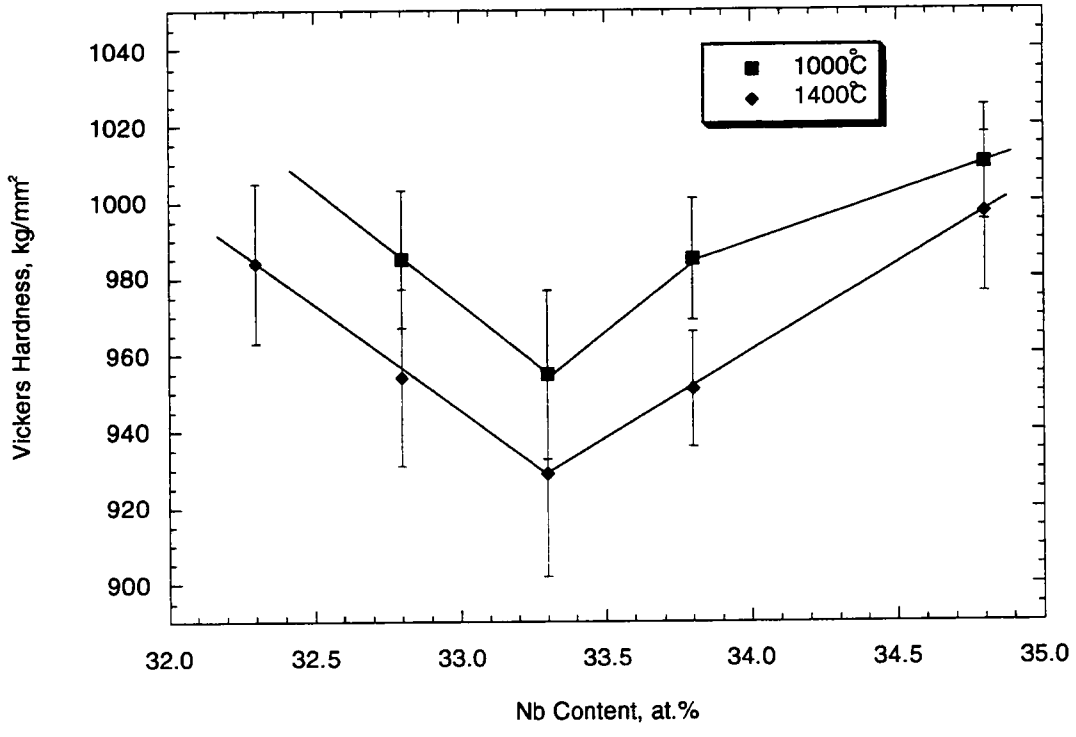


Fig. 20 Vickers Hardness versus Nb content for $NbCr_2$ alloys after quenching from 1400°C and 1000°C

The hardness as a function of the stoichiometry for the $NbCo_2$ alloys quenched from 1000°C is plotted in Fig. 21. It can be seen that as the composition deviates from the stoichiometry, the hardness of the Laves phase increases, i.e. anti-site substitution hardening was observed. This is similar to the situation in the $NbCr_2$ Laves phases.

The hardness as a function of the stoichiometry for the $NbFe_2$ alloys quenched from 1000°C is plotted in Fig. 22. It can be seen that as the composition deviates from the stoichiometry, the hardness of the Laves phase increases, i.e., anti-site substitution hardening was observed again. Thus, anti-site substitutional hardening is observed for both C15 ($NbCr_2$ and $NbCo_2$) and C14 ($NbFe_2$) structure alloys, indicating that anti-site substitutional hardening may be a general phenomenon for Laves phase alloys.

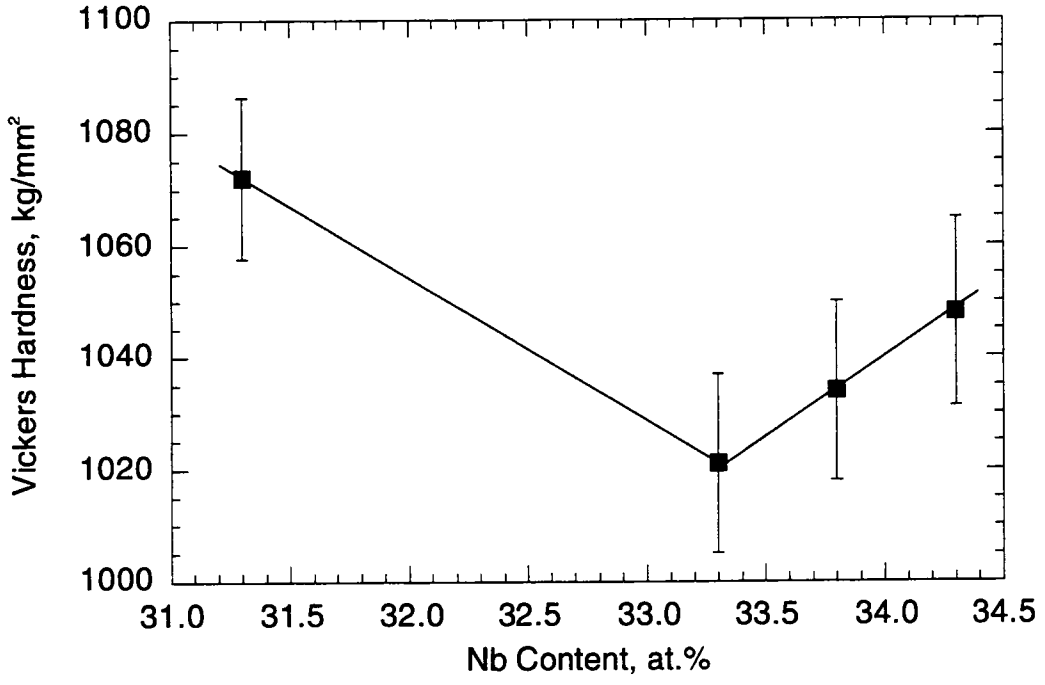


Fig. 21 Vickers Hardness versus Nb content for $NbCo_2$ alloys after quenching from 1000°C

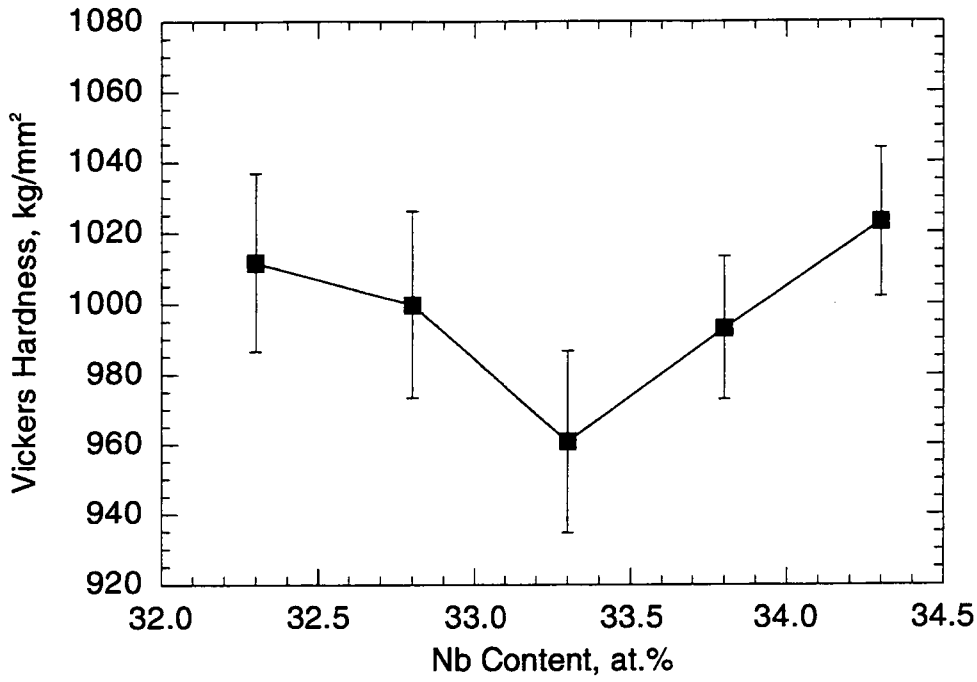


Fig. 22 Vickers Hardness versus Nb content for $NbFe_2$ alloys after quenching from 1000°C

The fracture toughness results as a function of the Nb content in $NbCr_2$ Laves phases after quenching from 1400°C and 1000°C are plotted in Fig. 23 and 24. The fracture toughness as a function of the Nb content for the $NbCo_2$ Laves phases after quenching from 1000°C is plotted in Fig. 25. Basically, the fracture toughness of the $NbCr_2$ and $NbCo_2$ alloys is close to 1 $MPa.m^{1/2}$. No effect of stoichiometry on the fracture toughness can be discerned. Even though the presence of the anti-site defects hardens the Laves phase (Figs. 20 and 21), they are not detrimental to the fracture toughness of the alloy. Furthermore, it is noted that the fracture toughness of the $NbCr_2$ alloys after quenching from 1400°C is similar to that of the alloys after quenching from 1000°C, i.e., the presence of thermal vacancies does not lead to the toughening of the Laves phases, even though they do soften the Laves phases (see Fig. 20).

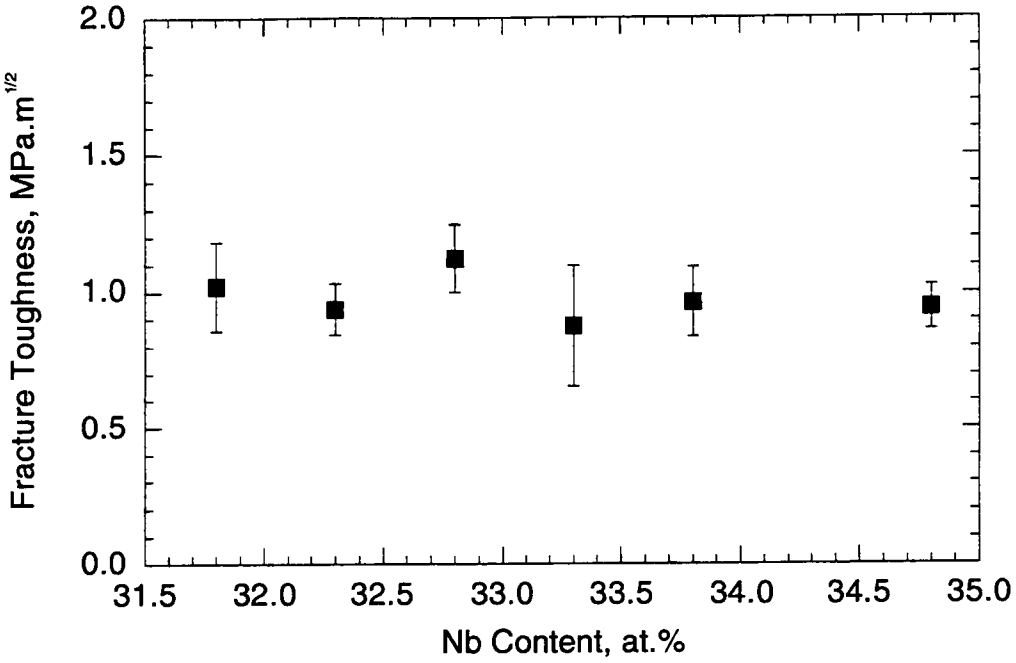


Fig. 23 Fracture toughness versus Nb content for $NbCr_2$ alloys after quenching from 1400°C

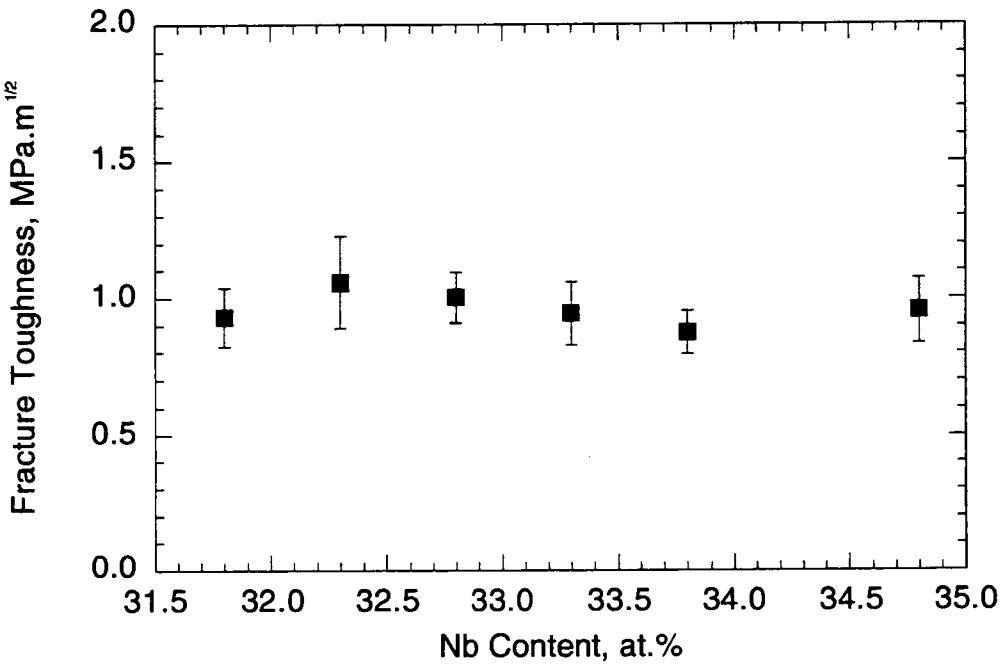


Fig. 24 Fracture toughness versus Nb content for $NbCr_2$ alloys after quenching from 1000°C

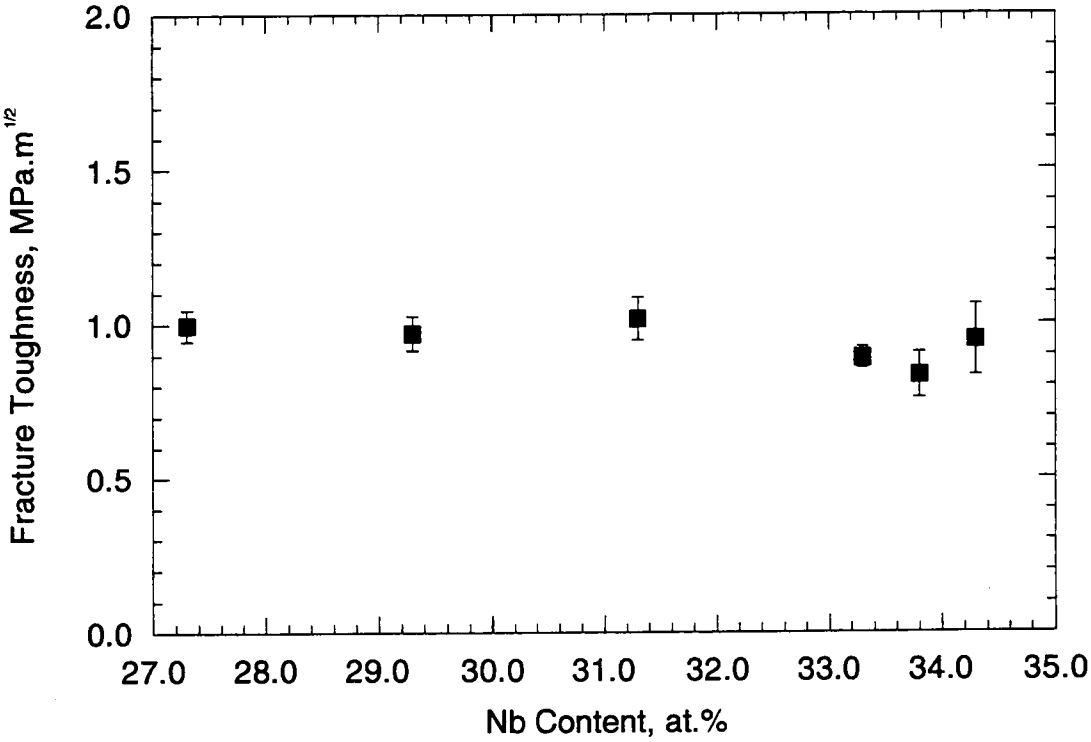


Fig. 25 Fracture toughness versus Nb content for $NbCo_2$ alloys

The fracture toughness results as a function of the Nb content for the $NbFe_2$ Laves phases after quenching from 1000°C is plotted in Fig. 26. Basically, the fracture toughness of the C14 $NbFe_2$ alloys is lower than that of C15 $NbCr_2$ and $NbCo_2$. No effect of stoichiometry on the fracture toughness can be discerned. Again, even though the presence of the anti-site defects hardens the Laves phase (Figs. 22), they are not detrimental to the fracture toughness of the alloy. Furthermore, it is noted that the fracture toughness of the two-phase alloys is higher than the single-phase alloys, which indicates that the μ phase may be tougher that the Laves phase.

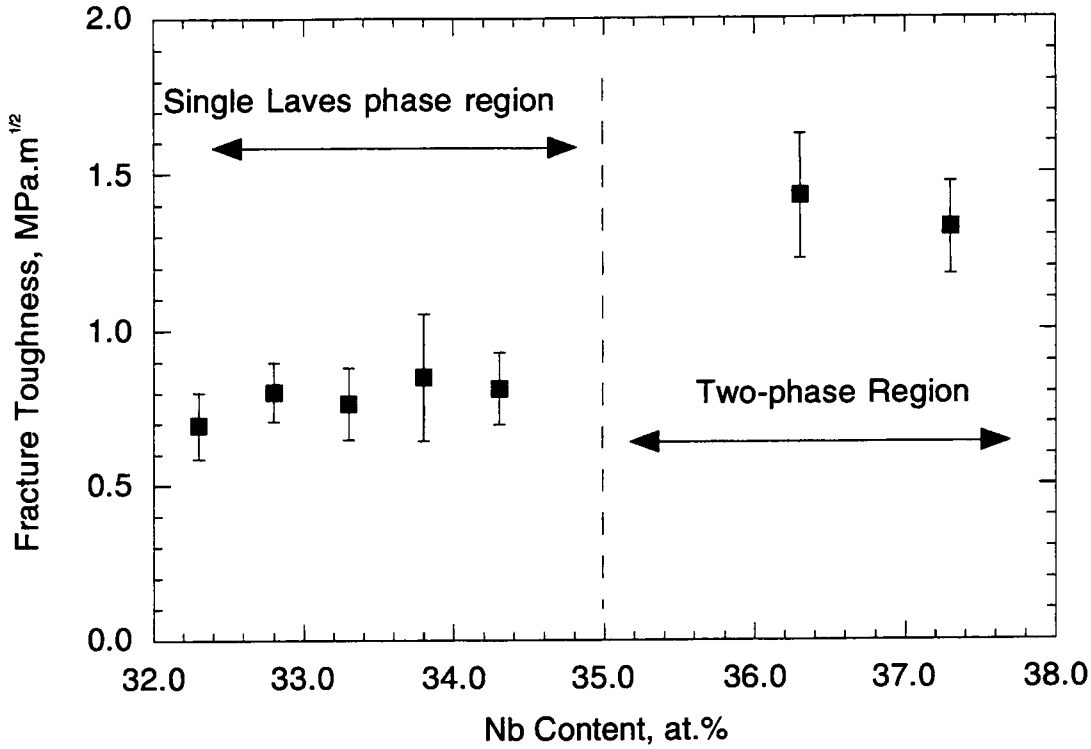


Fig. 26 Fracture toughness versus Nb content for $NbFe_2$ alloys

4. DISCUSSION

4.1 Defect Mechanisms in Binary Laves Phases

The study of point defects in intermetallic compounds is an interesting topic. Defect mechanisms are closely related to physical and mechanical properties, such as diffusivity, hardness, ductility, etc. A great deal of research effort has been devoted to the elucidation of the defect types in B2 structures, such as FeAl and NiAl [1, 25]. For example, it is now generally accepted that the defects in Ni-rich NiAl are of the anti-site type, i.e. the excess Ni will go to the Al sublattice site, while the excess Al in NiAl prefers to stay on its own sublattice, leading to the creation of vacancies on the Ni sublattice. Also, thermal vacancies can be easily generated in FeAl alloys by quenching from elevated temperatures [26], while the thermal vacancy concentration is much lower in NiAl [1] than in FeAl.

Previously, very limited studies have been undertaken to clarify the point defect mechanisms in Laves phases. Chen et al. [7] found from density measurements that both vacancy and anti-site defects are operating in the $TiCr_2$ Laves phase. Another study by Fleischer [27] found that anti-site substitution occurs on both sides of stoichiometry for the C15 $ZrCr_2$ Laves phase. Pargeter and Hume-Rothery [28] Saito and Beck [16] investigated the point defects in Co-rich $NbCo_2$ and $NbCo_3$ Laves phases and found that in both phases, the deviation from proper Laves stoichiometry result from the substitution of Co atoms for the Nb atoms. However, constitutional defects on the Nb-rich side were not studied. X-ray and neutron diffraction measurements [29] showed that for both $ZrFe_2$ and $TiFe_2$ the excess Fe atoms are associated with the sites of Zr- or Ti-atoms. The concentration variation of the lattice constants confirms such anti-site substitution mechanism. The constitutional defect structure of the $NbFe_2$ Laves phase was also investigated by measuring the lattice parameters on both sides of stoichiometry, and again anti-site substitution was found to be the defect mechanism [18]. Off-stoichiometry in the YAl_2 Laves phase was postulated to be accompanied by different defect mechanisms: the Y-rich side is accommodated by vacancies, while the Al-rich compositions result from anti-site substitution [30]. No work on the off-stoichiometric defects in $NbCr_2$ has been reported so far. From lattice parameter measurements, Thoma et al. [5, 14] postulate that constitutional vacancies on the Cr sublattice for the Nb-rich side of stoichiometry and anti-site substitution of Cr atoms on the Nb sites for the Cr-rich side of stoichiometry are probable defect mechanisms. It should be noted that in all of the above studies, the alloy compositions were not carefully controlled and vacancy concentrations in the Laves phases were not determined. Thus, no definitive conclusions on the defect mechanisms could be made from those studies.

The shape of the lattice parameter versus composition curve can provide valuable insight on constitutional defect mechanisms. For example, this type of information has

been used to successfully predict the constitutional defect mechanisms in a number of B2-ordered compounds [1]. These ideas can be extended to the present case by the consideration of Figs. 11, 14, and 17. The lattice parameter at the Cr, Co, or Fe-rich compositions is seen to increase with increasing Nb concentration. This is not surprising given that Nb has a larger atomic size than Cr, Co, or Fe. However, on the Nb-rich side of stoichiometry, the lattice parameter is seen to *increase* at an even greater rate with increasing Nb concentration for all these three Laves phase systems. This behavior suggests that the constitutional defect at Nb-rich compositions is Nb anti-site substitution. Only if a *decrease* in the rate of the lattice parameter change on the Nb-rich side of stoichiometry had been observed would constitutional vacancies be a possibility. The vacancy concentration results further confirm this conclusion unambiguously. The measured vacancy concentrations for all the single-phase alloys after quenching from 1000°C are essentially zero (Tables I, II, and III, and Figs. 13, 16, and 19), indicating that there are no constitutional vacancies in these Laves phases on either side of stoichiomtery. Thus, the constitutional defect mechanisms on both Cr-, Co-, or Fe-rich and Nb-rich sides of stoichiometry are anti-site substitution for the $NbCr_2$, $NbCo_2$, and $NbFe_2$ Laves phases.

4.2 Thermal Vacancy in Binary $NbCr_2$ Laves Phases

It is interesting that the measured vacancy concentration exhibits a maximum at the stoichiometric composition and decreases on both sides of stoichiometry for the $NbCr_2$ alloys when quenched from 1400°C. Since these vacancies were essentially annealed out at 1000°C (see Fig. 13), and since the constitutional defects in this compound have been established to be of the anti-site type, it is concluded that these are *thermal* vacancies. The shape of this curve may at first seem unique; however, a useful analog can be found when considering triple-defect B2 phases. This class of compounds has constitutional as well as thermal vacancies [1]. If the constitutional component is subtracted from the total vacancy

concentration, it is found that the thermal vacancy concentration exhibits a maximum at the stoichiometric composition, as is the case in our $NbCr_2$ system. This behavior is exhibited by the NiGa and CoGa compounds, for example. A convenient summary of such data is found in Ref. 1. A maximum in thermal vacancy concentration at the stoichiometric composition can be rationalized by considering that the increase in entropy associated with the introduction of vacancies will be the greatest at the stoichiometric composition where the degree of order is necessarily the highest. An interesting problem in the future will be to determine whether the thermal vacancies sit on the Cr-site, the Nb-site, or both.

4.3 Solid Solution Hardening in Binary Laves Phases

A point defect in a crystalline lattice is well known to cause hardening. This is referred to as solid solution hardening. Solid solution hardening has been extensively studied in B2 compounds [25]. Generally, it was found that in B2 compounds with anti-site defects, hardness exhibits a minimum at the stoichiometric composition, and deviation from stoichiometry causes hardening of the compounds, due to the presence of consitutional anti-site defects. For triple defect B2 compounds, the shape of the hardness versus composition curves was found to be not so simple and depends on the degree of thermal disorder. Also, vacancies were found to be a more potent hardener than the anti-site defects.

In the three Laves phases we studied, the hardness was also found to have a characteristic V-shape with a minimum occurring at the stoichiometric compositions (Figs. 20 - 22). Obviously, similar to anti-site B2 compounds, such off-stoichiometric hardening can be attributed to the presence of constitutional anti-site defects, which are the defect mechanism on both sides of stoichiometry in these Laves phases.

The hardness values of all $NbCr_2$ alloys after quenching from 1400°C were found to be lower than those after quenching form 1000°C. Since thermal vacancies are

incorporated into the compound after quenching from 1400°C (see Fig. 13), the above results indicate that vacancy causes softening, instead of hardening of the $NbCr_2$ Laves phases. Such vacancy-induced softening is very unique and has not been observed before. Also, this is in direct contrast to the effect of vacancy on the hardness in B2 compounds, where vacancy is a very potent hardener. The vacancy hardening in metals and B2 compounds are often correlated to an interaction between the stress field of a moving dislocation and that of the vacancy. The effect of vacancies in Laves phases is different from their effects in metals and B2 compounds, due to the fact that Laves phases have a topologically close-packed structure, and it is impossible for ordinary dislocations to move in the material. The presence of vacancies in Laves phases will make the structure less closely packed and possibly assist the synchroshear deformation of the alloy [31], thus leading to the solid solution softening of the alloys.

4.4 Fracture Toughness in Binary Laves Phases

The fracture toughness of the alloys does not change as a function of stoichiometry, indicating that the anti-site defect does not affect the deformability and fracture toughness of the materials.

It has been suggested that vacancies in Laves phases may assist the synchroshear mechanism, thus leading to the improvement in the deformability and toughness of the Laves alloys [31]. Chen et al. [7] attributed the toughness improvement in the off-stoichiometric $TiCr_2$ alloys to the presence of vacancies in the alloys. It was found that the quenching temperature, and thus, thermal vacancy, does not affect the crack propagation and fracture toughness behavior of the $NbCr_2$ alloys (Figs. 23 and 24). The vacancy-assisted synchroshear mechanism may not be able to operate in this system. However, the high residual thermal stress after quenching from 1400°C may also embrittle the $NbCr_2$ Laves phases, which may mask the effect of vacancy-assisted sychroshear deformation.

More work on point defects in Laves phases should be pursued, with the hope that constitutional vacancies, instead of thermal vacancies, may exist in certain Laves phases. Such systems will be suitable for examining if the vacancy-assisted synchroshear deformation and toughness improvement are possible in Laves phases.

5. CONCLUSIONS

Point defects in the binary $NbCr_2$, $NbCo_2$, and $NbFe_2$ systems have been clarified combining both bulk density and X-ray lattice parameter measurements. The vacancy concentrations in these systems after quenching from 1000°C are essentially zero. The constitutional defects on both sides of stoichiometry for these systems are of the anti-site type. Such defect mechanism is further supported by the change of the lattice parameter as a function of the stoichiometry. As the Nb content in the Laves phases increases, the lattice parameters on the Nb-rich side increase faster than on the Cr-, Co-, or Fe-rich side.

The previous postulation that constitutional vacancy is the defect mechanism on the Nb-rich side of $NbCr_2$ Laves phase is not correct. For the $NbCo_2$ system, it was found that about 0.7% solubility of Nb exists on the Nb-rich side. As in the $NbCr_2$ system, no consitutional vacancy was found for the Nb-rich compound. However, thermal vacancies exhibiting a maximum at the stoichiometric composition were obtained in $NbCr_2$ Laves phase alloys after quenching from 1400°C. These could be completely eliminated by annealing at 1000°C.

Anti-site hardening was found on both sides of stoichiometry for all three Laves phase systems studied. Furthermore, the thermal vacancies in $NbCr_2$ alloys after quenching from 1400°C were found to soften the Laves phases. The anti-site hardening of the Laves phases is similar to that of the B2 compounds, while the thermal vacancy softening is unique to the Laves phase. Both the anti-site defects and thermal vacancies do not significantly affect the fracture toughness of the Laves phases.

REFERENCES

1. Y.A. Chang and J.P. Neumann, Progr. Solid State Chem. 14 (1982) 221.
2. J.H. Wernick, in *Intermetallic Compounds*, J. H. Westbrook, ed., Wiley, New York (1967) 197.
3. A.K. Sinha, Progr. in Mater. Sci. 15 (Part 2) (1972) 79.
4. T.B. Massalski, in *Physical Metallurgy Part 1*, R. W. Cahn and P. Hassen, eds., North-Holland Physics Publishing, NY (1983) 190.
5. D.J. Thoma and J.H. Perepezko, J. of Alloys and Compounds 224 (1995) 330.
6. P.M. Hazzledine, K.S. Kumar, D.B. Miracle, and A.G. Jackson, MRS Symp. Proc. 288 (1992) 591.
7. K.C. Chen, S.M. Allen, and J.D. Livingston, MRS Symp. Proc. 364 (1994) 1406.
8. D.G. Ivey and D.O. Northwood, Z. Phys. Chem. N. F. 147 (1986) 191.
9. G. Sicking, E. Magomedbekov, R. Hempelmann, Ber. Bunsenges. Phys. Chem. 85 (1981) 686.
10. M. Takeyama and C.T. Liu, Mater. Sci. & Eng. A132 (1991) 61.
11. J.A. Cook, P.K. Liaw, and C.T. Liu, in *Fatigue and Fracture of Ordered Intermetallics*, W.O. Soboyejo, T.S. Srivatsan, and R.O. Ritchie, eds., TMS, Warrendale, PA (1995) 155.
12. J.A. Cook, P.K. Liaw, C.T. Liu, and S.B. Bhaduri, *in Proc. of the Johannes Weertman Symp.*, R.J. Arsenault et al., eds., TMS, Warrendale, PA (1996) 47.
13. K.S. Chan and D.L. Davidson, JOM 48 (1996) 62.
14. D.J. Thoma and J.H. Perepezko, Mater. Sci. & Eng. A156 (1992) 97.
15. J.H. Zhu, P.K. Liaw, and C.T. Liu, Mater. Sci. Eng. A239-240 (1997) 260.
16. S. Saito and P.A. Beck, Trans. Metall. Soc. AIME 218 (1960) 670.
17. T.B. Massalski, J.L. Murray, L.H. Bennett, and H. Baker, *Binary Alloy Phase Diagrams*, American Society for Metals, Metals Park, Ohio (1986).

18. A.W. Smith, J.A. Rogers, and R.D. Rawlings, Phys. Stat. Sol. (a) 15 (1973) K119.

19. E. Paul and L.J. Swartzendruber, Bulletin of Alloy Phase Diagrams, 7(3) (1986) 248.

20. J.M.Z. Bejarano, S. Gama, C.A. Ribeiro, and G. Effenberg, Z. Metallkd. 84(3) (1993) 160.

21. G.E. Dieter, *Physical Metallurgy*, Third Edition, McGraw-Hill, Inc. (1986) 331.

22. M. Sakai and R.C. Bradt, Inter. Mater. Rev. 38 (2) (1993) 53.

23. G.R. Anstis, P. Chantikul, B.R. Lawn, and D.B. Marshall, J. of Amer. Ceram. Soc. 64(9) (1981) 533.

24. H. Anton and P.C. Schmidt, Intermetallics 5 (1997) 449.

25. L. M. Pike, Y. A. Chang, and C. T. Liu, Acta Mater. 45 (1997) 3709.

26. J. P. Riviere, Mat. Res. Bull. 12 (1977) 995.

27. R.L. Fleischer, Scripta Metall. Mater. 27 (1992) 799.

28. J.K. Pargeter and W. Hume-Ruthery, J. Less-Common Met. 12 (1967) 366.

29. W. Brückner, K. Kleinstück, and G.E.R. Schulze, Phys. Stat. Sol. 23 (1967) 475.

30. J.C. Foley, D.J. Thoma, and J.H. Perepezko, Metall. Trans. 25A (1994) 230.

31. P.M. Hazzledine and P. Pirouz, Scripta Metall. et Mater. 28 (1993) 1277.

PART VI: CONCLUDING SUMMARY AND SUGGESTED FUTURE WORK

1. CONCLUDING SUMMARY

The purpose of this study was to gain a better understanding of the phase stability and point defect mechanisms in the Laves phases and improve the mechanical properties of the Laves phases through controlling phase stability and introducing constitutional defects.

The stability of the Laves phases was first studied in transition-metal $NbCr_2$-based systems, using the phase diagram information of binary X-Cr, Nb-X and ternary Nb-Cr-X systems. It was shown that when the atomic size ratios are kept identical, the average electron concentration factor, e/a, is the dominant factor in controlling the phase stability of $NbCr_2$-based transition-metal Laves phases. Such e/a and phase stability correlation was verified in the ternary Nb-Cr-Fe and Nb-Cr-Co Laves phase systems. The experimentally determined critical e/a values corresponding to the C15/C14/C15 phase transitions are close to those from the phase diagram survey. The critical e/a values for C15/C14 phase transitions are as follows: at $e/a < 5.77$, the C15 structure is stabilized; at $5.85 < e/a < 7.5$, the C14 structure is stable; with $e/a > 7.56$, the C15 structure is stabilized again. No intermediate structure is detected between the C15/C14 structures. As the Fe or Co content increases, the volume of 24-atom unit cell decreases linearly for both C15 and C14 structures, while the Vickers hardness increases over the whole C15 and C14 ranges. The fracture toughness is low for all the alloys. The fracture toughness of the C15 structure is greater than that of the C14 structure for the two ternary systems. No improvement in fracture toughness for alloys near the C15 and C14 phase boundaries and in the C15/C14 two-phase regions was observed.

The stability of the Laves phases was also considered from bond characteristics and the enthalpy of formation of the Laves phases. Enthalpies of formation of Laves phases are critically surveyed and reviewed. It was found that the bond characteristics in Laves phase are not necessarily metallic in nature for both non-transition metal Laves phases and Laves phases containing transition metals. There are metallic, covalent and ionic bonds, or a

mixed metallic-covalent-ionic bond. A thermodynamic interpretation is offered to explain the size-ratio limits for Laves phase formation. As the deviation from the ideal size ratio increases, the maximum negative enthalpy of formation decreases linearly, which is assumed to be due to the elastic strain energy expended in compressing the atoms. At the atomic size ratio R_A/R_B = 1.03 and 1.65, the enthalpies of formation reach zero. Further deviation in the R_A/R_B ratio from the ideal value will lead to the enthalpy of formation being positive. Thus, the free energy of formation becomes positive, due to the negligible entropy of formation term. Therefore, Laves phases can only be stabilized in certain atomic size R_A/R_B ratios. The enthalpies of formation calculated by the semiempirical Miedema model was found to be in good agreement with the available experimental data for transition-metal and Al lanthanide Laves phases. This means that Miedema's theory can be used to predict quantitatively, at least qualitatively, the enthalpies of formation of transition-metal and Al lanthanide Laves phase systems.

The constitutional defect mechanisms in the binary C15 $NbCr_2$ and $NbCo_2$, and C14 $NbFe_2$ Laves phase systems were clarified in this research. The constitutional defect mechanisms on both sides of stoichiometry in these three binary systems are the anti-site substitution. For the $NbCr_2$ alloys, it was shown that the previous postulation that constitutional vacancy is the defect mechanism at the Nb-rich side is not accurate. Furthermore, for this system, the vacancy concentrations after quenching from 1400°C were found to be much greater than after quenching from 1000°C, indicating the thermal nature of these vacancies. The thermal vacancies exhibited a maximum at the stoichiometric composition in $NbCr_2$ alloys quenched from 1400°C. These vacancies could be completely eliminated by annealing at 1000°C.

The hardness of the above alloys with various point defect concentrations was also determined, and the anti-site hardening was found in all of the three Laves phase systems. The presence of thermal vacancies was found to soften the Laves phases, instead of

hardening the alloys. The anti-site defect and thermal vacancies do not significantly affect the fracture toughness of the Laves phases.

2. SUGGESTED FUTURE WORK

This research has addressed several critical issues for Laves phase alloys. However, there are many remaining areas deserving further investigation. The following is a list of some challenging research areas for future studies:

(1) The understanding of the physical background of the e/a/phase stability correlation is needed in transition-metal Laves phases. There has been some research in this direction [1-5]; however, more theoretical calculations are needed to fully understand this phenomenon.

(2) Even though no intermediate structures were found between C14 and C15 for the ternary Nb-Cr-Fe and Nb-Cr-Co systems at 1000°C, there are indications that at 1200°C, C36 may exist in certain ranges between C15 and C14 [6]. Phase stability studies for these two ternary systems need to be undertaken after quenching from 1200°C. If a C36 structure exists, the fracture toughness of this structure needs to be characterized. Furthermore, it has been demonstrated that the heats of formation of Laves phases with C14, C15 and C36 structures are very close [7], indicating their stability is quite similar. The reason leading to the appearance and disappearance of the C36 structure should be clarified.

(3) More experimental determination of the enthalpy of formation (ΔH) of Laves phases with ΔH unknown should be conducted to further confirm the atomic size ratio dependence of the enthalpy of formation (Fig. 4, Part IV). Especially, enthalpies of formation of the two Laves phases, $ScAl_2$ and $BaPt_2$, with abnormal ΔH values should be determined using direct synthesis calorimetry.

(4) Our point defect study has been focused on C14 and C15 structures with R_A/R_B ratio smaller than the ideal one (1.225). It will be interesting to determine the defect mechanisms for Laves phases with R_A/R_B greater than 1.225. It is possible to obtain constitutional vacancies for Laves phases with $R_A/R_B > 1.225$, due to geometric considerations. Some examples will be $ZrCo_2$ and YFe_2, with R_A/R_B values of 1.28 and 1.414, respectively.

(5) For B2 phases, it has been found that the defect mechanism is closely related to the enthalpies of formation of the compounds. Actually, the defect structure of a specific B2 compound can often be predicted by considering the magnitude of the enthalpy of formation. Neumann has demonstrated that B2 compounds with negative ΔH smaller than 75 to 90 kJ/mole generally exhibit the anti-site defect structure, while compounds with a greater value generally exhibit the triple defect structure and have constitutional vacancies [8]. In other words, constitutional vacancies will be the preferred defect mechanism for compounds that are more strongly ordered, i.e., with higher absolute ΔH values. This empirical observation can be seen in Table I, which lists the ΔH values of several B2 compounds and was taken from Ref. 9.

Table I The enthalpies of formation of several B2 compounds

Compound	ΔH (kJ/mole)	Defect structure
FeCo	-30	Anti-site substitution
CuZn	-33.3	
AgMg	-55.2	
AuZn	-77.4	
FeAl	-75	Constitutional vacancy
CoAl	-162.3	
PdIn	-184.2	
NiAl	-207	

The ΔH values for $NbCr_2$, $NbCo_2$, and $NbFe_2$ are -21, -51, and -61.5 kJ/mole, respectively, from Table I and II of Part IV. Obviously, these values are in the same range with those of B2 compounds with anti-site defects. It is not surprising that only anti-site defects are observed for these Laves phases. It will be interesting to study the defect structures of those Laves phases with more negative enthalpy of formation, i.e., Laves phases with ΔH values close to those of B2 phases with constitutional vacancies. The possibility of the existence of constitutional vacancies will be higher for these Laves phases. Some examples of Laves phases with such characteristics will be $ZrCo_2$ and $ZrAl_2$ with ΔH equal to -113 and -138 kJ/mole.

(6) The thermal vacancies in different Laves phases should be studied and correlated with the stability of the Laves phases. Laves phases with high stability should be able to maintain their ordered state, thus less prone to the formation of thermal vacancies. It should be possible to find out some empirical relationship between the thermal vacancy concentration and enthalpy of formation in Laves phases. For those Laves phases with thermal vacancies, it will be interesting to determine whether the thermal vacancies sit on the A-site, the B-site, or both of the AB_2 Laves phases.

REFERENCES

1. S. Pei and T.B. Massalski, Acta Metall. Mater. 43 (1995) 2385
2. R.L. Johannes, R. Haydock, and V. Heine, Phys. Rev. Letters 36(7) (1976) 372.
3. Y. Ohta. and D.G. Pettifor, J. Phys.: Condens. Matter. 2 (1990) 8189.
4. F. Chu, M. Sob, R. Siegl, T.E. Mitchell, D.P. Pope, and S.P. Chen, Phil. Mag. B70 (1994) 881.
5. F. Chu, D.J. Thoma, Y. He, T.E. Mitchell, S.P. Chen, and J.H. Perepezko, Mat. Res. Soc. Symp. Proc. 364 (1995) 1089.
6. M. Grujicic, S. Tangrila, O.B. Cavin, W.D. Porter, and C.R. Hubbard, Mater. Sci. Eng. A160 (1993) 37.
7. S. Hong and C.L. Fu, "Phase Stability and Elastic Moduli of Cr_2Nb by First-Principles Calculations", submitted to Intermetallics (1998).
8. J. P. Neumann, Acta Metall. 28 (1980) 1165.
9. L.M. Pike, *"The Effect of Ternary Alloying on the Defect Structure and Mechanical Properties of B2 Compounds"*, Ph.D. Dissertation, University of Wisconsin - Madison (1997) 35.

VITA

Mr. Jiahong (John) Zhu was born in a small village surrounded by many beautiful rivers near Suzhou, P. R. China on Nov. 30, 1966. He received his Bachelor of Science degree in Physical Metallurgy from the Northeast Heavy-Machinery Institute in Helongjiang Province in July, 1988. He then went to graduate school in the Institute of Metallurgy and Materials Science, Shanghai University of Technology, under the instruction of Prof. X. J. Wan, and received his Master degree in Materials Science and Engineering in May, 1991. His thesis was entitled "Hydrogen Embrittlement of Intermetallic Alloys Based on Ni_3Al and Co_3Ti". After his graduation, he worked in the same institute for 3 years, continuing the research on environmental embrittlement and alloy design of interemetallic alloys. In August, 1994, he started his Ph.D. study in the Department of Materials Science and Engineering at University of Tennessee, Knoxville (UTK). His co-advisors were Dr. P. K. Liaw at UTK and Dr. C. T. Liu at ORNL. His dissertation was on the metallurgical factors controlling the phase stability and mechanical behavior of transition-metal Laves phase alloys. A Doctor of Philosophy degree was awarded on August 14, 1998.